
Doctoral Dissertations

Student Theses and Dissertations

1975

Design, fabrication, and application of uniformly distributed RC networks for use in electronic circuits

Michael Flynn Kavanaugh

Follow this and additional works at: https://scholarsmine.mst.edu/doctoral_dissertations



Part of the [Electrical and Computer Engineering Commons](#)

Department: **Electrical and Computer Engineering**

Recommended Citation

Kavanaugh, Michael Flynn, "Design, fabrication, and application of uniformly distributed RC networks for use in electronic circuits" (1975). *Doctoral Dissertations*. 269.

https://scholarsmine.mst.edu/doctoral_dissertations/269

This thesis is brought to you by Scholars' Mine, a service of the Missouri S&T Library and Learning Resources. This work is protected by U. S. Copyright Law. Unauthorized use including reproduction for redistribution requires the permission of the copyright holder. For more information, please contact scholarsmine@mst.edu.

DESIGN, FABRICATION, AND APPLICATION OF UNIFORMLY DISTRIBUTED
RC NETWORKS FOR USE IN ELECTRONIC CIRCUITS

by

MICHAEL FLYNN KAVANAUGH, 1940-

A DISSERTATION

Presented to the Faculty of the Graduate School of the

UNIVERSITY OF MISSOURI - ROLLA

In Partial Fulfillment of the Requirements for the Degree

DOCTOR OF PHILOSOPHY

in

ELECTRICAL ENGINEERING

1975

T3052
188 pages
c.1

Jack J. Bourquin *Ralph S. Carson*

Advisor

Eddie F. Fowler *O.R. Plummer*

246515

ABSTRACT

In the design of electronic circuits, both linear and non-linear, one of the goals is the reduction of the number of elements needed to complete the design. By using distributed RC networks a reduction in the number of elements by at least 50% is usually possible. This dissertation discusses several distributed RC networks, develops detailed design procedures for each, and applies them in the design of electronic circuits.

The indefinite admittance matrix (IAM) for the \overline{DRURC} (double-resistive uniformly distributed RC network) and the \overline{URC} (single-resistive uniformly distributed RC network), which have been previously derived, are used as the starting points for the development of the IAM's for the \overline{TURC} (tapped \overline{URC}) and the \overline{TDRURC} (tapped \overline{DRURC}), a new distributed network. The development of the IAM for the \overline{TDRURC} proceeds from the interconnection of two \overline{DRURC} 's such that the IAM's add. A similar procedure using \overline{URC} 's yields the IAM for the \overline{TURC} . These two IAM's, which have not been previously published, allow the derivation of the design equations necessary to apply these networks to electronic circuits.

These four distributed network elements (\overline{URC} , \overline{TURC} , \overline{DRURC} , and \overline{TDRURC}) are applied to the reduction in the numbers of elements needed for the following electronic circuits: RC-coupled amplifiers, multivibrator circuits, high-Q

(10 to 150) band-pass amplifiers, and phase-shift oscillators. The application to RC-coupled amplifiers is new, while the applications to band-pass amplifiers and phase-shift oscillators are significant advances to work that has been previously suggested. A prototype of each of the four distributed networks was built by the author in 1972 using a thin-film deposition method which is described in Chapter VII. The phase-shift oscillator, band-pass amplifier, and multivibrator circuits were also built and tested. The results compared favorably with predicted results.

The procedures for designing and fabricating uniformly distributed RC networks are reviewed in detail. A review of both thin-film fabrication by vacuum deposition and semiconductor fabrication by diffusion is included.

ACKNOWLEDGMENT

First, I would like to acknowledge the help of the Holy Spirit, for as Paul wrote to the Phillipians (4:13 KJV), "I can do all things through Christ which strengtheneth me". Without His support and help, the writing of any dissertation would have been impossible for me.

The compiling of a list of people who have contributed to the completion of my research would be a virtually endless task, however, a great debt of gratitude goes to Dr. J. J. Bourquin and the rest of my committee. Whatever this dissertation may be, the faults are in spite of the committee and not because of them. Two of my office-mates, Robert Egbert and Roger Hayes provided many an evening of discussions and circuit trouble-shooting and to them goes a vote of thanks for their help, both physical and spiritual. My wife, Nancy, put up with taking care of the children almost every night of the week while I was out at the office, as well as continually giving me the moral support I needed in order to finish. All too often the typist of a dissertation gets ignored. Mrs. Eunice French exhibited extreme patience and talent both with me and my handwriting. Finally, I wish to thank Northrop Institute of Technology, Inglewood, California, for the financial support given me through their Academic Leave Grant program.

TABLE OF CONTENTS

	PAGE
ABSTRACT	ii
ACKNOWLEDGMENT	iv
LIST OF FIGURES	xi
LIST OF TABLES	xv
I. INTRODUCTION.	1
A. GENERAL DISCUSSION.	1
1. Types	1
2. History	2
3. Literature Review	3
B. FABRICATION OF DISTRIBUTED NETWORKS	4
C. APPLICATIONS.	8
1. Filters	8
2. Logic and Switching Circuits.	8
3. Amplifier Circuits.	9
4. Oscillators	9
II. DOUBLE RESISTIVE \overline{URC}	11
A. INTRODUCTION.	11
1. History	11
2. Construction.	11
B. INDEFINITE ADMITTANCE MATRIX FOR THE \overline{DRURC}	12
1. Derivation.	12
2. Transfer Ratios	17

TABLE OF CONTENTS (cont'd)	PAGE
3. Reduction to \overline{URC}	20
C. DETERMINATION OF THE CAPACITANCE OF	
A \overline{DRURC}	22
III. TAPPED \overline{DRURC}	29
A. INTRODUCTION.	29
B. INTERCONNECTION OF \overline{DRURC} 's.	30
C. INDEFINITE ADMITTANCE MATRIX FOR THE	
\overline{TDRURC}	32
1. Development of the Indefinite	
Admittance Matrix	32
2. Relationship of K^* , K^{**} , Γ^* , and	
Γ^{**} to the \overline{TDRURC}	37
D. TRANSFER RATIOS	40
1. Introduction.	40
2. Voltage and Current Transfer	
Ratios.	40
3. Transfer Immittances.	45
IV. TAPPED \overline{URC}	46
A. INTRODUCTION.	46
B. INDEFINITE ADMITTANCE MATRIX DEVELOPMENT.	46
C. TRANSFER FUNCTIONS.	50
1. Voltage and Current Transfer	
Ratios.	50
2. Transfer Immittances.	52
D. CAPACITANCE DETERMINATION	53

TABLE OF CONTENTS (cont'd)	PAGE
V. APPLICATIONS	55
A. INTRODUCTION	55
B. LOGIC AND SWITCHING CIRCUITS	55
C. RC COUPLED AMPLIFIERS	59
1. Coupling Networks	59
a. Introduction	59
b. \overline{TURC}	59
(1) Driving-Point	
Admittances	59
(2) Frequency Response	62
c. \overline{TDRURC}	65
(1) Driving-Point	
Admittances	65
(2) Frequency Response	67
d. \overline{URC}	68
(1) Driving-Point	
Admittances	68
(2) Frequency Response	70
2. By-pass Networks	71
a. Introduction	71
b. Frequency Response	71
3. Summary	72
D. OSCILLATORS	73
1. Introduction	73
2. Analysis	73

TABLE OF CONTENTS (cont'd)	PAGE
E. FILTERS.	83
1. Passive Band-Reject.	83
2. Active Bandpass.	83
VI. DESIGN PROCEDURES AND EXAMPLES	90
A. INTRODUCTION	90
B. COUPLING NETWORKS.	91
1. Introduction	91
2. \overline{TURC}	93
3. \overline{TDRURC}	94
4. \overline{URC} (as in Figure 6-1)	95
5. \overline{DRURC}	96
6. \overline{URC} (as in Figure 6-2)	97
C. BY-PASS NETWORKS	99
D. AMPLIFIER CHARACTERISTICS.	99
1. Introduction	99
2. Input and Output Impedances.	99
3. Frequency Response	103
4. Comparison of Distributed Network and Lumped	108
a. Introduction	108
b. Input and Output Impedances.	108
c. Voltage Gain	109
5. Summary.	112
E. OSCILLATORS.	113
1. \overline{DRURC} Network Design	113
2. Active Block Design.	114

TABLE OF CONTENTS (cont'd)	PAGE
F. FILTERS	114
1. Passive Band Reject.	114
2. Active Bandpass.	118
G. LABORATORY VERIFICATION.	121
1. Capacitance Determination.	121
a. \overline{DRURC}	121
b. \overline{URC}	122
2. \overline{URC} By-pass.	123
VII. FABRICATION.	124
A. INTRODUCTION	124
B. FABRICATION METHODS.	124
1. Thin-film.	124
2. Semiconductor p-n Junction	131
C. RESISTORS.	134
1. Introduction and Design Equations.	134
a. Thin-Film.	134
b. Diffused Semiconductor	137
2. Geometry	138
D. CAPACITORS	140
1. Introduction and Design Equations.	140
a. Thin-Film.	141
b. Diffused Semiconductor	142
E. THIN-FILM DESIGN EXAMPLE	145
VIII. CONCLUSIONS.	146
A. SUMMARY.	146
B. SUGGESTIONS FOR FURTHER RESEARCH	149

TABLE OF CONTENTS (cont'd)	PAGE
BIBLIOGRAPHY.	153
VITA.	157
APPENDICES.	158
A. \overline{URC} IAM.	159
B. \overline{TURC} IAM	160
C. \overline{DRURC} IAM.	162
D. \overline{TDRURC} IAM	164
E. \overline{TURC} VOLTAGE RATIO AS ϕ APPROACHES INFINITY	166
F. MANUAL VERIFICATION OF THE LOWER 3-db FREQUENCY OF THE DISTRIBUTED NETWORK RC COUPLED AMPLIFIER	168
G. FREQUENCY RESPONSE CURVES OF THE DISTRIBUTED NETWORKS IN FIGURES 5-3 AND 6-1 AND THE \overline{DRURC} IN FIGURE 6-2.	169

LIST OF FIGURES

FIGURE NO.		PAGE
1-1.	Thin-film distributed network; L = total length, W = width of the distributed network	5
1-2.	Semiconductor p-n junction \overline{URC}	7
1-3.	Networks for use as emitter by-pass circuits	9
2-1.	Figure 1-1, modified slightly.	12
2-2.	Incremental section of \overline{DRURC}	13
2-3.	Standard symbol for \overline{DRURC} . R=rL, C=cL	16
2-4.	\overline{DRURC} set up for calculation of (a) voltage transfer ratio and (b) current transfer ratio	19
2-5.	\overline{DRURC} reduced to \overline{URC} by connecting terminals 2 and 3 and letting N = 0.	21
2-6.	\overline{DRURC} used as a passive notch filter	23
3-1.	Tapped \overline{DRURC} (\overline{TDRURC}).	29
3-2.	\overline{DRURC} 's with two additional terminals added to yield two six-terminal networks	31
3-3.	\overline{DRURC} 's of Figure 3-2 connected in parallel	31
3-4.	The six-terminal network resulting from the interconnection of the networks in Figure 3-2.	32
3-5.	Figure 3-1 repeated for convenience.	33
3-6.	(a) \overline{DRURC}_a and (b) \overline{DRURC}_b	38
3-7.	Figure 3-6 with the new values for R and C. R*, R**, C*, and C** are calculated from equations (3.3) and (3.4).	39
3-8.	Typical \overline{TDRURC} interstage coupling network with both source and load immittances.	41

LIST OF FIGURES (cont'd)

FIGURE NO.		PAGE
3-9.	Typical TDR $\overline{\text{URC}}$ interstage coupling network with both source and load admittances	43
4-1.	Tapped $\overline{\text{URC}}$ (T $\overline{\text{URC}}$)	47
4-2.	Equivalent circuit for a T $\overline{\text{URC}}$ used as an RC coupling network. The block represents Figure 4-1.	50
4-3.	T $\overline{\text{URC}}$ connected as a passive notch filter	53
5-1.	Monostable multivibrator using a DR $\overline{\text{URC}}$.	56
5-2.	Astable multivibrator utilizing DR $\overline{\text{URC}}$'s	58
5-3.	(a) Lumped version of a two-stage, RC coupled, bipolar amplifier. (b) Distributed RC version of (a).	60
5-4.	T $\overline{\text{URC}}$ set up for (a) output and (b) input driving-point admittance calculations. .	61
5-5.	Frequency response of a T $\overline{\text{URC}}$ used as an input coupling network	63
5-6.	TDR $\overline{\text{URC}}$ connected for calculations of (a) input admittance and (b) output admittance	66
5-7.	$\overline{\text{URC}}$ connected for calculation of (a) Y_i and (b) Y_0	69
5-8.	$\overline{\text{URC}}$ used as a replacement for a lumped RC emitter (or source) by-pass network .	71
5-9.	Feedback amplifier using a DR $\overline{\text{URC}}$ as the feedback network	74
5-10.	DR $\overline{\text{URC}}$ phase shift oscillator using a ICVS as a gain block	75
5-11.	Pole-zero diagram for (a) $\frac{G_1}{G_2}$ and (b) $\frac{H_1}{H_2}$ from equations (5.30)	78

LIST OF FIGURES (cont'd)

FIGURE NO.		PAGE
5-12.	Transistor realization of an ICVS	82
5-13.	Transistor-DR \overline{URC} phase-shift oscillator suitable for integration.	82
5-14.	Active bandpass filter using a DR \overline{URC} and an ideal operational amplifier. The DR \overline{URC} is oriented as shown in Figure 2-6.	84
5-15.	Q versus amplifier gain A for various values of R for the DR \overline{URC}	88
5-16.	Center frequency ϕ_o versus amplifier gain A for various values of R for the DR \overline{URC}	89
6-1.	Typical RC-coupled two-stage bipolar transistor amplifier: (a) lumped RC version [36], (b) distributed RC version.	92
6-2.	Typical RC-coupled two-stage JFET amplifier: (a) lumped RC version [36], (b) distributed RC version.	98
6-3.	Magnitude and phase response for the input impedance of the distributed network amplifier shown in Figure 6-1(b). $h_{ie} = 1500\Omega$, $h_{re} = 0$, $h_{fe} = 200$, $h_{oe} = 0.5 \times 10^{-4}$ mhos.	101
6-4.	Magnitude and phase response for the output impedance of the distributed network amplifier shown in Figure 6-1(b). $h_{ie} = 1500\Omega$, $h_{re} = 0$, $h_{fe} = 200$, $h_{oe} = 0.5 \times 10^{-4}$ mhos.	102
6-5.	(a) Equivalent circuit for Figure 6-1(b)	105
	(b) Magnitude and phase of voltage and current gain vs f(kHz) for distributed network amplifier shown in Figure 6-1(b). $h_{ie} = 1500\Omega$, $h_{re} = 0$, $h_{fe} = 200$, $h_{oe} = 0.5 \times 10^{-4}$ mhos	106
6-6.	DR \overline{URC} required for ICVS oscillator.	113
6-7.	Bipolar transistor current-controlled voltage-source (ICVS). R provides the needed value from equation (6.14)	115

LIST OF FIGURES (cont'd)

FIGURE NO.		PAGE
6-8.	Waveform of DR \overline{URC} phase shift oscillator	116
6-9.	Example schematic diagram of a DR \overline{URC} phase-shift oscillator suitable for integrated circuit design.	117
7-1.	Principal parts of a system for thin-film deposition.	125
7-2.	A simplified diffusion system for phosphorus	133
7-3.	Typical geometry for uniformly distributed resistance	139
8-1.	(a) Distributed RC parallel and (b) Distributed RC series replacement networks and the lumped RC counterparts . .	151
8-2.	Suggested RC distributed network replacements for (a) lead and (b) lag compensation networks.	152
G-1.	Magnitude of equation (4.8) versus $\phi = \omega RC$	170
G-2.	Magnitude of equation (3.13) versus $\phi = \omega(1+N)RC$	171
G-3.	Magnitude of equation (6.2) versus $\phi = \omega RC$	172
G-4.	Magnitude of equation (2.15) versus $\phi = \omega(1+N)RC$	173

LIST OF TABLES

TABLE NO.		PAGE
I.	Input and output impedance comparison between the lumped and distributed network amplifiers of Figure 6-1(a) and (b)	110
II.	Voltage gain comparison between the lumped and distributed network amplifiers of Figures 6-1(a) and (b). . . .	111
III.	Commonly used materials in thin film deposition	126
IV.	Sheet resistivities for materials used for thin film resistors. Thickness ranges from 200 Å down to 1 Å respectively.	136
V.	Several materials used for thin-film dielectrics	142

I. INTRODUCTION

A. GENERAL DISCUSSION

1. Types. Distributed networks are generally classified into one of two major classes: 1) uniform and 2) nonuniform. Within each major classification there are many subclassifications such as single resistive layer, multiresistive layer, RC, GRC, etc. This dissertation will deal with the uniformly distributed RC network. Under this subclassification will be two further groups: 1) single resistive-layer uniformly distributed RC network (hereafter called a $\overline{\text{URC}}$) and 2) double resistive-layer $\overline{\text{URC}}$ (hereafter called a $\overline{\text{DRURC}}$).

The term "uniformly distributed" means that for a given distributed network, the width of the network (see Figure 1-1) is a constant. Therefore, the per-unit length resistance and per-unit length capacitance become constants as well. In actual practice, this is impossible to obtain exactly, but deviations are difficult to detect or predict. Another assumption is that no change in the per-unit resistance or per-unit capacitance occurs along the width of the network. Of course, this assumption is ideal, but if the width is sufficiently small compared to the length, the assumption is essentially valid.

"Nonuniformly distributed" indicates that the network elements are distributed along the length in some fashion other than uniform (i.e., they are now functions of the position along the network). In terms of fabrication and analysis, the most common nonuniformly distributed networks are the linear taper and the exponential taper. These tapers are the manner in which a given parameter of the distributed network varies with respect to the length (i.e., $r = f(x)$ where f is the function described by the type of taper-- linear, exponential, etc., and x is some distance less than or equal to the total length). Other types of nonuniform distributed networks have been described in the literature [1,2,3]. As discussed in the next major section (B - Fabrication of Distributed Networks), the nonuniform network presents some difficulty in fabrication.

2. History. Although the methods useful for the analysis of distributed networks have been a part of electrical engineering for many years, the majority of the distributed networks discussed in this dissertation are new. A distributed network is described by partial differential equations, and distributed networks may be used to simulate certain classes of partial differential equations [4]. The partial differential equations are similar in form to those describing an LC transmission line.

Some of the early modern work in the analysis, design and application of distributed networks was done by Happ and Castro [5], Wyndrum [6], Smith and Cooper [7] and Smith [8]. These were done from an idealized analysis point of view with little if any aim toward practical realization of the distributed network. The main thrust then was to develop an understanding of and the mathematical descriptions for the distributed network. Primarily because of the ease of fabrication, the earliest distributed networks were the \overline{URC} type; however, as interest grew, other types were investigated. One of the first divergences from the \overline{URC} was the \overline{UGRC} where the effects of the conductance of the dielectric layer were investigated. The effect of non-zero conductance is to add a circuit parameter which modifies the frequency response characteristics of the resultant network [9].

3. Literature Review. Recent literature (since 1965) and research has been concerned with the use of the distributed RC network in the areas of active and passive synthesis of filters. For example, considerable work has been done in the area of active filters [1,15,23,24] where one or more \overline{URC} 's have been used to advantage in obtaining a desirable low-pass frequency response. Some work has also been done with band-pass filters where a \overline{URC} and either a lumped resistor in series with the conductive layer or a

lumped capacitor across the resistive layer has been used to replace the Twin-T network [24]. (The Twin-T may also be replaced by a $\overline{\text{DRURC}}$ as is seen in Chapters II and V.)

In the area of applications of distributed networks to amplifier design, suggestions were made by Lin [25] and Castro, et al [28] that it might be possible to replace the lumped RC networks with distributed RC networks. They drop the topic after brief discussions and no other authors have pursued it any further. Lemke [27] has used URC's to replace the lumped RC networks in an FM discriminator. Good frequency response is claimed by Lemke for the performance of this discriminator.

The drawback in most applications of distributed networks to electronic circuit design is the inability to fabricate a large capacitance in the distributed network [25,26]. No work has been published that suggests a large (e.g., 10 μ Farads) capacitance can be obtained in an integrated circuit.

B. FABRICATION OF DISTRIBUTED NETWORKS

Two methods are presently available for the fabrication of distributed networks: 1) deposition of thin films and 2) growth of semiconductor p-n junctions. Both methods are feasible and practical, but the choice of method depends upon the equipment available and the intended application. In an application demanding the use of semiconductor integrated

circuits, the semiconductor p-n junction method would be the most practical, because it can then be formed along with the remainder of the circuit. If, however, the intended application is to merely investigate the properties of the distributed network or where the network need not be incorporated into the total circuit as completely as with integrated circuits, then the thin-film method would be preferable due to the ease with which the method yields a distributed network. Ease here refers to capital outlay for equipment and accuracy of results. Both of the above methods are described in more detail in Chapter VII, but for purposes of introduction each will be described briefly here.

The method of thin-film deposition deposits each of the layers shown in Figure 1-1 as a thin film. Depending upon the type of distributed network (\overline{URC} or \overline{DRURC}) one or both of the conductive layers may exhibit a high total

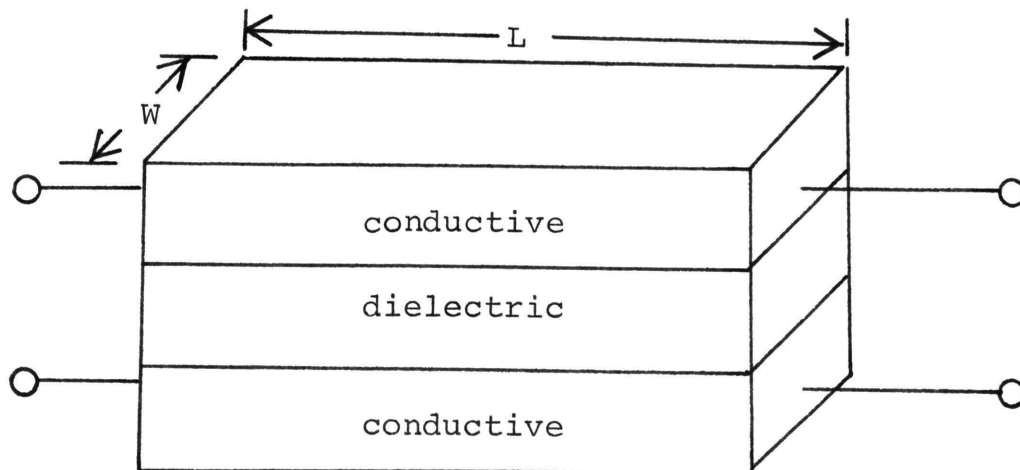


Figure 1-1. Thin-film distributed network; L = total length, W = width of the distributed network.

resistance (500Ω to $2M\Omega$ typically). The method is essentially one of heating the material to be deposited to its melting point and allowing the resulting vapors to condense onto a substrate (the substrate is not shown in Figure 1-1). The thickness is monitored, and when the desired thickness of material has been deposited onto the substrate the process is stopped. The operation is carried out under a high vacuum to allow deposition to take place with lower temperatures and also to help prevent oxidation of the heated material by removing as much oxygen as possible from the system.

Semiconductor p-n junction distributed networks make use of the doping of the p and n layers to provide the necessary resistance. The capacitance needed for the network is provided by the capacitance of the depletion region (or barrier capacitance) that results when the p-n junction is reverse biased. The semiconductor p-n junction method is more difficult to control, without expensive, sophisticated equipment, when producing a desired distributed network because the resistance is dependent upon the level of impurities in each layer and the material used for each layer. In addition, the capacitance is dependent upon the reverse bias that is applied across the p-n junction [11]. Since the width of the depletion layer is determined by the impurity density and the width determines the capacitance, considerable variation in capacitance occurs with a variation in impurity level. Another capacitance, called diffusion

capacitance [11] also exists across the p-n junction under the condition of forward bias. This capacitance may be as large as 20μ farads, but is shunted by the low resistance across the forward-biased junction and is, therefore, impractical. Figure 1-2 shows a p-n junction distributed network. Since the capacitance depends upon the amount of reverse bias applied across the p-n junction, normally the p-type layer will be highly doped so that the conductance of the lower layer will be very high. Normally the common terminal is considered negative and to insure reverse bias, this will necessitate the p layer becoming the common layer. Generally, the resistance of that lower layer will be considered approximately zero.

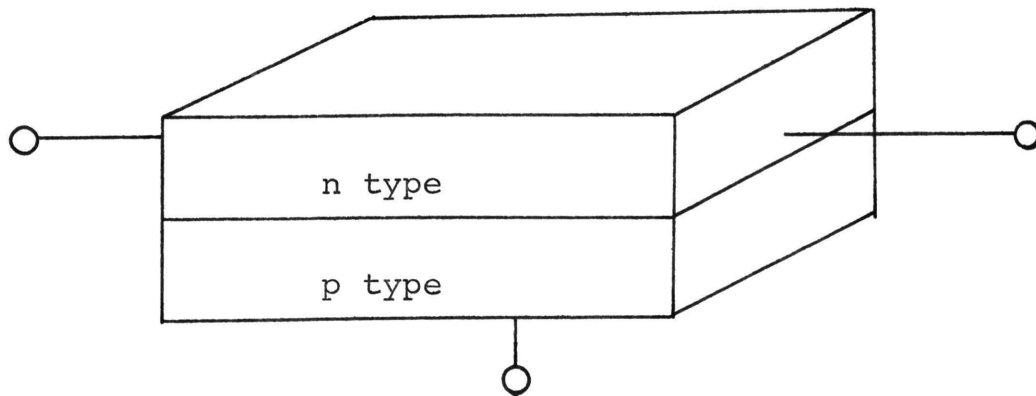


Figure 1-2. Semiconductor p-n junction \overline{URC} .

C. APPLICATIONS

1. Filters. Low-pass, high-pass, and notch filters may be synthesized with distributed networks. The performance of these filters (in terms of number of elements, rate of roll-off, etc.) is comparable to the lumped version [14,15]. With the addition of an operational amplifier, bandpass filters may be made (Chapter V and [28]) that exhibit frequency response characteristics as good as those made with lumped components.

With lumped components, many procedures are available for the synthesis of both active [12] and passive [13] filters. Fortunately, most of these procedures work equally well with distributed networks and much work has been done in this area [14,15].

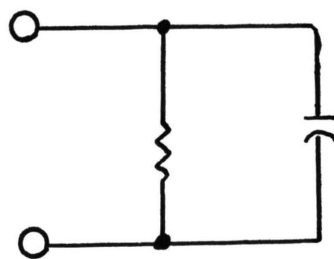
2. Logic and Switching Circuits. There are many applications in the field of switching and logic circuits open to the use of distributed networks.

Hayes [16] has developed both a one-shot and an astable multivibrator utilizing distributed networks which produce good quality waveforms. The frequency of the output is dependent upon the RC product of the distributed network used. For the one shot, a \overline{URC} is used and for the multivibrator, two $DR\overline{URC}$'s are used to replace the RC networks

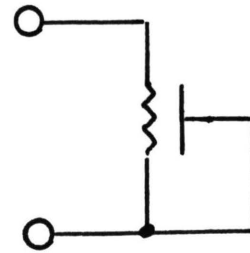
in the lumped versions. Schematic diagrams of these circuits are found in Chapter V.

3. Amplifier Circuits. Theoretically, distributed networks can be used to replace all of the lumped RC network combinations in an RC-coupled amplifier.

For example [25,28], the emitter by-pass network shown in Figure 1-3(a) can be replaced by the \overline{URC} shown in Figure 1-3(b). The frequency response of the distributed network can be shown to be as good as the lumped network.



(a) Lumped Parallel RC



(b) Distributed RC Parallel

Figure 1-3. Networks for use as emitter by-pass circuits.

The collector resistor, coupling capacitor, and base-biasing resistors between two bipolar transistors can be replaced by one $TDR\overline{URC}$ (tapped $DR\overline{URC}$). (See Figure 6-1 for a schematic diagram illustrating this application.)

4. Oscillators. RC phase-shift oscillators are

dependent upon obtaining 180° phase shift between input and output of the RC network used in the feedback loop of an active device. This type of oscillator may be made using a single $\overline{\text{URC}}$ as the feedback network, because the phase shift from input to output continues to increase as a function of frequency. Therefore, at some frequency the phase shift will be the desired 180° , and the oscillations will occur. DRURC's may also be used in phase-shift oscillators.

The application of uniformly distributed RC networks to both amplifiers and oscillators is discussed in Chapters V and VI. Other authors [5,25,28] have made suggestions concerning applications to amplifiers and oscillators but have not treated the topic in as much detail as done in this dissertation.

II. DOUBLE RESISTIVE $\overline{\text{URC}}$

A. INTRODUCTION

1. History. The double resistive $\overline{\text{URC}}$ ($\overline{\text{DRURC}}$) was first proposed by Happ and Castro [5] in 1960. Their approach was to develop the indefinite admittance matrix (IAM) describing the $\overline{\text{DRURC}}$. The $\overline{\text{DRURC}}$ forms a building block for further types of distributed networks (the $\overline{\text{TDRURC}}$ and $\overline{\text{TURC}}$). Although, as shown in Chapters V and VI, there are many applications to electronic circuit design for the $\overline{\text{DRURC}}$, very little work has been done [5,28,29]. Most of the past work has centered upon either single resistive or multilayer $\overline{\text{URC}}$'s. As is seen in the next subsection on construction of the $\overline{\text{DRURC}}$, it may resemble a multilayer $\overline{\text{URC}}$ but there are some differences.

2. Construction. A physical view of the $\overline{\text{DRURC}}$ is shown in Figure 1-1 which is modified slightly and repeated below. r is given in ohms per meter, c in farads per meter and N is a positive constant. In the case of a $\overline{\text{URC}}$, $N = 0$, and the bottom layer becomes a ground plane with a per-unit resistance much less than r .

When compared with the typical multilayer distributed network [1,22], it can be seen that the $\overline{\text{DRURC}}$ is a multilayer $\overline{\text{URC}}$ with no low resistance conducting layer. The

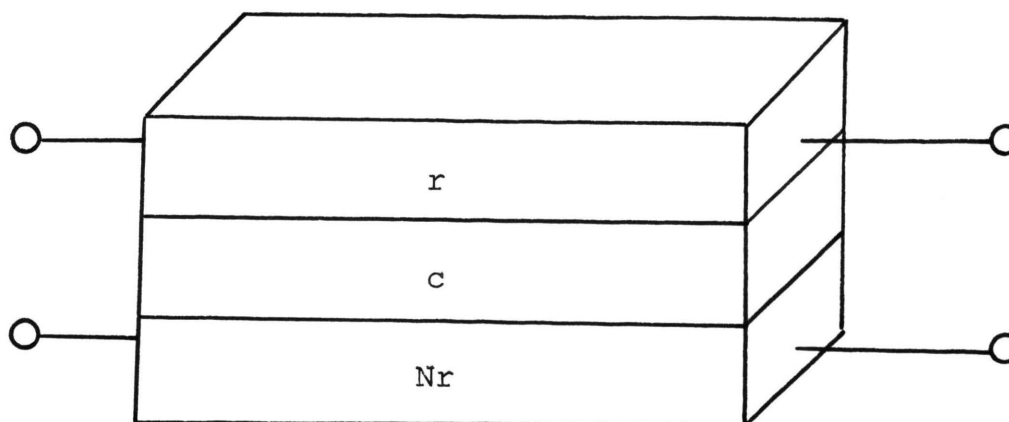


Figure 2-1. Figure 1-1, modified slightly.

multilayer \overline{URC} would have another dielectric layer below the Nr layer and a high conductance ground plane layer beneath that.

B. INDEFINITE ADMITTANCE MATRIX FOR THE $DR\overline{URC}$

1. Derivation. An incremental section of the RC ladder line representing a Δx section of a $DR\overline{URC}$ is shown in Figure 2-2. The following analysis is similar to that found in references [5] and [11]. Writing a Kirchhoff's Voltage Law expression for the outermost loop yields

$$e(x, j\omega) = ri_1(x, j\omega) \Delta x + e(x + \Delta x, j\omega) - Nri_2(x, j\omega) \Delta x$$

or

$$e(x, j\omega) - e(x+\Delta x, j\omega) = ri_1(x, j\omega) \Delta x - Nri_2(x, j\omega) \Delta x. \quad (2.1)$$

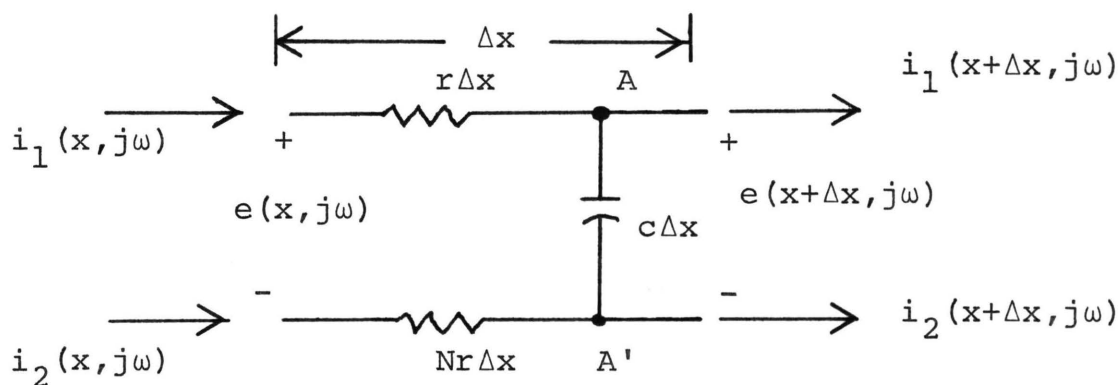


Figure 2-2. Incremental section of DRURC.

Dividing both sides of (2.1) by Δx and taking the limit $\Delta x \rightarrow 0$, yields

$$\frac{\partial}{\partial x} e(x, j\omega) = -ri_1(x, j\omega) + Nri_2(x, j\omega). \quad (2.2)$$

Now, writing a Kirchhoff's Current Law expression at both A and A' gives

$$i_1(x, j\omega) = j\omega c\Delta x e(x+\Delta x, j\omega) + i_1(x+\Delta x, j\omega)$$

and

$$i_2(x, j\omega) = -j\omega c \Delta x e(x+\Delta x, j\omega) + i_2(x+\Delta x, j\omega)$$

or

$$i_1(x, j\omega) - i_1(x+\Delta x, j\omega) = j\omega c \Delta x e(x+\Delta x, j\omega) \quad (2.3a)$$

$$i_2(x, j\omega) - i_2(x+\Delta x, j\omega) = -j\omega c \Delta x e(x+\Delta x, j\omega). \quad (2.3b)$$

After dividing by Δx and taking the limit, $\Delta x \rightarrow 0$, equations (2.3) become

$$\frac{\partial}{\partial x} i_1(x, j\omega) = -j\omega c e(x, j\omega) \quad (2.4a)$$

and

$$\frac{\partial}{\partial x} i_2(x, j\omega) = j\omega c e(x, j\omega). \quad (2.4b)$$

By comparing the expressions in equations (2.4) it can be seen that

$$\frac{\partial}{\partial x} i_1(x, j\omega) = - \frac{\partial}{\partial x} i_2(x, j\omega) = -j\omega c e(x, j\omega). \quad (2.5)$$

Integrating (2.5) with respect to x yields an expression relating $i_1(x, j\omega)$ and $i_2(x, j\omega)$.

$$i_1(x, j\omega) = - i_2(x, j\omega) + f(j\omega). \quad (2.6)$$

Substituting (2.6) into (2.2) yields

$$\frac{\partial}{\partial x} e(x, j\omega) = i_2(x, j\omega)(1+N)r - rf(j\omega). \quad (2.7)$$

Differentiating (2.7) with respect to x and substituting (2.4b) into the result gives

$$\frac{\partial^2}{\partial x^2} e(x, j\omega) = j\omega c(1+N)re(x, j\omega). \quad (2.8)$$

The solutions for equation (2.4) and equation (2.8) subject to the boundary conditions $e(x, j\omega)$ and $i(x, j\omega)$ evaluated at $x = 0$ and $x = L$, give the voltages at each end and the currents $i_1(x, j\omega)$ and $i_2(x, j\omega)$.

Redrawing the $\overline{\text{DRURC}}$ gives Figure 2.3 (which is the accepted symbol for a $\overline{\text{DRURC}}$) and letting

$$i_1 = i_1(0, j\omega) \quad (2.9a)$$

$$i_2 = i_2(0, j\omega) \quad (2.9b)$$

$$i_3 = -i_2(L, j\omega) \quad (2.9c)$$

$$i_4 = -i_1(L, j\omega) \quad (2.9d)$$

yields the terminal currents; L is the total physical length of the \overline{DRURC} .

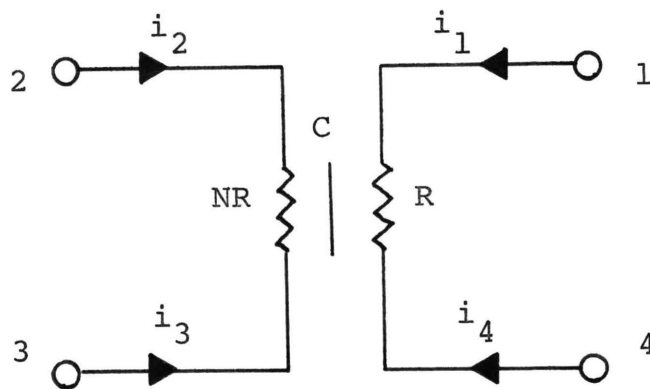


Figure 2-3. Standard symbol for \overline{DRURC} . $R = rL$, $C = cL$.

The terminal voltages may be found from the four terminal-pair voltages,

$$e(0, j\omega) = V_{12} = V_1 - V_2 \quad (2.10a)$$

$$e(L, j\omega) = V_{43} = V_4 - V_3 \quad (2.10b)$$

$$V_{14} = \int_0^L i_1(x, j\omega) r dx = V_1 - V_4 \quad (2.10c)$$

$$V_{23} = \int_0^L i_2(x, j\omega) N r dx = V_2 - V_3. \quad (2.10d)$$

The relationship of the terminal currents of equations (2.9) and the terminal voltages of equations (2.10) yields the

indefinite admittance matrix (IAM) of (2.11) [5,25]. This IAM is used as the basis for the computer programs of Appendices A-D. The elements of (2.11) are calculated by use of the program in Appendix C.

$$\frac{1}{(1+N)R} \begin{bmatrix} \left(\frac{\Gamma}{\tanh \Gamma} + N\right) & \left(1 - \frac{\Gamma}{\tanh \Gamma}\right) & \left(\frac{\Gamma}{\sinh \Gamma} - 1\right) & \left(-\frac{\Gamma}{\sinh \Gamma} - N\right) \\ \left(1 - \frac{\Gamma}{\tanh \Gamma}\right) & \left(\frac{\Gamma}{\tanh \Gamma} + \frac{1}{N}\right) & \left(-\frac{\Gamma}{\sinh \Gamma} - \frac{1}{N}\right) & \left(\frac{\Gamma}{\sinh \Gamma} - 1\right) \\ \left(\frac{\Gamma}{\sinh \Gamma} - 1\right) & \left(-\frac{\Gamma}{\sinh \Gamma} - \frac{1}{N}\right) & \left(\frac{\Gamma}{\tanh \Gamma} + \frac{1}{N}\right) & \left(1 - \frac{\Gamma}{\tanh \Gamma}\right) \\ \left(-\frac{\Gamma}{\sinh \Gamma} - N\right) & \left(\frac{\Gamma}{\sinh \Gamma} - 1\right) & \left(1 - \frac{\Gamma}{\tanh \Gamma}\right) & \left(\frac{\Gamma}{\tanh \Gamma} + N\right) \end{bmatrix} \quad (2.11)$$

where

$$\Gamma \triangleq \sqrt{j\omega(1+N)RC}.$$

2. Transfer Ratios. As discussed in Chapters V and VI, the voltage transfer ratio V_1/V_3 and the current transfer ratio $(-I_1)/I_3$ are the two that are needed in

most applications. For these applications, terminal 2 of the DR \overline{URC} is connected to the supply and is therefore at AC ground, and terminal 4 is usually connected directly to DC ground; these assumptions then give rise to the network of Figure 2-4 with terminals 2 and 4 grounded which is then used to develop the above two transfer ratios [28].

Figure 2-4(a) shows the DR \overline{URC} appropriately connected to develop the voltage transfer ratio, and Figure 2-4(b) is then used for development of the current transfer ratio. Both transfer ratios will take into account source and load immittances. For Figure 2-4(a), since both terminals 2 and 4 are grounded, the rows and columns numbered 2 and 4, respectively, will be eliminated from the matrix of (2.11). This operation yields two equations

$$I_1 = Y_{11}V_1 + Y_{13}V_3 \quad (2.12)$$

and

$$I_3 = Y_{31}V_1 + Y_{33}V_3. \quad (2.13)$$

Writing a node equation at terminal 3 and solving for V_3 ,

$$V_3 = \frac{V_{in}Y_s - V_1Y_{31}}{Y_s + Y_{33}}. \quad (2.14)$$

Letting $I_1 = -Y_L V_{out}$, $V_1 = V_{out}$ and substituting these plus

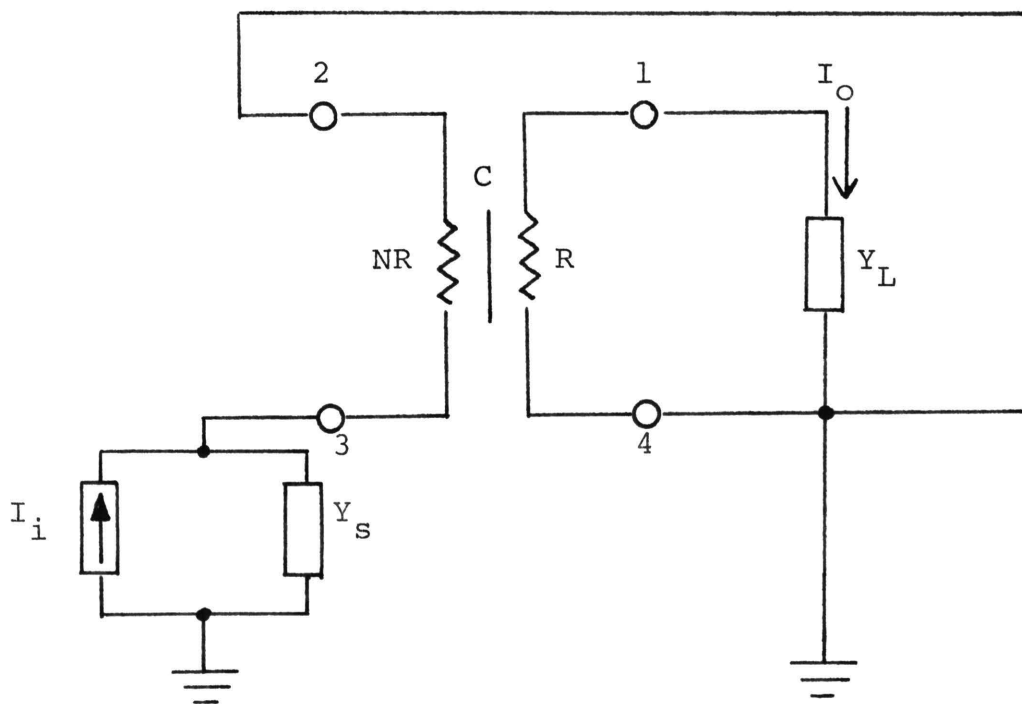
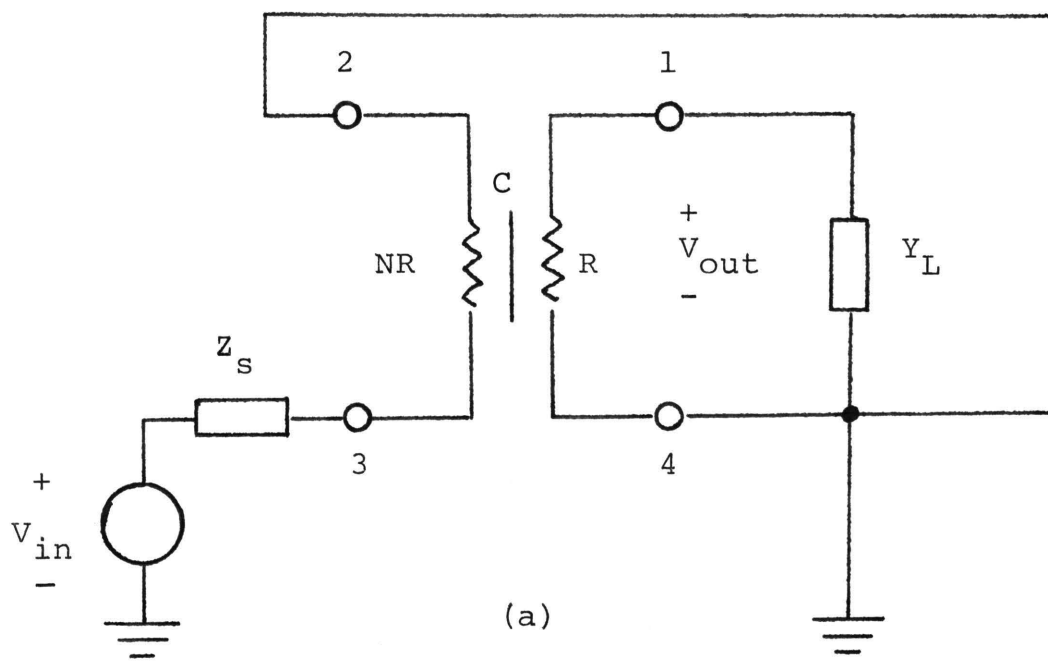


Figure 2-4. $\overline{\text{DRURC}}$ set up for calculation of (a) voltage transfer ratio and (b) current transfer ratio.

(2.14) into (2.12) gives, after some algebraic manipulation, the desired voltage transfer ratio.

$$\frac{V_{\text{out}}}{V_{\text{in}}} = \frac{-Y_{13}Y_s}{(Y_s + Y_{33})(Y_L + Y_{11}) - Y_{13}Y_{31}} \quad (2.15)$$

The current transfer ratio can be calculated using Figure 2.4(b) and writing a node equation at terminal 3 and solving for V_3 ,

$$V_3 = \frac{I_i - Y_{31}V_1}{Y_s + Y_{33}} \quad (2.16)$$

Letting $I_1 = -I_0$, $V_1 = I_0 Z_L$, substituting (2.16) into (2.12) and manipulating gives

$$\frac{I_0}{I_i} = \frac{-Y_L Y_{13}}{(Y_L + Y_{11})(Y_s + Y_{33}) - Y_{13}Y_{31}} \quad (2.17)$$

Therefore equations (2.15) and (2.17) give the desired transfer functions for the DR $\overline{\text{URC}}$. The immittance transfer functions Z_T ($Z_T = \frac{V_0}{I_i}$) and Y_T ($Y_T = \frac{I_0}{V_i}$) may be found by dividing (2.17) by Y_L and multiplying (2.15) by Y_L , respectively.

3. Reduction to $\overline{\text{URC}}$. The DR $\overline{\text{URC}}$ may be reduced to a $\overline{\text{URC}}$ by appropriate terminal connections and by letting $N = 0$. If, in Figure 2-3, $N = 0$ and terminals 2 and 3 are connected together a $\overline{\text{URC}}$ results and is shown in Figure 2-5.

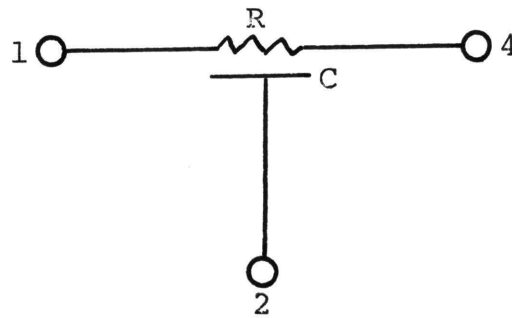


Figure 2-5. \overline{DRURC} reduced to \overline{URC} by connecting terminals 2 and 3 and letting $N = 0$.

The IAM for Figure 2-5 is found from (2.11) and is shown in (2.18) [5]. The numerical

$$\frac{\theta}{R} \begin{bmatrix} \left(\frac{1}{\tanh \theta}\right) & \left(\frac{1}{\sinh \theta} - \frac{1}{\tanh \theta}\right) & \left(-\frac{1}{\sinh \theta}\right) \\ \left(\frac{1}{\sinh \theta} - \frac{1}{\tanh \theta}\right) & \left(\frac{2}{\tanh \theta} - \frac{2}{\sinh \theta}\right) & \left(\frac{1}{\sinh \theta} - \frac{1}{\tanh \theta}\right) \\ \left(-\frac{1}{\sinh \theta}\right) & \left(\frac{1}{\sinh \theta} - \frac{1}{\tanh \theta}\right) & \left(\frac{1}{\tanh \theta}\right) \end{bmatrix} \quad (2.18)$$

$$\theta \triangleq \sqrt{j\omega RC}.$$

values for the elements of (2.18) are calculated by use of the program in Appendix A. (Note: terminal 4 of Figure

2-5 is represented by column 3 of (2.18) in this program). Applications in the design of electronic amplifiers and oscillators involving the use of the IAM of (2.18) are discussed in Chapters V and VI. References [5] and [28] suggest these applications but give only brief discussions.

C. DETERMINATION OF THE CAPACITANCE OF A $\overline{\text{DRURC}}$

Since the capacitance of a $\overline{\text{DRURC}}$ is not "lumped" at one location, it is impossible to measure directly. The value of capacitance is an important parameter in design (cf: Chapter VI), and a check is needed to determine if the value of capacitance obtained during the fabrication process is the desired value.

One of the methods that could be used to determine the value of capacitance would be to calculate the capacitance directly from a knowledge of the dimensions and physical properties of the resistive layers (it is assumed that both the resistive layers have identical geometry) and the dielectric layer. Since the dimensions of the resistive layers are quite small (0.1 inch width would be large) and the thickness of the dielectric layer is difficult to control accurately, the above method of capacitance determination is of doubtful practical value.

A novel method that makes use of the frequency response characteristics of the $\overline{\text{DRURC}}$ ([12] and [30]) is the easiest to use in determining the capacitance. The essence of this

method is one of measuring the frequency at which the \overline{DRURC} will act as a notch filter. Substituting that measured notch frequency into an expression for notch frequency (as a function of R , C , and N) and solving for C will yield the value of capacitance for the \overline{DRURC} .

The \overline{DRURC} used as a notch filter is shown in Figure 2-6. Note that terminal 3 is "floating", and the \overline{DRURC}

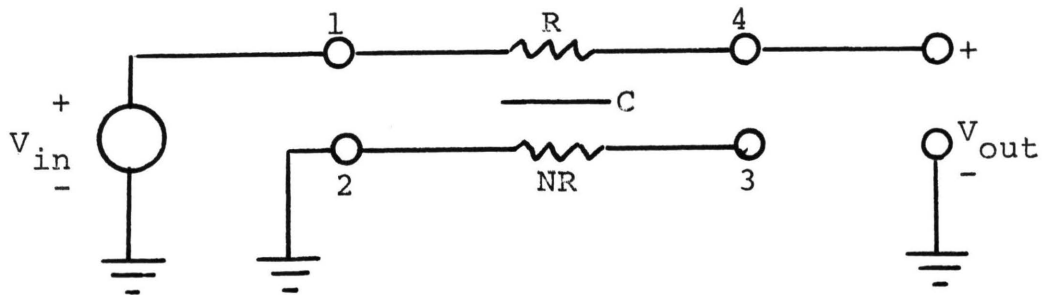


Figure 2-6. \overline{DRURC} used as a passive notch filter.

is now used as a 3-terminal network with terminal number 3 "suppressed". The method of obtaining the IAM from equation (2.11) of the network of Figure 2-3 that has one terminal suppressed is explained in Balabanian and Bickart [18]. The IAM for Figure 2-6 is shown in (2.19).

$$\begin{bmatrix} Y_{11}^* & Y_{12}^* & Y_{14}^* \\ Y_{21}^* & Y_{22}^* & Y_{24}^* \\ Y_{41}^* & Y_{42}^* & Y_{44}^* \end{bmatrix} \quad (2.19a)$$

where

$$Y_{11}^* = \frac{1}{(1+N)R} \left[\frac{N\Gamma^2 \tanh \Gamma + \Gamma + N\Gamma(2\operatorname{sech} \Gamma + N)}{N\Gamma + \tanh \Gamma} \right]$$

$$Y_{12}^* = Y_{21}^* = \frac{1}{(1+N)R} \left[\frac{\Gamma(1-N)(\operatorname{sech} \Gamma - 1) - N\Gamma^2 \tanh \Gamma}{N\Gamma + \tanh \Gamma} \right] \quad (2.19b)$$

$$Y_{14}^* = Y_{41}^* = \frac{1}{R} \left[\frac{-(N\Gamma + \Gamma \operatorname{sech} \Gamma)}{N\Gamma + \tanh \Gamma} \right]$$

$$Y_{22}^* = \frac{1}{(1+N)R} \left[\frac{N\Gamma^2 \tanh \Gamma + 2\Gamma(1 - \operatorname{sech} \Gamma)}{N\Gamma + \tanh \Gamma} \right]$$

$$Y_{24}^* = Y_{42}^* = \frac{1}{R} \left[\frac{\Gamma(\operatorname{sech} \Gamma - 1)}{N\Gamma + \tanh \Gamma} \right] \quad (2.19c)$$

$$Y_{44}^* = \frac{1}{R} \left[\frac{\Gamma(1+N)}{N\Gamma + \tanh \Gamma} \right]$$

Since terminal 4 is open circuited (or the load

impedance at terminal 4 is very much larger than R), the current at terminal 4 can be neglected. This yields

$$0 = Y_{41}^* V_1 + Y_{44}^* V_4. \quad (2.20)$$

Letting $V_1 = V_{in}$, $V_4 = V_{out}$, and solving for the voltage transfer ratio gives

$$\frac{V_{out}}{V_{in}} = \frac{-Y_{41}^*}{Y_{44}^*}. \quad (2.21)$$

Substituting the expressions for Y_{41}^* and Y_{44}^* from equations (2.19) into equation (2.21) gives the desired voltage transfer ratio for the DRURC passive notch filter as

$$\frac{V_{out}}{V_{in}} = \frac{1 + N \cosh \Gamma}{(1+N) \cosh \Gamma}. \quad (2.22)$$

The notch frequencies are determined by the zeros of $1 + N \cosh \Gamma = 0$. Letting $\Gamma = \sqrt{j\omega(1+N)RC} = \sqrt{j}\varnothing$, means that some value of \varnothing gives a zero of (2.22). Letting $\varnothing = \omega(1+N)RC = \omega/\omega_0$ and rearranging the numerator of equation (2.22) yields

$$\cosh \sqrt{j} \omega/\omega_0 = -\frac{1}{N}. \quad (2.23)$$

Since

$$\sqrt{j} \omega/\omega_0 = \sqrt{\omega/2\omega_0} (1+j) = u(1+j) \quad (2.24)$$

equation (2.23) now becomes

$$\cosh u \cos u - j \sinh u \sin u = -1/N. \quad (2.25)$$

Equating real and imaginary parts from both sides of (2.25) gives

$$\cosh u \cos u = -\frac{1}{N} \quad (2.26)$$

and

$$\sinh u \sin u = 0. \quad (2.27)$$

Equation (2.27) is satisfied for

$$u = n\pi, \quad n = 0, \pm 1, \pm 2, \pm 3, \dots$$

Choosing $n = \pm 1$ gives $u = \sqrt{\omega/2\omega_0} = \pm\pi$. Solving for ω , and noting that

$$\omega_0 = \frac{1}{(1+N)RC} \quad (2.28)$$

gives [28]

$$\omega = \frac{19.75}{(1+N)RC} \quad (2.29)$$

Substituting $u = \pm\pi$ into equation (2.26) yields

$$\cosh(\pm\pi) \cos(\pm\pi) = -\frac{1}{N}, \quad (2.30)$$

or, since $\cosh(\pm\pi) = \cosh(\pi)$ and $\cos(\pm\pi) = \cos(\pi) = -1$, equation (2.30) becomes

$$\cosh(\pi) = \frac{1}{N}. \quad (2.31)$$

Solving equation (2.31) for N yields

$$N = 0.08627. \quad (2.32)$$

This, then, indicates that for $N = 0.08627$, a true zero of transmission exists for the $DR\overline{URC}$ passive notch filter at $\omega = 19.75$. For N not equal to 0.08627 the transmission factor is no longer zero and, as seen from equation (2.29),

a slight shift in frequency also occurs.

With the use of equation (2.29) and assuming N to be small enough to produce a measurable notch, the capacitance of a \overline{DRURC} can be determined. The resulting expression for capacitance then becomes

$$C = \frac{19.75}{\omega(1+N)R} \quad (2.33)$$

where R is the DC resistance of the layer with the highest resistance.

III. TAPPED $\overline{\text{DRURC}}$

A. INTRODUCTION

Occasionally it may be advantageous to utilize both the full resistance of one side of the $\overline{\text{DRURC}}$ and to "tap" one side in order to make a voltage divider. The result becomes the five-terminal network shown in Figure 3-1. The indefinite admittance matrix of equation (2.11) is, therefore, no longer directly applicable, and a new IAM must be derived.

Since the IAM for a $\overline{\text{DRURC}}$ is already available, it is convenient to combine two $\overline{\text{DRURC}}$'s together to produce a tapped $\overline{\text{DRURC}}$ ($\overline{\text{TDRURC}}$). From Figure 3-1 it may be seen that a tapped $\overline{\text{DRURC}}$ may be thought of as two $\overline{\text{DRURC}}$'s connected in cascade.

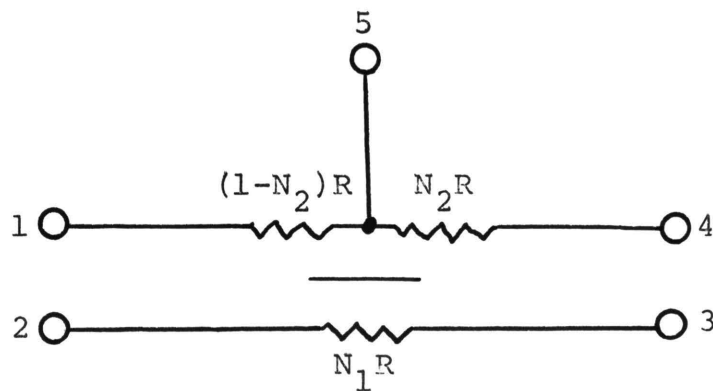


Figure 3-1. Tapped $\overline{\text{DRURC}}$ ($\overline{\text{TDRURC}}$).

It is desired to use the IAM for the $\overline{\text{DRURC}}$, since it is already available, and conversion to another set of parameters would introduce undesirable complexity into the calculations. In order to use the IAM directly, the two networks must be connected in parallel (see Leon and Wintz [19]).

B. INTERCONNECTION OF $\overline{\text{DRURC}}$'s

The addition of two more terminals to each of two $\overline{\text{DRURC}}$'s yields the two six-terminal networks shown in Figure 3-2. When the two networks shown in Figure 3-2 are connected in parallel as shown in Figure 3-3, the result is a six-terminal network. The six-terminal network may now be seen to be the cascade combination of two four-terminal $\overline{\text{DRURC}}$'s.

The resultant IAM for the six-terminal network of Figure 3-3 is found by merely adding together the IAM's of each of the two networks in Figure 3-2.

The addition of the two extra terminals onto each $\overline{\text{DRURC}}$ in Figure 3-2 does not add to the overall complexity of the networks.

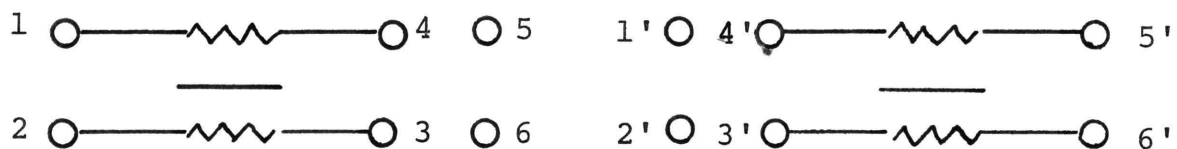


Figure 3-2. DRURC's with two additional terminals added to yield two six-terminal networks.

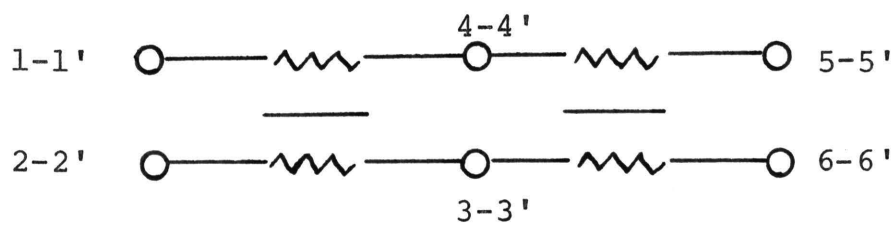


Figure 3-3. DRURC's of Figure 3-2 connected in parallel.

C. INDEFINITE ADMITTANCE MATRIX FOR THE $\overline{\text{TDRURC}}$

1. Development of the Indefinite Admittance Matrix.
 Designate the unprimed $\overline{\text{DRURC}}$ in Figure 3-2 as $\overline{\text{DRURC}}_a$ and the primed $\overline{\text{DRURC}}$ as $\overline{\text{DRURC}}_b$.

The network in Figure 3-4 is the desired network except for terminal 3 and the renumbering of the terminals to match Figure 3-1. The suppression of terminal 3 will yield the desired network and the desired IAM for the $\overline{\text{TDRURC}}$ (Figure 3-1).

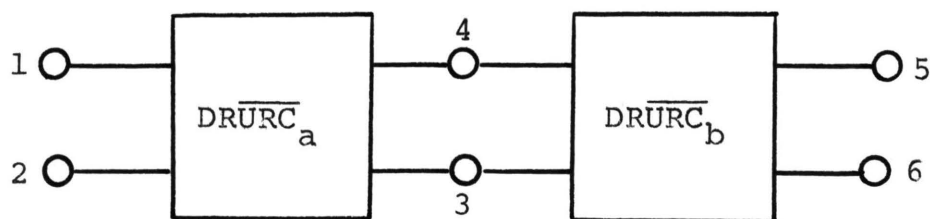


Figure 3-4. The six-terminal network resulting from the interconnection of the networks in Figure 3-2.

Suppression of terminal 3 may be carried out in a number of ways [13,17]. The method used here comes from Balabanian and Bickart [18].

Renumbering the $\overline{\text{TDR}}_{\text{URC}}$ terminals of Figure 3-4 to match those of Figure 3-1 yields the $\overline{\text{TDR}}_{\text{URC}}$ of Figure 3-5 and its associated IAM shown in (3.1). Due to the IAM properties of a passive network [18] only 10 of the 25 elements need be specified explicitly. The elements of (3.1) are listed in equation (3.2).

$$\begin{bmatrix}
 Y_{11} & Y_{12} & Y_{13} & Y_{14} & Y_{15} \\
 Y_{21} & Y_{22} & Y_{23} & Y_{24} & Y_{25} \\
 Y_{31} & Y_{32} & Y_{33} & Y_{34} & Y_{35} \\
 Y_{41} & Y_{42} & Y_{43} & Y_{44} & Y_{45} \\
 Y_{51} & Y_{52} & Y_{53} & Y_{54} & Y_{55}
 \end{bmatrix} \quad (3.1)$$

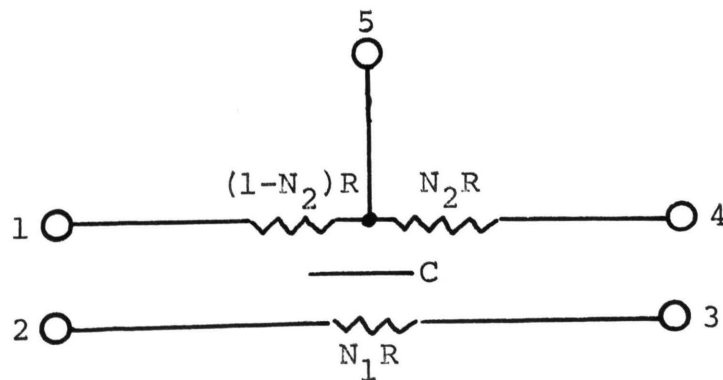


Figure 3-5. Figure 3-1 repeated for convenience.

$$l_1 = K^* (\Gamma^* \coth \Gamma^* + \frac{1}{N_1}) - \frac{(K^*)^2 (\Gamma^* \operatorname{csch} \Gamma^* - 1)^2}{K^* (\Gamma^* \coth \Gamma^* + \frac{1}{N_1}) + K^{**} (\Gamma^{**} \coth \Gamma^{**} + \frac{1}{N_1})}$$

here K^* , Γ^* , K^{**} , and Γ^{**} are shown in equations (3.3) and 8.4),

$$l_2 = K^* (1 - \Gamma^* \coth \Gamma^*) + \frac{(K^*)^2 (\Gamma^* \operatorname{csch} \Gamma^* - 1) (\Gamma^* \operatorname{csch} \Gamma^* + \frac{1}{N_1})}{K^* (\Gamma^* \coth \Gamma^* + \frac{1}{N_1}) + K^{**} (\Gamma^{**} \coth \Gamma^{**} + \frac{1}{N_1})} \quad (3.2a)$$

$$y_{13} = \frac{K^* K^{**} (\Gamma^* \operatorname{csch} \Gamma^* - 1) (\Gamma^{**} \operatorname{csch} \Gamma^{**} + \frac{1}{N_1})}{K^* (\Gamma^* \coth \Gamma^* + \frac{1}{N_1}) + K^{**} (\Gamma^{**} \coth \Gamma^{**} + \frac{1}{N_1})}$$

$$y_{14} = \frac{-K^* K^{**} (\Gamma^* \operatorname{csch} \Gamma^* - 1) (\Gamma^{**} \operatorname{csch} \Gamma^{**} - 1)}{K^* (\Gamma^* \coth \Gamma^* + \frac{1}{N_1}) + K^{**} (\Gamma^{**} \coth \Gamma^{**} + \frac{1}{N_1})}$$

$$y_{15} = - \sum_{i=1}^4 y_{1i}$$

$$y_{21} = y_{12}$$

$$l_2 = K^* (\Gamma^* \coth \Gamma^* + \frac{1}{N_1}) - \frac{(K^*)^2 (\Gamma^* \operatorname{csch} \Gamma^* + \frac{1}{N_1})^2}{K^* (\Gamma^* \coth \Gamma^* + \frac{1}{N_1}) + K^{**} (\Gamma^{**} \coth \Gamma^{**} + \frac{1}{N_1})}$$

$$Y_{23} = - \frac{K^* K^{**} (\Gamma^* \operatorname{csch} \Gamma^* + \frac{1}{N_1}) (\Gamma^{**} \operatorname{csch} \Gamma^{**} + \frac{1}{N_1})}{K^* (\Gamma^* \operatorname{coth} \Gamma^* + \frac{1}{N_1}) + K^{**} (\Gamma^{**} \operatorname{coth} \Gamma^{**} + \frac{1}{N_1})} \quad (3.2b)$$

$$Y_{24} = \frac{K^* K^{**} (\Gamma^* \operatorname{csch} \Gamma^* + \frac{1}{N_1}) (\Gamma^{**} \operatorname{csch} \Gamma^{**} - 1)}{K^* (\Gamma^* \operatorname{coth} \Gamma^* + \frac{1}{N_1}) + K^{**} (\Gamma^{**} \operatorname{coth} \Gamma^{**} + \frac{1}{N_1})}$$

$$Y_{25} = - \sum_{i=1}^4 Y_{2i}$$

$$Y_{31} = Y_{13}$$

$$Y_{32} = Y_{23} \quad (3.2c)$$

$$Y_{33} = K^{**} (\Gamma^{**} \operatorname{coth} \Gamma^{**} + \frac{1}{N_1}) - \frac{(K^{**})^2 (\Gamma^{**} \operatorname{csch} \Gamma^{**} + \frac{1}{N_1})^2}{K^* (\Gamma^* \operatorname{coth} \Gamma^* + \frac{1}{N_1}) + K^{**} (\Gamma^{**} \operatorname{coth} \Gamma^{**} + \frac{1}{N_1})}$$

$$Y_{34} = K^{**} (1 - \Gamma^{**} \operatorname{coth} \Gamma^{**}) + \frac{(K^{**})^2 (\Gamma^{**} \operatorname{csch} \Gamma^{**} + \frac{1}{N_1}) (\Gamma^{**} \operatorname{csch} \Gamma^{**} - 1)}{K^* (\Gamma^* \operatorname{coth} \Gamma^* + \frac{1}{N_1}) + K^{**} (\Gamma^{**} \operatorname{coth} \Gamma^{**} + \frac{1}{N_1})}$$

$$Y_{35} = - \sum_{i=1}^4 Y_{3i}$$

$$Y_{41} = Y_{14}$$

$$Y_{42} = Y_{24} \quad (3.2d)$$

$$Y_{43} = Y_{34}$$

$$Y_{44} = K^{**} (\Gamma^{**} \coth \Gamma^{**} + N_1) - \frac{(K^{**})^2 (\Gamma^{**} \operatorname{csch} \Gamma^{**} - 1)^2}{K^* (\Gamma^* \coth \Gamma^* + \frac{1}{N_1}) + K^{**} (\Gamma^{**} \coth \Gamma^{**} + \frac{1}{N_1})}$$

$$Y_{45} = - \sum_{i=1}^4 Y_{4i}$$

$$Y_{51} = Y_{15}$$

$$Y_{52} = Y_{25}$$

(3.2e)

$$Y_{53} = Y_{35}$$

$$Y_{54} = Y_{45}$$

$$Y_{55} = - \sum_{i=1}^4 Y_{5i}$$

Values for the elements of (3.1) are calculated by use of the program in Appendix D.

2. Relationship of K^* , K^{**} , Γ^* , and Γ^{**} to the $\overline{\text{TDRURC}}$.

It is necessary to investigate the $\overline{\text{TDRURC}}$ of Figures 3-1 and 3-5 in more detail in order to determine exactly the expressions for K^* , K^{**} , Γ^* , and Γ^{**} in terms of the R and C of the $\overline{\text{TDRURC}}$. Figure 3-6 shows the two component $\overline{\text{DRURC}}$'s that, when connected together, form the $\overline{\text{TDRURC}}$. In Figure 3-6, the R and C are, respectively, the total resistance of the top layer and the total capacitance between the layers of the $\overline{\text{TDRURC}}$. Since it is desired to relate each of these networks to the original $\overline{\text{DRURC}}$ in Chapter II, Figure 2-3, the R and C of each of the networks in Figure 3-6 need to be modified.

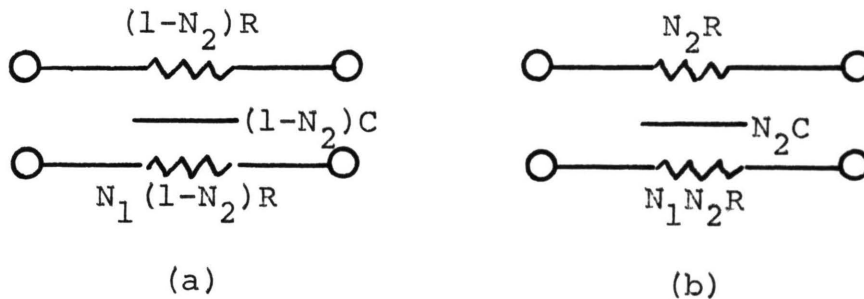


Figure 3-6. (a) \overline{DRURC}_a and (b) \overline{DRURC}_b .

Letting $(1-N_2)R = R^*$, $(1-N_2)C = C^*$ and $N_1(1-N_2)R = N_1R^*$, network (a) of Figure 3-6 becomes Figure 3-7 (a). Letting $N_2R = R^{**}$, $N_2C = C^{**}$ and $N_1N_2R = N_1R^{**}$ yields Figure 3-7 (b). Comparison of Figures 3-7 (a) and (b) with Figure 2-3 shows that they are indeed the same network with different R and C values. The constant multiplier K as well as the complex variable Γ of the matrix (2.11) are both different for networks (a) and (b) of Figure 3-7. The constant multiplier K and the complex variable Γ are calculated in equations (3.3) and (3.4) for each of the two \overline{DRURC} 's. Substitution of the expressions for K^* and Γ^* into the matrix of (2.11) yields the IAM for the network of Figure 3-6 (a). A similar operation

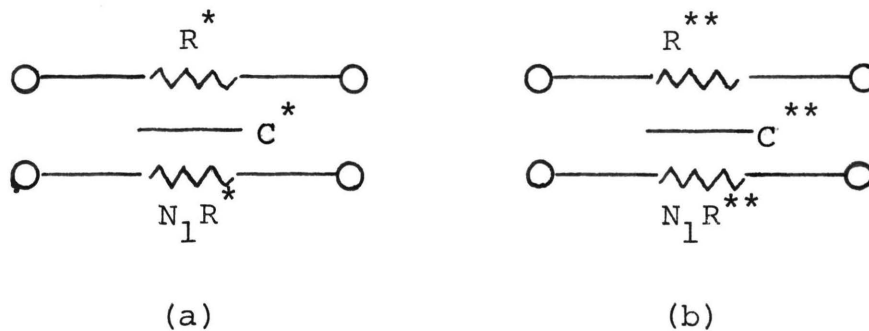


Figure 3-7. Figure 3-6 with the new values for R and C. R^* , R^{**} , C^* , and C^{**} are calculated from equations (3.3) and (3.4).

$$K^* = \frac{1}{(1+N_1)R^*} = \frac{1}{(1+N_1)(1-N_2)R}$$

$$\Gamma^* = \sqrt{j\omega(1+N_1)R^*C^*} = \sqrt{j\omega(1+N_1)(1-N_2)^2 RC} \quad (3.3)$$

$$\Gamma^* = (1-N_2) \sqrt{j\omega(1+N_1)RC}$$

$$K^{**} = \frac{1}{(1+N_1)R^{**}} = \frac{1}{(1+N_1)N_2R}$$

$$\Gamma^{**} = \sqrt{j\omega(1+N_1)R^{**}C^{**}} = \sqrt{j\omega(1+N_1)N_2^2RC} \quad (3.4)$$

$$\Gamma^{**} = N_2\sqrt{j\omega(1+N_1)RC}$$

using K^{**} and Γ^{**} yields the IAM for Figure 3-6 (b). Now each of the parameters in equations (3.2) can be calculated in terms of the total resistance and capacitance of the $\overline{\text{TDRURC}}$.

D. TRANSFER RATIOS

1. Introduction. At the present time, the $\overline{\text{TDRURC}}$ is designed to be used as a distributed network replacement for the interstage coupling network between two transistor stages. Since the two transistor stages may be either bipolar, FET, or a combination, both the voltage and current transfer functions are needed. In order to cover all the possibilities, the transfer immittances are derived as well.

2. Voltage and Current Transfer Ratios. Under the application referenced above, Figure 3-8 shows a typical interstage coupling network with a voltage source, source

impedance and a load admittance. Normally, terminals 1 and 2 would be connected to the voltage supply and would, therefore, be at A.C. ground potential. Terminal 4 would be at both A.C. and D.C. ground potential. The input voltage is V_i , and the output voltage is V_0 .

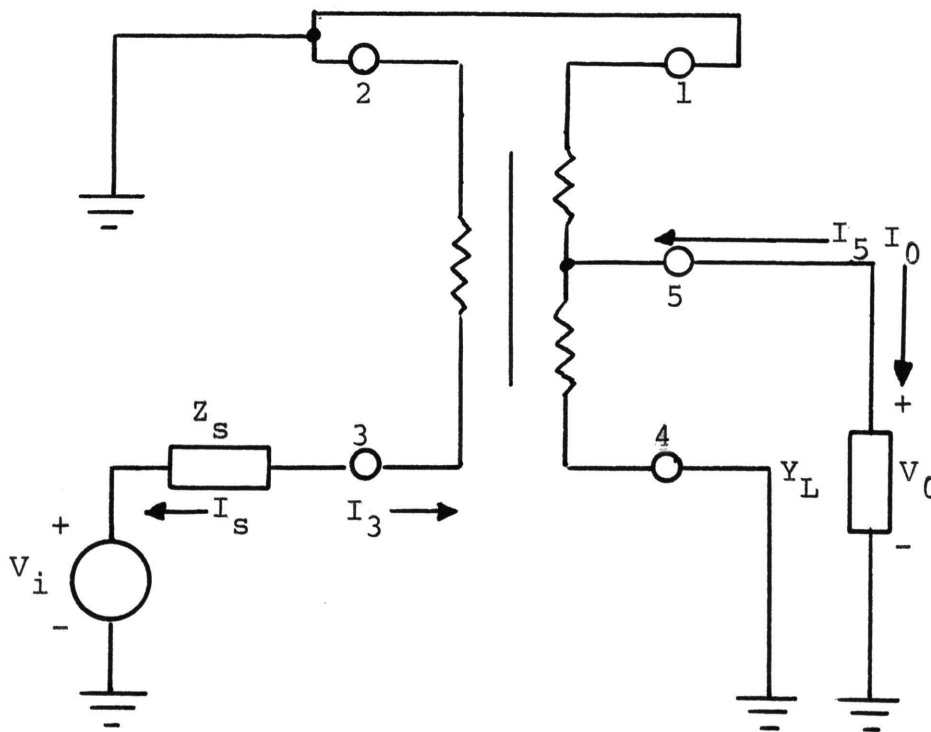


Figure 3-8. Typical TDRURC interstage coupling network with both source and load immittances.

Writing a node equation at terminal 3 yields

$$I_s + I_3 = 0$$

$$Y_s(V_3 - V_i) + Y_{33}V_3 + Y_{35}V_5 = 0. \quad (3.5)$$

Solving (3.5) for V_3 gives

$$V_3 = \frac{Y_s V_i - Y_{35} V_5}{Y_s + Y_{33}}. \quad (3.6)$$

A similar node equation at terminal 5 yields

$$Y_{53}V_3 + Y_{55}V_5 + Y_L V_0 = 0. \quad (3.7)$$

Substitution of (3.6) into (3.7) and noting that $V_5 = V_0$ yields the desired voltage transfer ratio of equation (3.8) where the Y_{ij} are those of the TDR \overline{URC} .

$$\frac{V_0}{V_i} = \frac{-Y_s Y_{53}}{(Y_L + Y_{55})(Y_s + Y_{33}) - Y_{53} Y_{35}} \quad (3.8)$$

If Y_s approaches infinity equation (3.8) becomes

$$\frac{V_0}{V_i} \approx \frac{-Y_{53}}{Y_L + Y_{55}}. \quad (3.9)$$

Additionally, if Y_L approaches 0, equation (3.9) becomes

$$\frac{V_0}{V_i} \cong \frac{-Y_{53}}{Y_{55}} \quad (3.10)$$

An example where equation (3.9) would be valid is where a MOSFET source follower stage is being coupled to a MOSFET common-source stage.

If the current transfer ratio is desired, Figure 3-9 may be used. Again, terminals 1, 2 and 4 are considered to be at A.C. ground and both source and load admittance are present.

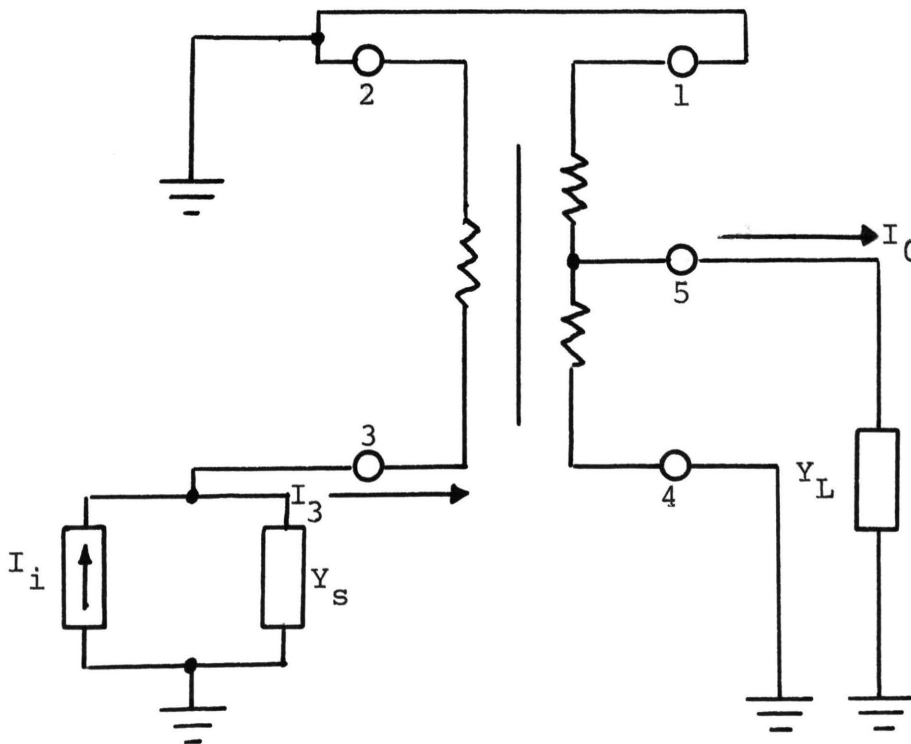


Figure 3-9. Typical TDRURC interstage coupling network with both source and load admittances.

Since the input signal source I_i and the associated admittance Y_s of Figure 3-9 are related to the input voltage source and the associated source admittance of Figure 3-8 by a Norton's transformation of equation (3.11) and $I_0 = V_0 Y_L$,

$$I_i = V_i Y_s, \quad (3.11)$$

multiplication by Y_L and division by Y_s of equation (3.8) yields the desired ratio.

$$\left(\frac{V_0}{V_i}\right) \left(\frac{Y_L}{Y_s}\right) = \frac{V_0 Y_L}{V_i Y_s} = \frac{I_0}{I_i} \quad (3.12)$$

$$\frac{I_0}{I_i} = \frac{-Y_{53} Y_L}{(Y_L + Y_{55})(Y_s + Y_{33}) - Y_{53} Y_{35}}. \quad (3.13)$$

Letting $Y_s \rightarrow 0$ and $Y_L \rightarrow \infty$, the current transfer ratio in equation (3.13) becomes

$$\frac{I_0}{I_i} \cong -\frac{Y_{53}}{Y_{33}}. \quad (3.14)$$

These cases stated above are discussed in a more practical vein and applied to the design of RC-coupled amplifiers in Chapters V and VI.

3. Transfer Immittances. Occasionally the need arises for a transfer function of a "mixed" type (i.e., voltage-current or current-voltage). This gives rise to the transfer immittances

$$Z_T = \frac{V_0}{I_i} \quad (3.15)$$

and

$$Y_T = \frac{I_0}{V_i} \quad (3.16)$$

For the determination of Z_T , Figure 3-9 and equation (3.13) may be used. Dividing both sides of (3.13) by Y_L and noting that $I_0 = Y_L V_0$ yields the transfer impedance

$$Z_T = \frac{V_0}{I_i} = \frac{-Y_{53}}{(Y_{33} + Y_s)(Y_L + Y_{55}) - Y_{53}Y_{35}} \quad (3.17)$$

A similar procedure involving Figure 3-8 and equation (3.8) (note that $I_0 = Y_L V_0$) gives the transfer admittance of equation (3.18).

$$Y_T = \frac{I_0}{V_i} = \frac{-Y_L Y_s Y_{53}}{(Y_L + Y_{55})(Y_s + Y_{33}) - Y_{53}Y_{35}} \quad (3.18)$$

IV. TAPPED \overline{URC}

A. INTRODUCTION

The next step in the development beyond the $TDR\overline{URC}$ of the previous chapter is to place a tap on the resistive layer of a \overline{URC} . This gives rise to the tapped \overline{URC} or $T\overline{URC}$.

The input coupling capacitor and base-biasing resistors of a bipolar transistor amplifier may be replaced by a $T\overline{URC}$. The tap will be placed so as to provide the proper DC bias for the transistor. As is seen in Chapter V the frequency response is comparable to the lumped elements that are replaced by the $T\overline{URC}$. In the case of a FET amplifier the $T\overline{URC}$ can be replaced by a \overline{URC} where the total resistance would provide the gate biasing. In the case of a MOSFET, biased to operate in the enhancement mode [11], the $T\overline{URC}$ may again be used with the tap connected to the gate terminal and the drain supply across the total resistance of the $T\overline{URC}$. The $T\overline{URC}$ resistive layer then provides the required positive bias for enhancement mode operation.

B. INDEFINITE ADMITTANCE MATRIX DEVELOPMENT

The $T\overline{URC}$ (shown in Figure 4-1) may be thought of as two \overline{URC} 's connected in cascade. The point where the resistive layers are connected together forms the tap on the $T\overline{URC}$.

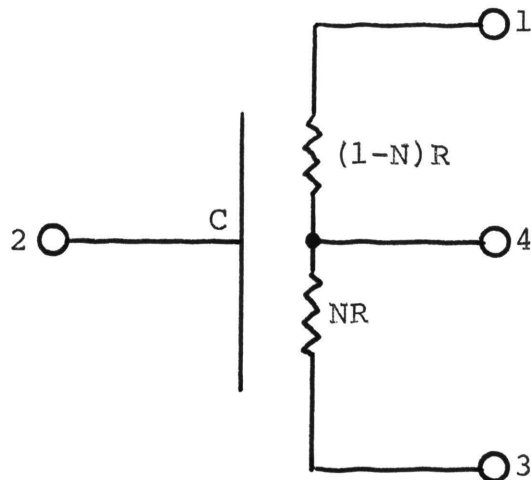


Figure 4-1. Tapped \overline{URC} (\overline{TURC}).

If a comparison is made between Figure 4-1 and Figure 3-5, it can be seen that the \overline{TURC} is actually a \overline{TDRURC} that has been modified by letting N_1 go to zero.

The IAM for the \overline{TURC} is obtained using the same method as used in Chapter III to develop the IAM for the \overline{TDRURC} . Two \overline{URC} 's (each with two additional terminals added) are connected in parallel such that the IAM's will add together.

The result of the IAM development is shown in equation (4.1). Equations (4.2) express the individual elements of equation (4.1) in terms of the hyperbolic functions. Values for the elements of (4.1) are calculated by use of the program in Appendix B.

$$\begin{bmatrix}
 Y_{11} & Y_{12} & Y_{13} & Y_{14} \\
 Y_{21} & Y_{22} & Y_{23} & Y_{24} \\
 Y_{31} & Y_{32} & Y_{33} & Y_{34} \\
 Y_{41} & Y_{42} & Y_{43} & Y_{44}
 \end{bmatrix} \quad (4.1)$$

$$Y_{11} = \frac{\theta^*}{R} [\coth \theta^*]$$

$$Y_{12} = \frac{\theta^*}{R} \left[\frac{1 - \cosh \theta^*}{\sinh \theta^*} \right]$$

(4.2a)

$$Y_{13} = 0$$

$$Y_{14} = \frac{\theta^*}{R} [-\operatorname{csch} \theta^*]$$

$$Y_{21} = Y_{12}$$

$$Y_{22} = -2 \left[\frac{\theta^*}{R} \left(\frac{1 - \cosh \theta^*}{\sinh \theta^*} \right) + \frac{\theta^{**}}{R^{**}} \left(\frac{1 - \cosh \theta^{**}}{\sinh \theta^{**}} \right) \right] \quad (4.2b)$$

$$Y_{23} = \frac{\theta^{**}}{R^{**}} \left[\frac{1 - \cosh \theta^{**}}{\sinh \theta^{**}} \right]$$

$$Y_{24} = \frac{\theta^*}{R} \left[\frac{1 - \cosh \theta^*}{\sinh \theta^*} \right] - \frac{\theta^{**}}{R^{**}} \left[\frac{1 - \cosh \theta^{**}}{\sinh \theta^{**}} \right].$$

$$Y_{31} = Y_{13}$$

$$Y_{32} = Y_{23}$$

$$Y_{33} = \frac{\theta^{**}}{R^{**}} [\coth \theta^{**}] \quad (4.2c)$$

$$Y_{34} = \frac{\theta^{**}}{R^{**}} [-\operatorname{csch} \theta^{**}]$$

$$Y_{41} = Y_{14}$$

$$Y_{42} = Y_{24} \quad (4.2d)$$

$$Y_{43} = Y_{34}$$

$$Y_{44} = \frac{\theta^*}{R^*} [\coth \theta^*] + \frac{\theta^{**}}{R^{**}} [\coth \theta^{**}]$$

where

$$\theta^* = (1-N) \sqrt{j\omega RC}$$

$$\theta^{**} = N \sqrt{j\omega RC}$$

(4.3)

$$R^* = (1-N)R$$

$$R^{**} = NR$$

C. TRANSFER FUNCTIONS

1. Voltage and Current Transfer Ratios. The majority of $\overline{\text{TURC}}$ applications will involve the voltage transfer ratio since most signal sources may be represented as a voltage source in series with some impedance.

The typical application for the $\overline{\text{TURC}}$ is as a replacement for a lumped RC coupling network. Figure 4-2 illustrates the equivalent circuit for just such an application of the $\overline{\text{TURC}}$.

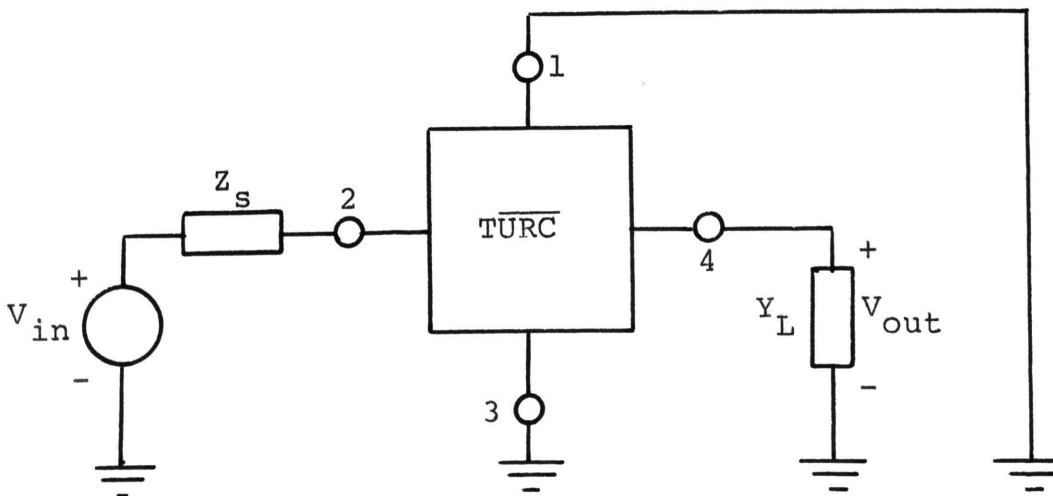


Figure 4-2. Equivalent circuit for a $\overline{\text{TURC}}$ used as an RC coupling network. The block represents Figure 4-1.

Z_s represents the source impedance and Y_L represents the input admittance of the amplifier stage to which the $\overline{\text{TURC}}$ is connected. Terminal 1 is connected to the supply voltage for the amplifier.

Writing a Node equation at terminal 2 gives

$$(V_2 - V_{in}) Y_s + Y_{22}V_2 + Y_{24}V_4 = 0. \quad (4.4)$$

Solving (4.4) for V_2 and letting $V_4 = V_{out}$,

$$V_2 = \frac{V_{in} Y_s}{Y_s + Y_{22}} - \frac{V_{out} Y_{24}}{Y_s + Y_{22}}. \quad (4.5)$$

A similar Node equation at terminal 4 (with $I_4 = -I_0 = -V_{out}Y_L$) gives, after some algebraic manipulation,

$$\frac{V_{out}}{V_{in}} = \frac{-Y_s Y_{42}}{(Y_L + Y_{44})(Y_s + Y_{22}) - Y_{42}Y_{24}}. \quad (4.6)$$

Equation (4.6) gives the desired voltage transfer ratio of the $\overline{\text{TURC}}$ as a function of both load admittance (Y_L) and source admittance (Y_s). If the situation arises where the signal source is represented by a current source and a current transfer ratio is therefore needed, the desired current transfer ratio is given by equation (4.7). The

$$\frac{I_{out}}{I_{in}} = \frac{-Y_L Y_{42}}{(Y_L + Y_{44})(Y_s + Y_{22}) - Y_{42}Y_{24}} \quad (4.7)$$

network, from which equation (4.7) was derived, is the same as Figure 4-2 except that the $V_{in} - Z_s$ combination is replaced by its Norton equivalent, an $I_{in} - Y_s$ combination.

2. Transfer Immittances. The immittance transfer ratios for the \overline{TURC} are obtained from equations (4.6) and (4.7). The admittance transfer ratio (Y_T) is found by multiplying equation (4.6) by the load admittance Y_L and noting that $I_0 = V_{out} Y_L$. The admittance transfer ratio then becomes

$$Y_T = \frac{I_0}{V_{in}} = \frac{-Y_s Y_L Y_{42}}{(Y_L + Y_{44})(Y_s + Y_{22}) - Y_{42} Y_{24}} \quad (4.8)$$

To obtain the impedance transfer ratio (Z_T), equation (4.7) is divided by Y_L . Noting that $V_{out} = I_{out}/Y_L$, equation (4.7) becomes

$$Z_T = \frac{V_{out}}{I_{in}} = \frac{-Y_{42}}{(Y_L + Y_{44})(Y_s + Y_{22}) - Y_{42} Y_{24}} \quad (4.9)$$

Therefore, the desired immittance transfer ratios are given by equations (4.8) and (4.9).

D. CAPACITANCE DETERMINATION

The problem of determining the value of the distributed capacitance for a $\overline{\text{TURC}}$ is as acute as it is for both the $\overline{\text{DRURC}}$ and the $\overline{\text{TDRURC}}$.

As in Chapter II, Section C, the capacitance can be determined by connecting the $\overline{\text{TURC}}$ such that it acts as a notch filter. The connection of a lumped resistor between terminal 2 and ground of the $\overline{\text{TURC}}$ in Figure 4-1 yields Figure 4-3 which acts as a passive notch filter. Terminal 4 is left open circuited.

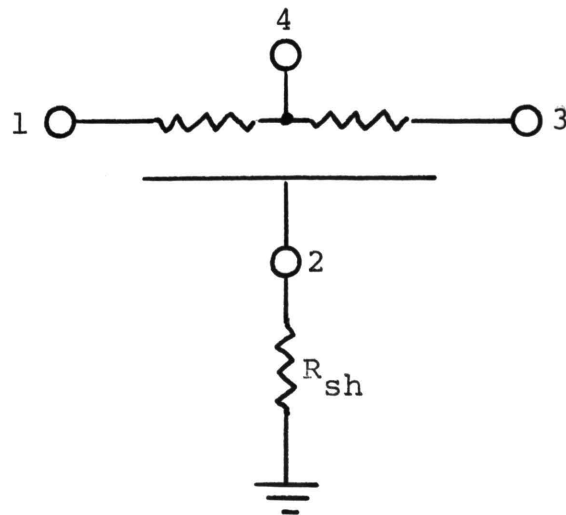


Figure 4-3. $\overline{\text{TURC}}$ connected as a passive notch filter.

The voltage transfer ratio $\frac{V_3}{V_1}$ for the network in Figure 4-3 is [12]

$$\frac{V_3}{V_1} = \frac{\alpha + u \sinh u}{\alpha \cosh u + u \sinh u} \quad (4.10)$$

where $\alpha = \frac{R}{R_{sh}}$ and $u = \sqrt{\frac{\omega}{\omega_0}} (1+j)$ and $\omega_0 = \frac{2}{RC}$.

A transmission null occurs for $\frac{\omega}{\omega_0}$ such that $\alpha + u \sinh u = 0$. The frequency at which a null occurs is found to be $\frac{\omega}{\omega_0} = 5.62$, or $\omega = 5.62 \omega_0$. In terms of the total resistance and capacitance of the \overline{TURC} , the null occurs at [12]

$$\omega \approx \frac{11.20}{RC} . \quad (4.11)$$

The value of C at such a frequency becomes

$$C = \frac{11.2}{2\pi f R} \quad (4.12)$$

for $\alpha = 17.8$.

The notch, for $\alpha = 17.8$, is quite narrow [12] (typically $0.01 \frac{\omega}{\omega_0}$) and deep (typically about -60 db) and is, therefore, quite easy to measure. Examples of this, and for the \overline{DRURC} as well, are shown in Chapter VI.

V. APPLICATIONS

A. INTRODUCTION

Now that the expressions for the transfer ratios have been developed for the \overline{DRURC} , \overline{TDRURC} , and \overline{TURC} , four general areas of application are discussed. In section B on logic and switching circuits, applications of the \overline{DRURC} to multivibrator design are discussed. Section C is concerned with the application of \overline{URC} , \overline{TURC} , \overline{DRURC} , and \overline{TDRURC} networks to amplifier design. The main thrust here is to replace the lumped RC networks with one of the four distributed RC networks listed above. Sections D and E discuss the application of the \overline{DRURC} to oscillator design and bandpass filter design, respectively.

B. LOGIC AND SWITCHING CIRCUITS

A monostable multivibrator using a \overline{DRURC} is shown in Figure 5-1. As can be seen by comparison with a lumped RC version [20, p. 370], the \overline{DRURC} replaces the collector resistor of Q_1 , the coupling capacitor and the base resistor for Q_2 . The pulse duration for the circuit of Figure 5-1 is found to be [16]

$$t = 0.197\tau \quad (5.1)$$

where

$$\tau = (1+N)RC. \quad (5.2)$$

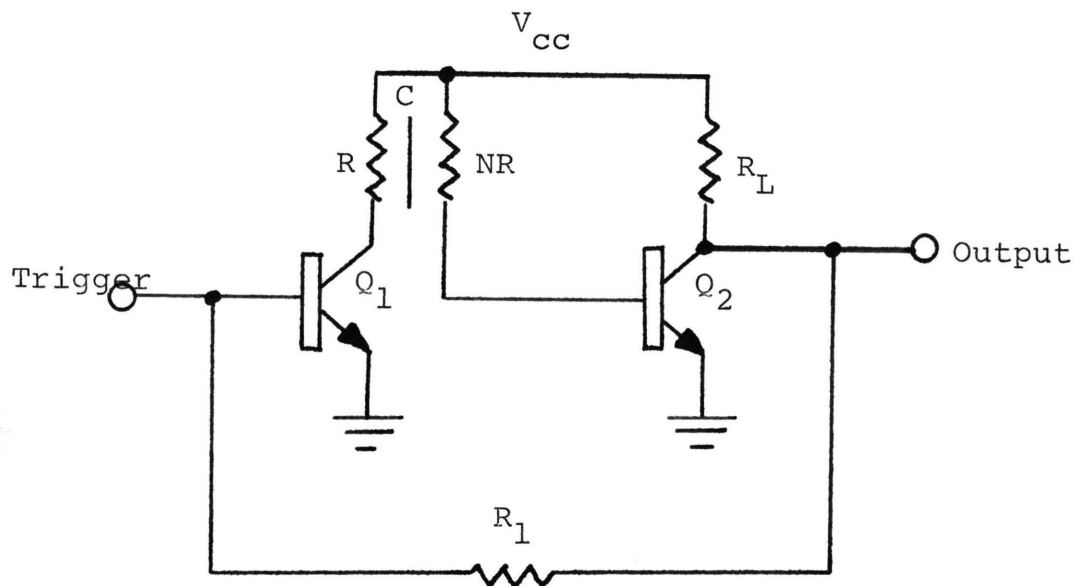


Figure 5-1. Monostable multivibrator using a DRURC.

These equations are derived using the assumption that $V_{CC} \gg V_{CESAT} \approx 0$ and $V_{BE} \approx 0$. Equation (5.2) may be compared to a similar pulse-duration equation for the lumped-RC version shown in equation (5.3). The comparison for a given pulse duration of $t=250\mu$ seconds and an $R=5$ k ohms

$$t = 0.69\tau \quad (5.3)$$

where

$$\tau = RC \quad (5.4)$$

yields (from equations (5.1) and (5.2)) a capacitance of 0.0231μ Farads for a $\overline{\text{DRURC}}$ ($N = 10$). A similar calculation for a lumped version, using equations (5.3) and (5.4), yields a capacitance value of 0.00725μ Farads. Therefore, although a reduction in size of the total network results from the use of a $\overline{\text{DRURC}}$, an increase in the needed capacitance occurs. As can be seen, the increase in capacitance is on the order of 3.2. Since large distributed network capacitance is difficult to obtain, this then is one disadvantage to the use of distributed networks in the design of logic and switching circuits.

An astable multivibrator using two $\overline{\text{DRURC}}$'s has also been proposed by Hayes [16]. This multivibrator uses $\overline{\text{DRURC}}$'s to replace all of the lumped RC combinations. In particular, each $\overline{\text{DRURC}}$ replaces the collector resistor of one transistor, the coupling capacitor between the two transistors, as well as the base bias resistor of the other transistor. Figure 5-2 shows an astable multivibrator with $\overline{\text{DRURC}}$'s replacing the lumped RC components. A lumped RC version of Figure 5-2 is found in reference [20], page 385.

The expression governing the period of the output waveform is an extension of the analysis done for the monostable circuit. Q_1 , and the associated $\overline{\text{DRURC}}$, as well as Q_2 and the associated $\overline{\text{DRURC}}$, may each be considered as a monostable multivibrator. Adding the expressions for pulse duration

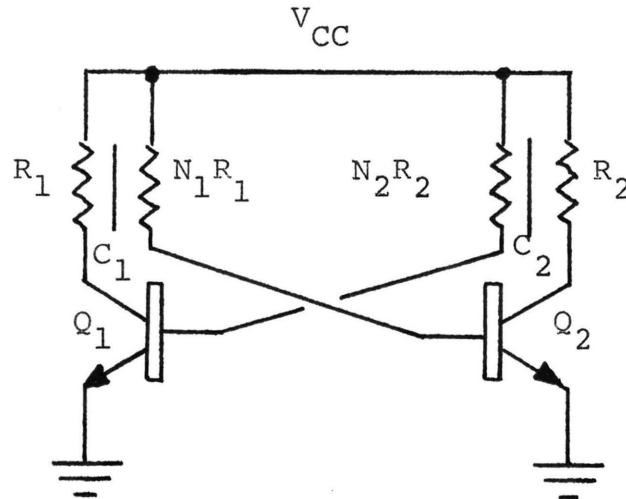


Figure 5-2. Astable multivibrator utilizing DRURC's.

(see equations (5.1) and (5.2)) for each yields

$$T = 0.197 [C_1(1+N_1)R_1 + C_2(1+N_2)R_2] \quad (5.5)$$

where T is the period of the output waveform.

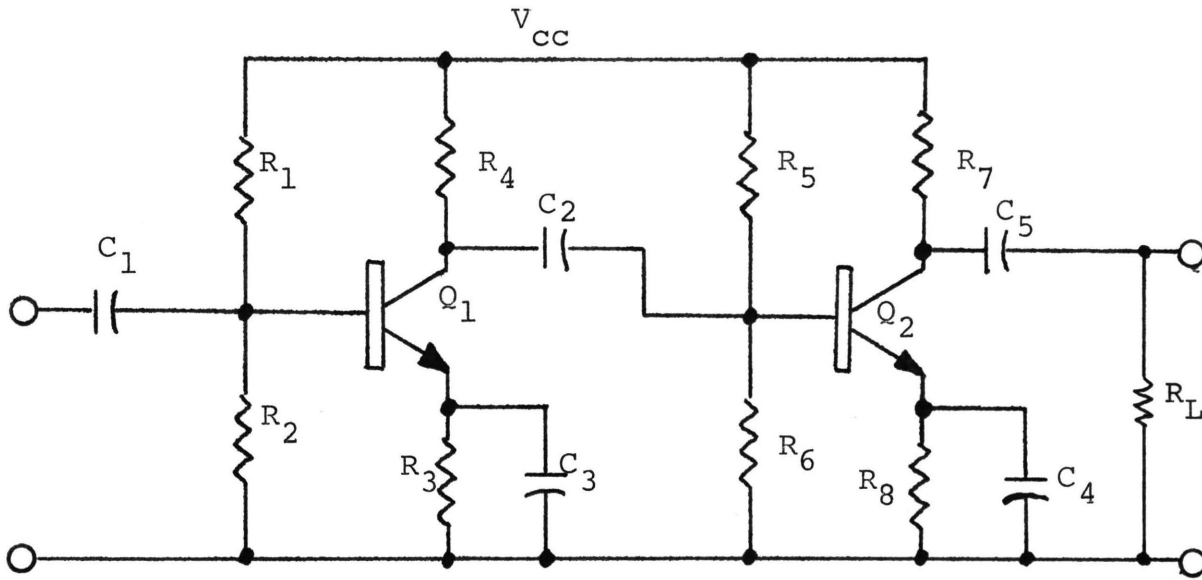
The ratio of "on" time to "off" time for the pulse train may be adjusted by varying the component values in equation (5.5). The analysis is based on having the transistors in saturation during the "on" time and completely cut off during the "off" time. In other words, the time needed by the transistor to go from cut off to saturation, and vice versa, is neglected.

C. RC COUPLED AMPLIFIERS

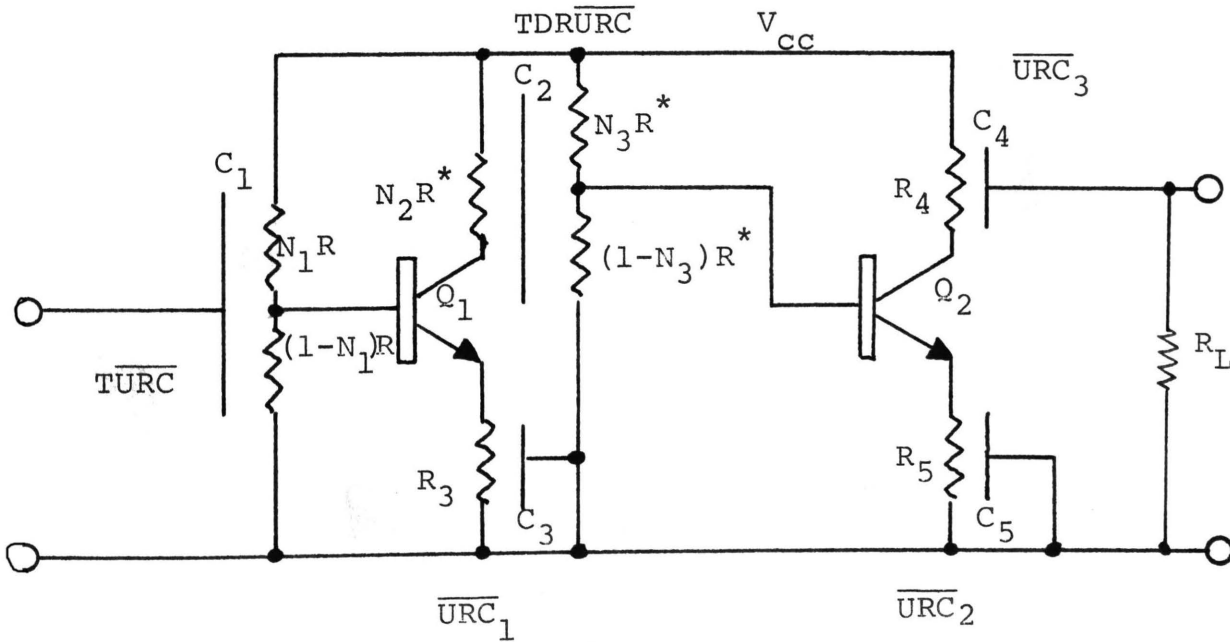
1. Coupling Networks.

a. Introduction. Theoretically, distributed RC networks can be used to replace all the lumped RC network combinations in an RC-coupled amplifier. As inspection of Figure 5-3(b) shows, the input coupling capacitor as well as the base biasing resistors for Q_1 may be replaced by a single \overline{TURC} . The collector resistor of Q_1 , the coupling capacitor between Q_1 and Q_2 , and the base biasing resistors for Q_2 may be replaced by a single $TDR\overline{URC}$. A single \overline{URC} may be used to replace the collector resistor of Q_2 as well as the output coupling capacitor. Each of these distributed networks exhibits more attenuation than does the lumped RC combination it replaces; this attenuation is overcome by increasing the gain of the appropriate stage.

b. \overline{TURC} . (1) Driving-Point Admittances. The frequency response of the coupling network is covered in the next subsection; here the driving point immittances are discussed. The AC equivalent circuit of the \overline{TURC} with source and load immittances connected is shown in Figures 5-4 (a) and (b). Figure 5-4 is similar to Figure 4-2, and the block in Figure 4-2 may be used in place of the \overline{TURC} in Figure 5-4. The terminal numbering in Figure 5-4 is arranged to match that of Figure 4-1.



(a)



(b)

Figure 5-3. (a) Lumped version of a two-stage, RC coupled, bipolar amplifier.
 (b) Distributed RC version of (a).

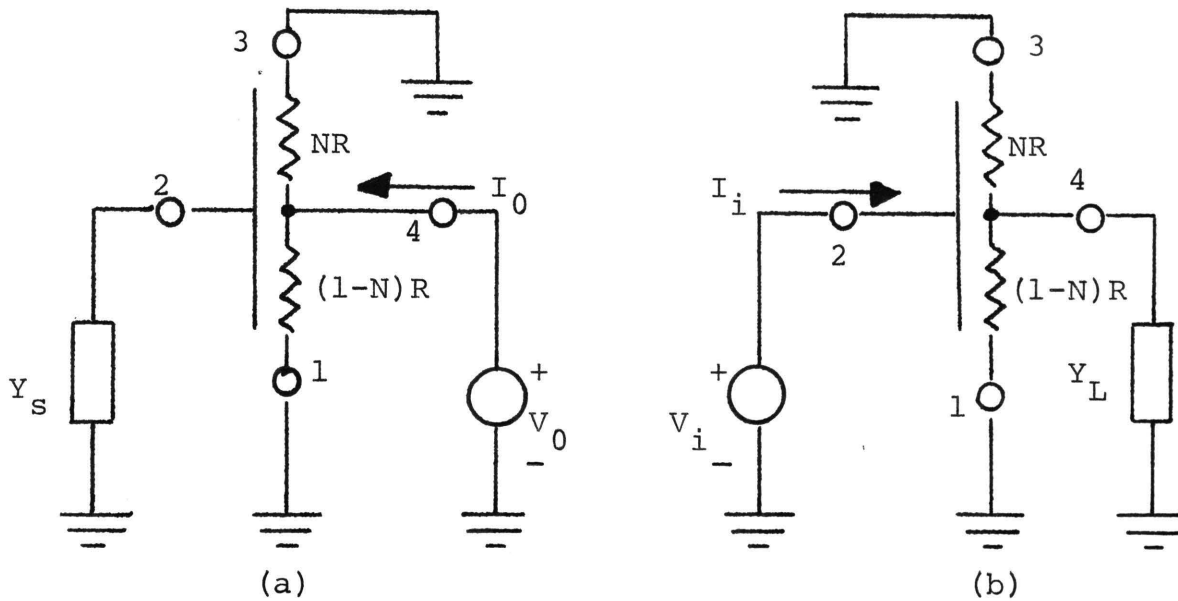


Figure 5-4. $\overline{\text{TÜRĈ}}$ set up for (a) output and (b) input driving-point admittance calculations.

Letting $Y_0 = \frac{I_0}{V_0}$, and applying routine network analysis to Figure 5-4(a), yields

$$Y_0 = \frac{I_0}{V_0} = \frac{I_4}{V_4} = Y_{44} - \frac{Y_{24} Y_{42}}{Y_S + Y_{22}}. \quad (5.6a)$$

The Y_{ij} are those of the $\overline{\text{TÜRĈ}}$ and are given in terms of the elements of the Y_{ij} for a $\overline{\text{URĈ}}$ by equations (4.2). A similar analysis of Figure 5-4(b) shows the input admittance, Y_i , to be

$$Y_i = Y_{22} - \frac{Y_{24} Y_{42}}{Y_L + Y_{44}}. \quad (5.6b)$$

It is tempting to try to reduce the complexity of equations (5.6) by assuming that the magnitude of Y_S is much less than

the magnitude of Y_{22} and the magnitude of Y_L is much less than the magnitude of Y_{44} . However, inspection of equations (4.2) shows that the calculation of the Y_{ij} magnitudes is a formidable task that is best carried out on the computer. Additionally, the concern here is to provide some guide to design of the $\overline{\text{TURC}}$ for application as an input coupling network irrespective of the magnitudes of Y_s or Y_L .

In most applications, R_1 is related to R_2 by $R_1 = kR_2$ (see Figure 5-3(a)) and, therefore, $N_1R = k(1-N_1)R$ for the $\overline{\text{TURC}}$. The above relationship yields

$$N_1 = \frac{k}{k+1}, \quad k > 1. \quad (5.7)$$

Of course, N_1 and R are chosen so as to meet the bias requirements of Q_1 . These requirements on N_1 and R are met using standard design techniques for bipolar transistor bias networks [10].

(2) Frequency Response. As is seen in Figure 5-5, the frequency response for the $\overline{\text{TURC}}$ of Figure 4-2, used as shown in Figure 5-3 (b), compares favorably to that of a lumped RC input coupling network for $\phi < 1360$. This response curve is obtained by plotting the magnitude of equation (4.6) versus ϕ ($\phi = \omega RC$). The 3-db ($0.707 A_{v_{\max}}$) points occur at $\phi = 9.2$ and 1360. Unfortunately the frequency response curve begins to drop off and approaches

zero as ϕ is increased. The "flat" region is, however, broad enough to allow application as a replacement for the RC lumped version in some medium bandwidth applications.

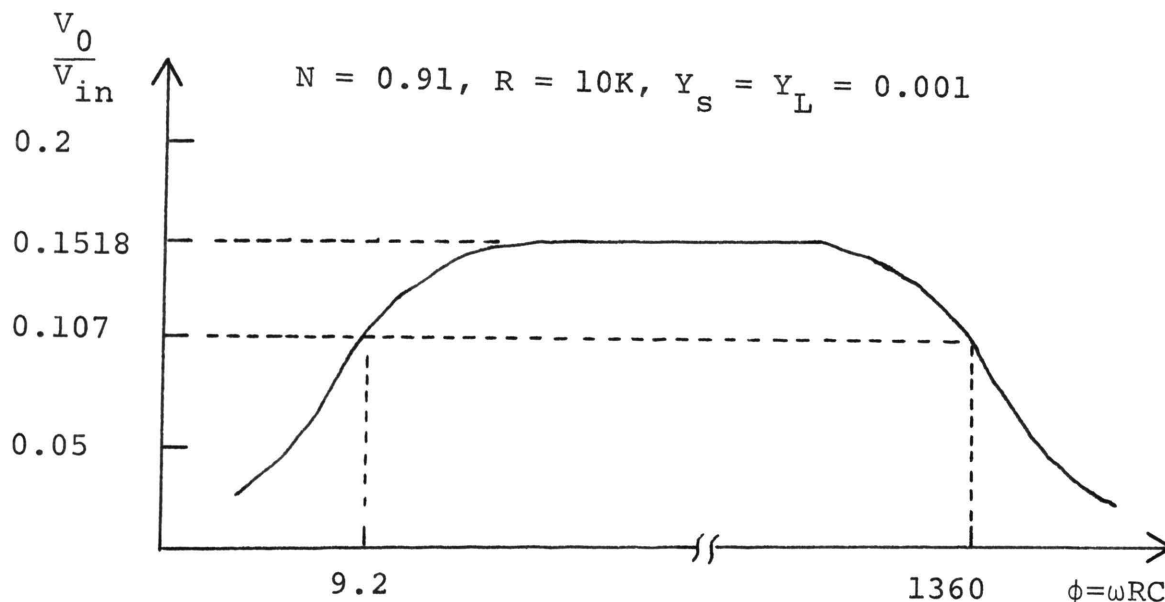


Figure 5-5. Frequency response of a \overline{TURC} used as an input coupling network.

The fact that the voltage transfer ratio of the \overline{TURC} does go to zero is explained by the distributed capacitance. Inspection of Figure 5-3(b) shows that, since C is distributed along the total resistive length, there will be some value of ϕ for which the signal source is presented with an impedance, the magnitude of which approaches zero as ϕ approaches infinity. From a mathematical point of view, the transfer function, equation (4.6), is seen to approach zero as ϕ approaches infinity (see Appendix E). Since $\phi = \frac{\omega}{\omega_0} = \omega RC$, the upper and lower 3-db frequencies then become

$$\omega_{3db} = \frac{\phi_{3db}}{RC}. \quad (5.8)$$

The resistance R and the number N are determined by the bias requirements of the transistor used; the capacitance of C determines the 3-db frequencies.

Therefore, solving equation (5.8) for C,

$$C = \frac{\phi_{3db}}{R \omega_{3db}} = \frac{\phi_{3db}}{2\pi R f_{3db}}. \quad (5.9a)$$

For the values used in Figure 5-5, C becomes (for $\phi_{3db}=9.2$)

$$C = \frac{1.46}{f_{3db}} \times 10^{-4} \text{ Farads}. \quad (5.9b)$$

The lumped RC version coupling capacitor value is

$$C = \frac{1}{2\pi(R_s + R_B) f_{3db}} \quad (5.10a)$$

where R_s = source resistance and R_B = parallel combination of R_1 and R_2 in Figure 5-3(a). Assuming $R_s = 1$ k ohms and $R_B = 820$ ohms,

$$C = \frac{8.74}{f_{3db}} \times 10^{-5} \text{ Farads}. \quad (5.10b)$$

Unfortunately, a single expression appropriate for all values of N, R and C is extremely difficult to obtain, and,

as a result, equation (5.9) is good only for those values used. In designing the $\overline{\text{TURC}}$, a computer program would be used to determine the magnitude of equation (4.6) versus ϕ for a given value of N and R. From this tabulated data, the value of $\phi_{3\text{db}}$ is determined. Once the $\phi_{3\text{db}}$ value is obtained, it is substituted into equation (5.11) to determine the needed value of C.

$$C = \frac{\phi_{3\text{db}}}{2\pi R f_{3\text{db}}} . \quad (5.11)$$

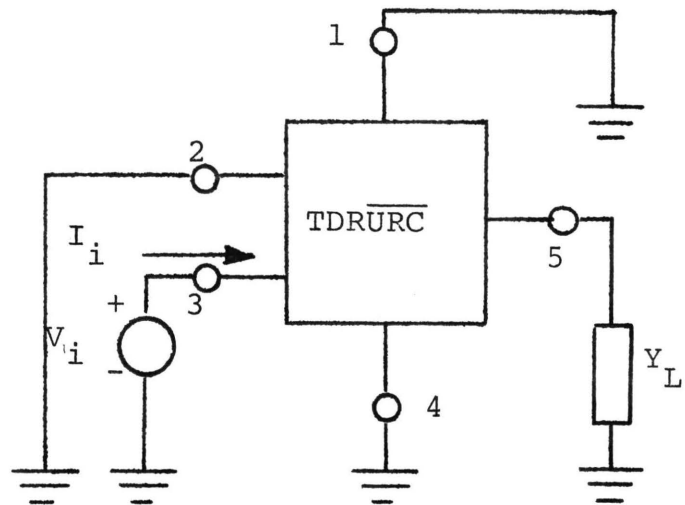
c. $\overline{\text{TDRURC}}$. (1) Driving-Point Admittances. The $\overline{\text{TDRURC}}$ in block form is shown in Figures 5-6(a) and (b) arranged for input and output admittance calculations. Routine analysis using the elements of the IAM for a $\overline{\text{TDRURC}}$ (see matrix of (3.1)) yields the input and output admittances

$$Y_i = Y_{33} - \frac{Y_{35} Y_{53}}{Y_L + Y_{55}} \quad (5.12a)$$

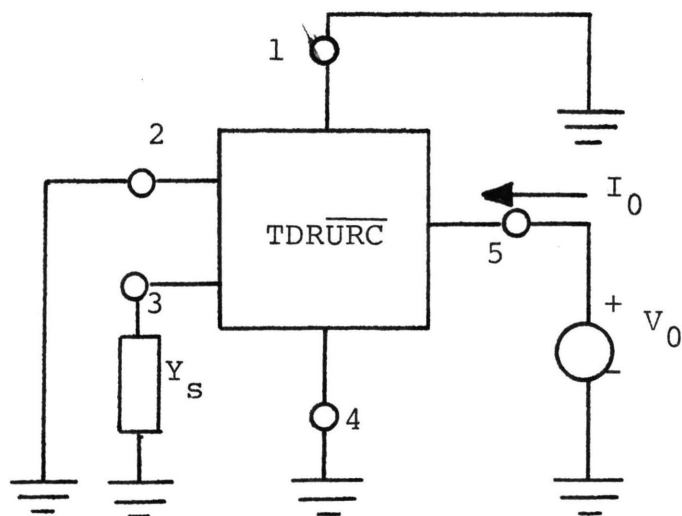
and

$$Y_o = Y_{55} - \frac{Y_{35} Y_{53}}{Y_s + Y_{33}} . \quad (5.12b)$$

As before in equations (5.6) it is extremely difficult



(a)



(b)

Figure 5-6. $\overline{\text{TDRURC}}$ connected for calculations of (a) input admittance and (b) output admittance.

to determine the relative magnitudes of Y_{55} and Y_{33} such that Y_L and Y_S may be ignored. Examination of equations (3.2) shows that determination of the magnitudes of Y_{55} and Y_{33} is even more difficult than for Y_{22} and Y_{44} of the $\overline{\text{TURC}}$. A program exists for the calculation of the numerical values of Y_{55} and Y_{33} ; this program is listed in Appendix D.

(2) Frequency Response. The frequency response for a $\overline{\text{TDRURC}}$ used as an interstage coupling network is very similar in shape to that of a lumped network. The difficulty with design lies in the fact that the resistance layers of the $\overline{\text{TDRURC}}$ are connected to two different transistors. If R^* is changed, the value of N_2 (refer to Figure 5-3) must be changed to account for the needed value of collector resistance on the previous amplifier. The value of N_3 is approximately the same as the value of N_1 for the $\overline{\text{TURC}}$. This leaves two variables, N_2 and N_3 , that need to be chosen to accommodate the design of the output network of Q_1 and the bias network of Q_2 .

The expression that will be used in Chapter VI is the ratio of the base current of Q_2 to the collector current of Q_1 . This ratio is the same as that found in Chapter III in connection with Figure 3-9, equation (3.13) and is repeated below as equation (5.13).

$$\frac{I_0}{I_i} = \frac{-Y_{53}Y_L}{(Y_L+Y_{55})(Y_S+Y_{33}) - Y_{53}Y_{35}} \quad (5.13)$$

Accordingly, each design necessitates the use of a computer to generate data needed for a plot similar to that of Figure G-2, Appendix G.

The values for the N's can be calculated from a knowledge of the resistance needed to properly bias the transistors. For example, in Figure 5-3(a), assume $R_4 = 5 \text{ k ohms}$ and $R_5 + R_6 = 100 \text{ k ohms}$. Therefore, $N_2 R^* = 5 \text{ k ohms}$ and $N_3 R^* + (1-N_3)R^* = R^* = 100 \text{ k ohms}$ and

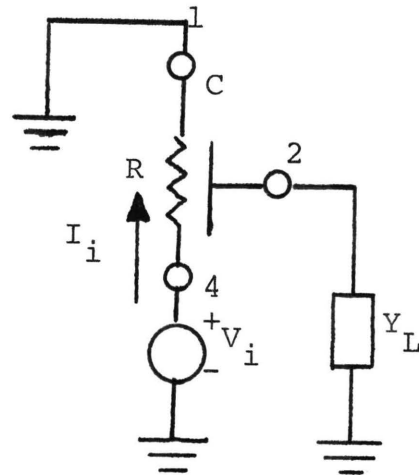
$$N_2 = \frac{5 \text{ k}}{100 \text{ k}} = 0.05. \quad (5.14)$$

N_3 is assumed to have the same value as N_1 of the $\overline{\text{TURC}}$ if Q_1 and Q_2 are identical. The $\phi_{3\text{db}}$ values for the $\overline{\text{TDRURC}}$ can be obtained from a plot of the magnitude of equation (5.13) versus ϕ ($\phi = \omega(1+N)RC$). An example of such a plot is shown in Figure G-2 of Appendix G.

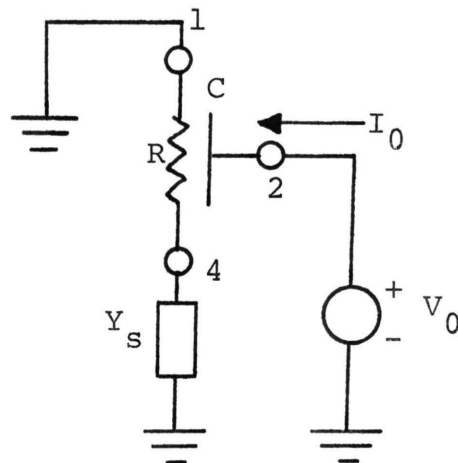
d. $\overline{\text{URC}}$. (1) Driving-Point Admittances. For the $\overline{\text{URC}}$ used as the last coupling network, the driving-point admittances may be found using Figures 5-7(a) and (b). Writing a node equation at terminal 2 of Figure 5-7(a) and solving for V_2 yields

$$V_2 = - \frac{Y_{24} V_i}{Y_L + Y_{22}}. \quad (5.15)$$

Equation (5.15) substituted into a node equation at terminal



(a)



(b)

Figure 5-7. \overline{URC} connected for calculation of (a) Y_i and (b) Y_0 .

4 gives

$$Y_i = Y_{44} - \frac{Y_{24}Y_{42}}{Y_L + Y_{22}}. \quad (5.16)$$

A similar approach applied to Figure 5-7(b) gives the desired output admittance Y_0 .

$$Y_0 = Y_{22} - \frac{Y_{42}Y_{24}}{Y_s + Y_{44}}. \quad (5.17)$$

(2) Frequency Response. The output coupling network for the amplifier of Figure 5-3(b) is a \overline{URC} . The expression for the voltage transfer ratio of a \overline{URC} can be found by straightforward analysis of a network similar to that of Figure 5-7(a). The difference is that the output immittance of the transistor driving the \overline{URC} (Q_2 of Figure 5-3(b)) must be taken into account.

Taking into account the output admittance of Q_2 (represented below by Y_s), analysis of Figure 5-7(a) yields

$$V_2 = \frac{-Y_{24}V_4}{Y_{22} + Y_L}. \quad (5.18a)$$

This, combined with a similar expression for V_4 ,

$$V_4 = \frac{V_i Y_s - Y_{42} V_2}{Y_s + Y_{44}} \quad (5.18b)$$

gives the desired voltage transfer ratio (let $V_2 = V_0$) as

$$\frac{V_0}{V_i} = \frac{Y_{24}Y_s}{Y_{24}Y_{42} - (Y_{22}+Y_L)(Y_{44}+Y_s)}. \quad (5.19)$$

The Y_{ij} terms are found in the matrix (2.18).

This network, like the $\overline{\text{TDRURC}}$, has several variables that must be specified before a design can be undertaken; the R of the $\overline{\text{URC}}$, the output admittance of the transistor, and the load admittance must be given.

2. By-pass Networks

a. Introduction. The $\overline{\text{URC}}$, connected as shown in Figure 1-3(b), can be used to replace the lumped RC emitter by-pass network shown in Figure 1-3(a) [25,28]. Figure 1-3(b) is repeated as Figure 5-8 for reference.

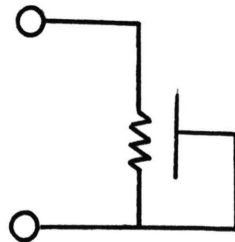


Figure 5-8. $\overline{\text{URC}}$ used as a replacement for a lumped RC emitter (or source) by-pass network.

b. Frequency Response. Analysis of the response of the $\overline{\text{URC}}$ shown in Figure 5-8 utilizes equation (4.2). Routine analysis, similar to that performed on the previous distributed networks yields the following expression [25].

$$\left| \frac{z_{in}}{R} \right| = \frac{1}{\sqrt{\phi}} \frac{\cosh \sqrt{2\phi} - \cos \sqrt{2\phi}}{\cosh \sqrt{2\phi} + \cos \sqrt{2\phi}} \frac{1}{2} \quad (5.20)$$

The value of ϕ that causes the numerical value of equation (5.20) to become 0.707 is found to be $\phi = 2.61$. This value of ϕ is confirmed by writing a program to plot equation (5.20) versus ϕ in tabular form and by substituting $\phi = 2.61$ into equation (5.20). Lin [25] has found the value to be $\phi = 2.0$ but is in error.

$$\phi = \omega RC = 2.61. \quad (5.21)$$

Or, solving for the capacitance,

$$C = \frac{2.61}{2\pi f R}, \quad (5.22a)$$

where f is the desired 3-db frequency for the by-pass network, and R is the resistance of the resistive layer. The capacitance needed for the lumped RC version is

$$C = \frac{1}{2\pi f R}. \quad (5.22b)$$

3. Summary. The distributed RC network, although attractive for use in an RC-coupled amplifier, has several drawbacks. Calculation of the values for the needed capacitances must be carried out with the aid of graphs derived from computer-generated data. These capacitances, for the audio frequency range, are larger than those presently available. In addition, the bandwidth of the

amplifier using these distributed networks is narrower than that of a lumped RC version.

D. OSCILLATORS

1. Introduction. Several oscillators utilizing distributed networks have been discussed [25,28]. The oscillator discussed here is different in that it uses the \overline{DRURC} to replace some of the network elements in the gain block thereby reducing the number of components needed to build the gain block. This oscillator is still basically a feedback amplifier with the \overline{DRURC} providing the feedback (see Figure 5-9).

As with all phase-shift oscillators, the feedback network is used to provide the proper amount of feedback such that the total phase shift around the closed loop is some multiple of 360° . In this manner, a feedback amplifier can be made to oscillate at a given frequency provided the open loop gain at that frequency is high enough to overcome the losses through the feedback network.

2. Analysis. The \overline{DRURC} phase-shift oscillator, using a current-controlled voltage-source (ICVS), is shown in Figure 5-10. Due to the low input impedance of the ICVS, terminal 2 is at ground potential while terminals 1 and 3 are connected to the common side of the ICVS. Routine analysis of the \overline{DRURC} feedback network yields the transfer admittance

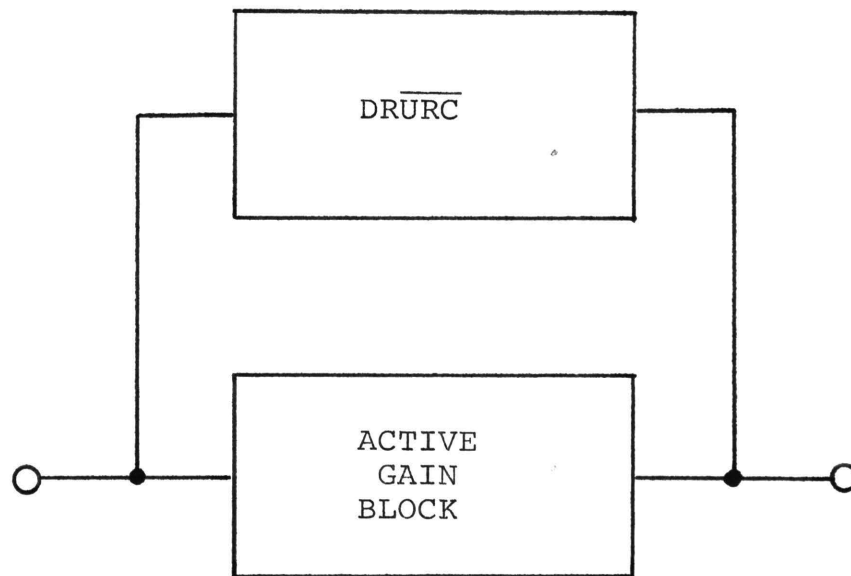


Figure 5-9. Feedback amplifier using a \overline{DRURC} as the feedback network.

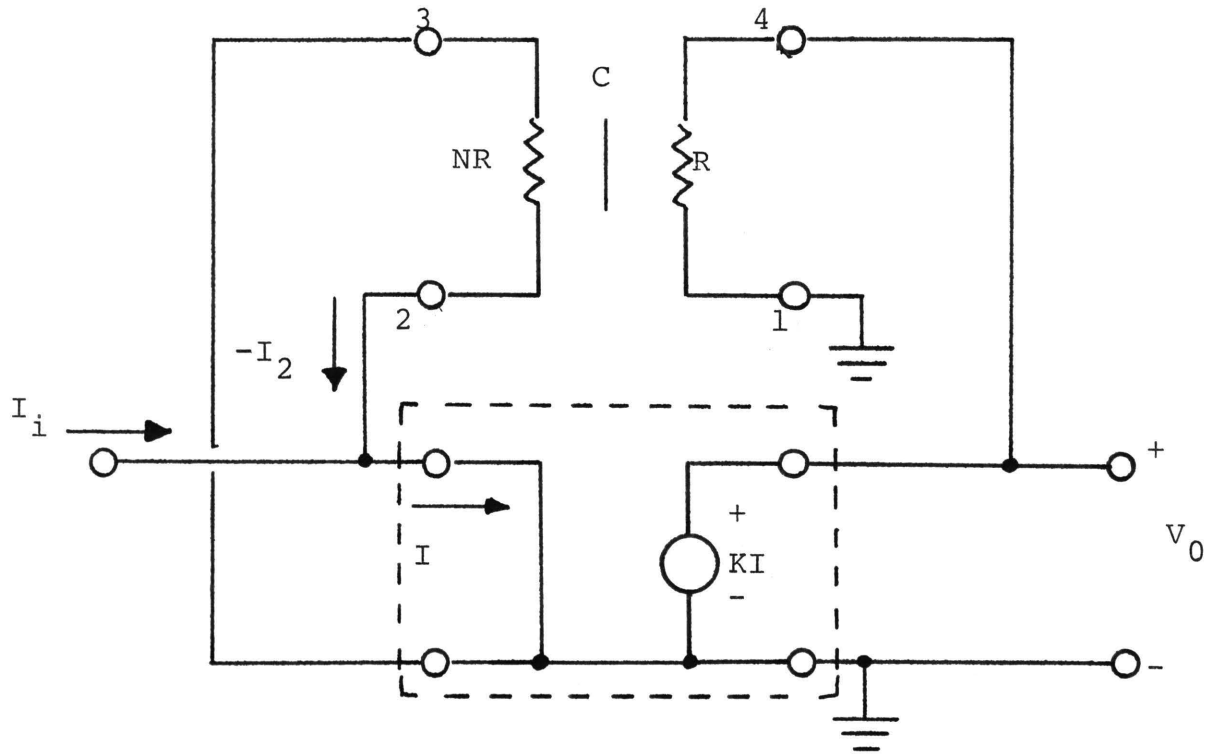


figure 5-10. \overline{DRURC} phase shift oscillator using a ICVS as a gain block.

$$-\frac{I_2}{V_4} = -Y_{24} = -\frac{1}{(1+N)R} \left[\frac{\Gamma}{\sinh \Gamma} - 1 \right]. \quad (5.23)$$

Using $e^\Gamma = W$ [31], equation (5.23) can be written as

$$-\frac{I_2}{V_4} = -\frac{1}{(1+N)R} \left[\frac{2W\Gamma - W^2 + 1}{W^2 - 1} \right]. \quad (5.24)$$

The closed loop gain $\frac{V_0}{I_i}$ of Figure 5-10 may be derived as shown below

$$I = I_i - I_2 \quad (5.25)$$

$$V_0 = KI = K(I_i - I_2). \quad (5.26)$$

Substituting $-I_2$ from equation (5.23), and noting that $V_4 = V_0$, yields

$$\frac{V_0}{I_i} = \frac{K}{1 + K Y_{24}}. \quad (5.27)$$

For oscillations to occur, $1 + K Y_{24}$ must equal zero, or

$$K^* \left[\frac{2W\Gamma - W^2 + 1}{W^2 - 1} \right] = -1 \quad (5.28)$$

here

$$K^* = \frac{K}{(1+N)R} \quad (5.29)$$

and K = transfer impedance magnitude of the ICVS.

Rewriting equation (5.28) so as to put it in the form

$$\frac{G_1(\Gamma)}{G_2(\Gamma)} \frac{H_1(W)}{H_2(W)} = -1, \quad (5.30a)$$

gives

$$\frac{2K^*}{1-K^*} \frac{\Gamma W}{W^2 - 1} = -1. \quad (5.30b)$$

From equation (5.30b) it is seen that

$$\left| \frac{2K^*}{1-K^*} \right| \cdot \left| \Gamma \right| \cdot \left| \frac{W}{W^2 - 1} \right| = 1 \quad (5.31)$$

and

$$\angle \Gamma + \angle \frac{W}{W^2 - 1} = \pm (2n-1)(180^\circ) \quad (5.32)$$

for $n = 1, 2, 3, \dots$

Therefore, a root-locus approach [31] may be used to determine the characteristics of Figure 5-10 such that the needed gain and the frequency of oscillation are obtained. This method is the same as the root-locus constructed in one plane, except that it is constructed in two planes: the Γ plane and the W plane.

The poles and zeros of equation (5.30b) are shown in Figure 5-11. The procedure is one of picking a test point

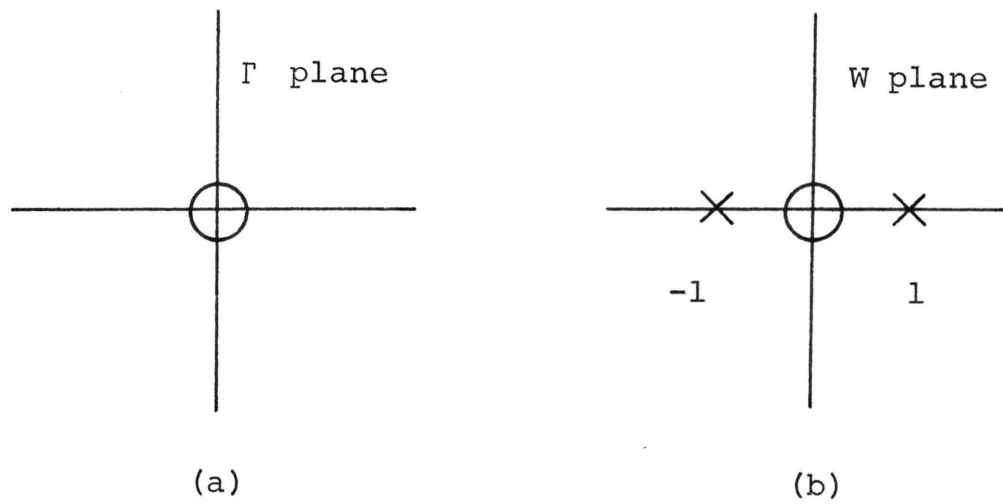


Figure 5-11. Pole-zero diagram for (a) $\frac{G_1}{G_2}$ and
 (b) $\frac{H_1}{H_2}$ from equations (5.30).

Γ_t and mapping this test point into a test point in the W plane, W_t , by using

$$W_t = e^{\Gamma_t}. \quad (5.33)$$

An angle measurement is made in the Γ plane on the Γ_t test point and in the W plane on the W_t test point. If these measurements satisfy equation (5.32), a point on the root locus has been found.

For analysis of oscillators the procedure is greatly simplified because the point desired is a point on the boundary of the stability region of the Γ plane. This boundary is a radial line that makes a $\pm 45^\circ$ angle with the positive real axis of the Γ plane. In this case the procedure is simplified because the angle in the Γ plane will always be 45° for points along the 45° radial line.

The test point $\Gamma_t = 3.92 + j 3.92$ yields a $W_t = 50.2 \angle 225^\circ$. The angle measurements satisfy equation (5.32). The magnitude criterion, equation (5.31), is satisfied by substituting into it the magnitudes from the Γ and W planes. The magnitude from the Γ plane is found to be $3.92 \sqrt{2}$ or 5.55, and that from the W plane is 1.99×10^{-2} . These values substituted into equation (5.31) give

$$\left| \frac{2K^*}{1-K^*} \right| = \frac{1}{(5.55)(1.99 \times 10^{-2})} = 9.05. \quad (5.34)$$

From equations (5.34) and (5.29) the value of K for the ICVS is found to be

$$K = 0.82(1+N)R. \quad (5.35)$$

Also, since $\Gamma = \sqrt{j\omega(1+N)RC} = 3.92(1+j)$, the frequency of oscillation is given by

$$f = \frac{30.75}{2\pi(1+N)RC}. \quad (5.36)$$

Castro, et al. [28] obtained an expression similar to equation (5.36) for a notch network; however, their distributed network is basically a low-pass configuration whereas the distributed network shown in Figure 5-10 is basically a high-pass configuration.

A practical realization of the ICVS used in Figure 5-10 is shown in Figure 5-12 [32]. The needed low input impedance is provided by the forward biased base-emitter junction of Q_1 and the needed low output impedance by the emitter-follower configuration of Q_2 . The transfer impedance of the ICVS is

$$K = \frac{V_0}{I_i} \cong h_{fb_1} R. \quad (5.37)$$

Figure 5-13 shows an exceptionally simple oscillator.

Proper choices of geometry and process parameters will allow Figure 5-12 to have a transfer impedance given by equation (5.37) and suitable for use in Figure 5-13. Example values for V_1 , V_2 , R_1 , R_2 , C , and N for Figure 5-13 are shown in Chapter VI, Section E. Figure 5-13 could easily be integrated using standard solid-state fabrication techniques. This would allow an extremely simple oscillator to be fabricated on a chip using minimum space.

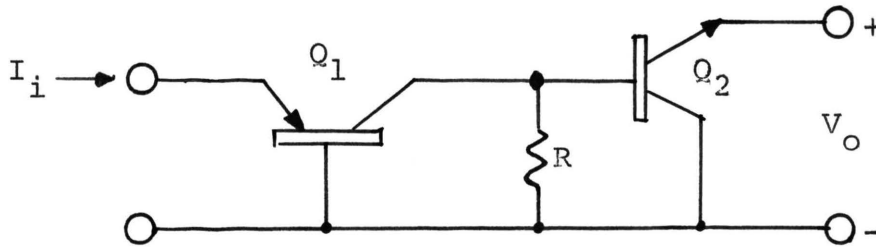


Figure 5-12. Transistor realization of an ICVS.

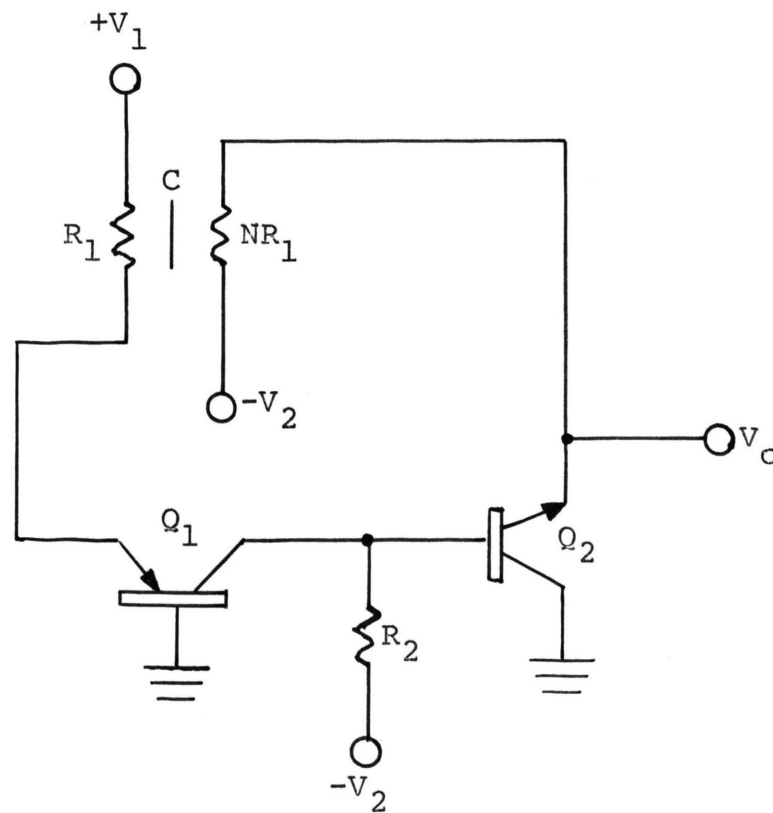


Figure 5-13. Transistor-DRURC phase-shift oscillator suitable for integration.

E. FILTERS

1. Passive Band-Reject. A passive band-reject filter [28] (notch filter) can be made from a \overline{DRURC} . The configuration and analysis are the same as that of the network used to determine the capacitance of a \overline{DRURC} , Figure 2-6. The frequency of the notch is given by equation (2.29) which is repeated in equation (5.38) for reference. The best range

$$f = \frac{19.75}{2\pi(1+N)RC} \quad (5.38)$$

for N is 0.05 to 0.5. Outside of these limits, N is such that the notch depth and width are too shallow and too wide, respectively, to provide the response needed for a good notch filter. As shown in equation (2.32), $N = 0.08627$ gives a true zero of transmission at the frequency given by equation (5.38). At $N = 0.05$, the attenuation and bandwidth are 30db and $\Delta\phi = 2$, while at $N = 0.5$, the attenuation and bandwidth are approximately 10db and $\Delta\phi = 10$.

There are not nearly as many applications for passive notch filters as for active bandpass filters, but the active bandpass filter described in the next section uses the passive notch filter to obtain a bandpass characteristic.

2. Active Bandpass. An active bandpass filter [28] using a \overline{DRURC} and a high gain operational amplifier is shown in Figure 5-14. The operational amplifier is assumed to have

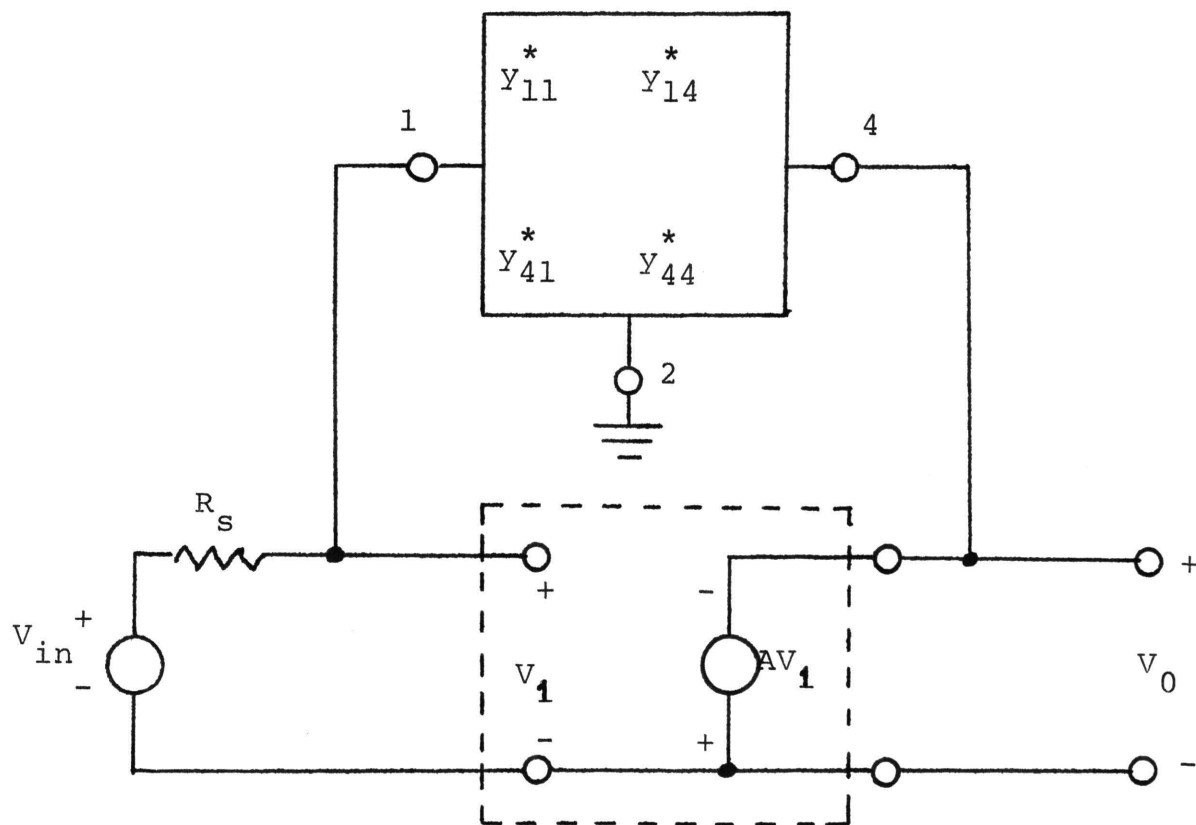


Figure 5-14. Active bandpass filter using a \overline{DRURC} and an ideal operational amplifier. The \overline{DRURC} is oriented as shown in Figure 2-6.

characteristics that approximate the ideal case. Writing a node equation for V_1 and solving yields

$$V_1 = \frac{V_{in}}{1 + y_{11}^* R_s - Ay_{14}^* R_s} \quad (5.39)$$

Noting that $V_0 = -AV_1$ gives [44]

$$\frac{V_0}{V_{in}} = \frac{-A}{1 + y_{11}^* R_s - Ay_{14}^* R_s} \quad (5.40)$$

The problem of obtaining an expression for Q (or bandwidth) has yet to be solved. However, by inspecting plots of the magnitude of equation (5.40) in db versus ϕ ($\phi = \omega(1+N)RC$) for various combinations of R for the $DR\overline{URC}$ and open-loop amplifier gain A , the curves of Figure 5-15 and 5-16 result. These curves allow the design of a bandpass amplifier when center frequency and either bandwidth or Q are specified. The Q in Figure 5-15 is found by dividing the value of ϕ at which the magnitude of equation (5.40) has a maximum value by the difference between the values of ϕ at which the magnitude is down by 3 db from the maximum value. That this results in an expression for Q can be seen from equation (5.41)

$$\frac{\phi_0}{\phi_2 - \phi_1} = \frac{\omega_0(1+N)RC}{\omega_2(1+N)RC - \omega_1(1+N)RC} = \frac{\omega_0}{\omega_2 - \omega_1} = Q \quad (5.41)$$

where

ω_0 = center frequency

ω_2 = upper 3 db frequency

ω_1 = lower 3 db frequency.

For values of open-loop amplifier gain A below 1000, Figure 5-16 shows that ϕ_0 changes markedly with a change in A . However, as the gain A is increased beyond 1000, the dependence of ϕ_0 upon A decreases to the point where ϕ_0 becomes relatively independent of changes in A . This set of curves (Figure 5-16) allows the designer to determine the needed value of capacitance to realize the desired center frequency for the filter.

In using the curves, Figure 5-15 is entered at a point corresponding to the desired value of Q . Once a value of R is chosen (the choice is arbitrary but should be limited to values greater than 1 k Ω due to the small value of N) the needed open-loop gain is determined from the horizontal axis. By locating on Figure 5-16 the point of intersection of the curve representing the previously chosen value of R and the vertical line corresponding to the determined value of A , the value of ϕ_0 is found. The necessary value of C then becomes

$$C = \frac{\phi_o}{\omega_o (1+N) R} \cdot \quad (5.42)$$

The use of these curves is illustrated in Chapter VI by way of a design example for an IF amplifier for an FM receiver.

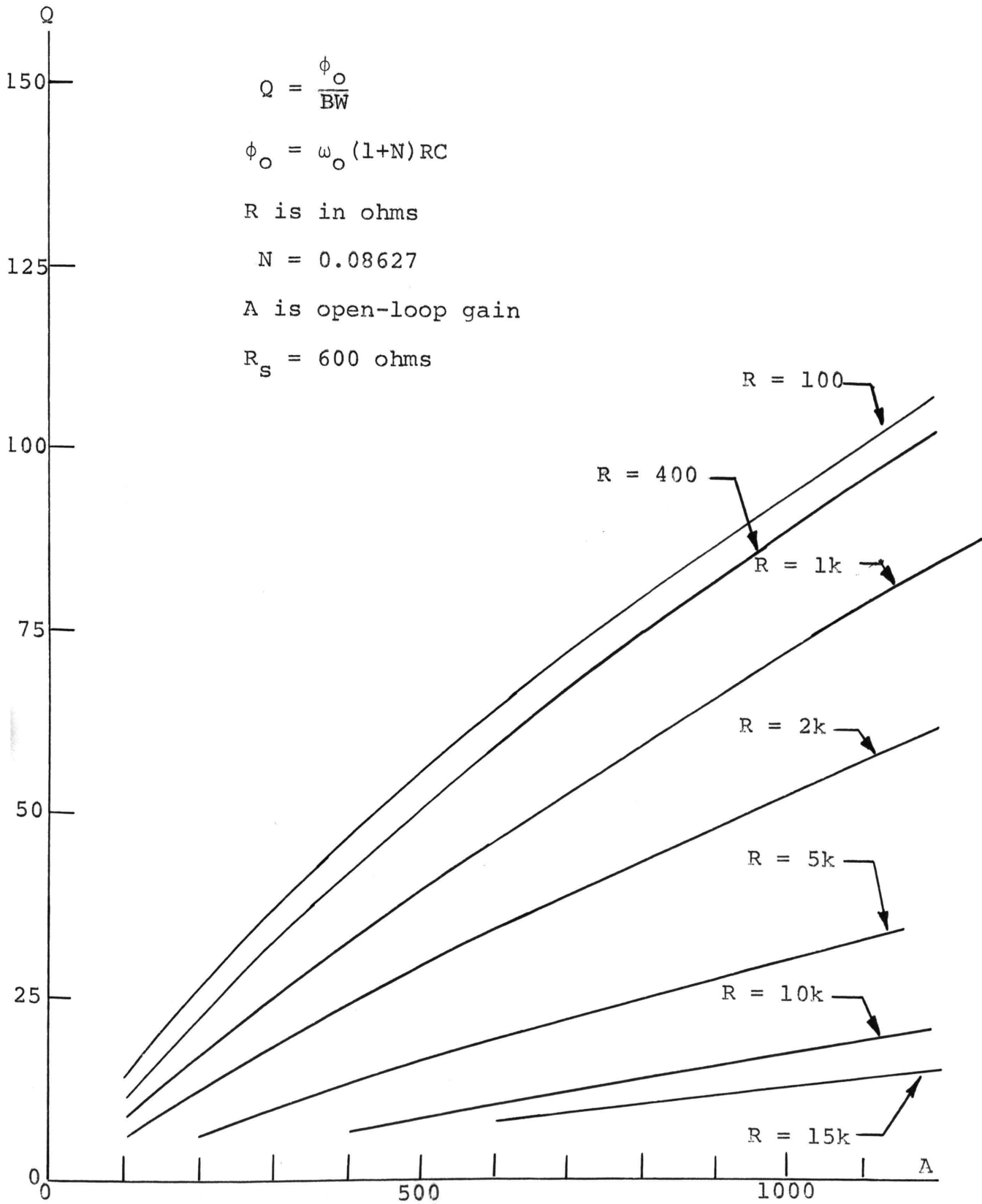


Figure 5-15. Q versus amplifier gain A for various values of R for the DRURC.

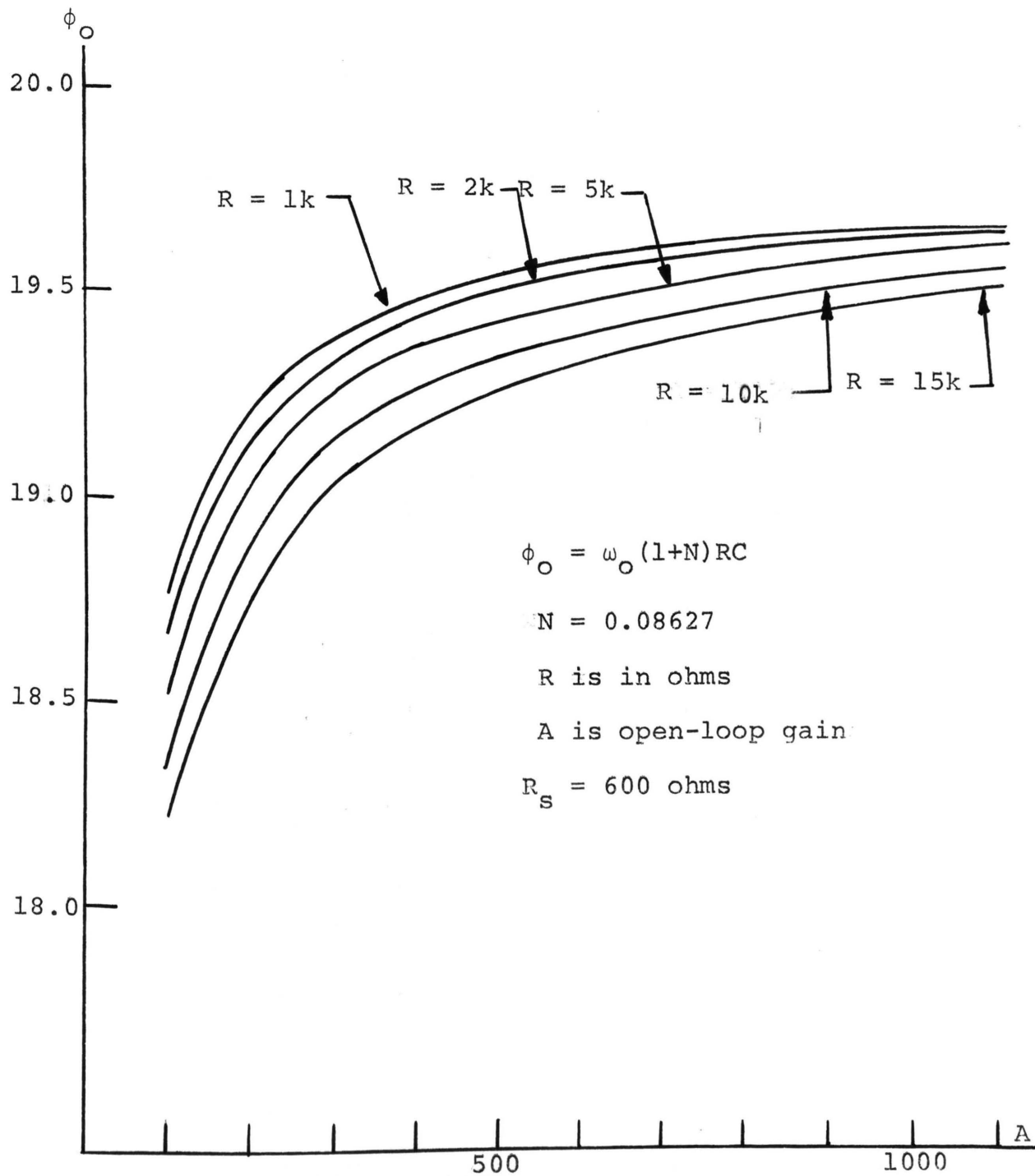


Figure 5-16. Center frequency ϕ_0 versus amplifier gain A for various values of R for the DRURC.

VI. DESIGN PROCEDURES AND EXAMPLES

A. INTRODUCTION

This chapter discusses several design examples illustrating the use of the equations and design curves developed in Chapters I through V. Most of the procedures illustrated in Sections B through D are for the bipolar transistor, although field effect transistors (FET's) are included as examples in the subsection on $\overline{\text{DRURC}}$'s. The procedure for bypass network design is basically the same for either bipolar transistors or FET's--this is discussed in Section C. Section D discusses the characteristics of a two-stage bipolar transistor amplifier using distributed networks.

The design of oscillators using the $\overline{\text{DRURC}}$ is discussed in Section E. The method of design is one of analysis applied to design based mostly on the method of multiple-plane root locus developed by Bourquin [31]. The oscillators are of the RC phase-shift variety which, unlike those found in [28], use the $\overline{\text{DRURC}}$ to provide the D.C. bias for the gain block as well as the necessary feedback for oscillation. The oscillator is amenable to the techniques of monolithic, silicon-chip fabrication. Section F is concerned with design procedures applicable to band-elimination and band-pass filters. The band-elimination filters are passive networks using the $\overline{\text{DRURC}}$, while the bandpass filters are active networks using the band-elimination filter in the

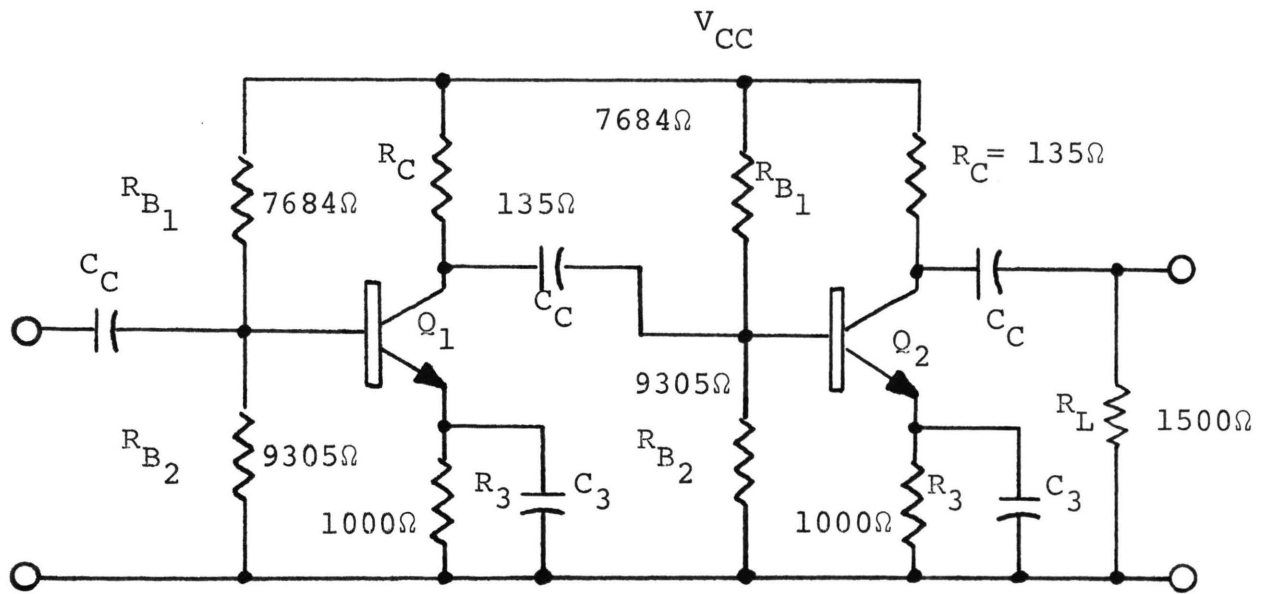
feedback loop of an operational amplifier. The design curves from Chapter V are applied to the design of a finite-gain bandpass filter.

B. COUPLING NETWORKS

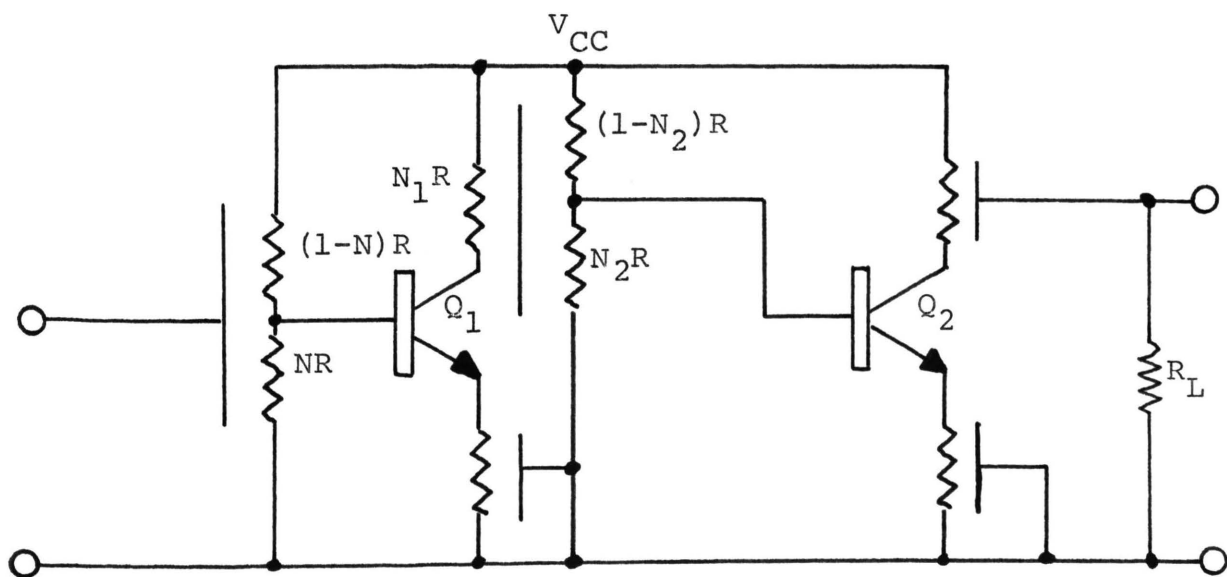
1. Introduction. The schematic diagram of a typical two-stage RC-coupled bipolar transistor amplifier is shown in Figure 6-1(a). The same amplifier with all of the lumped RC components replaced by distributed RC networks is shown in Figure 6-1(b). As is discussed in Chapter VII, each of the distributed RC networks may be fabricated with about the same difficulty as fabricating an integrated circuit capacitor.

Not only is there comparative ease of fabrication, but the number of elements to be fabricated is reduced. In Figure 6-1(a) there are 13 lumped two terminal elements; in Figure 6-1(b) there are 5 distributed RC network components. Most of the capacitors used in this chapter have values that are not available using the present technology for fabricating distributed networks. The values that are presently available are limited at the upper end by approximately 0.03μ farads [26]. Due to the sizes involved in integrated circuit, the capacitance limit is considerably smaller (on the order of 50 p farads).

In the calculations that follow, the lower 3-db frequency to be designed for is 1.0 kHz. The lower 3-db



(a)



(b)

Figure 6-1. Typical RC-coupled two-stage bipolar transistor amplifier: (a) lumped RC version [36], (b) distributed RC version.

frequencies of the by-pass circuits are assumed to be much lower than 1.0 kHz. Since three distributed coupling networks are cascaded, the lower 3-db frequency for each becomes 509.8 Hz. At present, there is no formula to allow the calculation of the 3-db frequencies for each of several cascaded networks if the networks do not possess identical, single poles. The development of such an expression would be a significant contribution to the state-of-the-art design of cascaded amplifiers.

It has been the experience of the author that only a small error occurs when the standard expression for use with networks having identical, single poles [10,36,44] is applied to cascaded distributed networks in amplifier design. The distributed networks used in this chapter do not have single poles, but it is assumed that the dominant-pole effect is pronounced enough to allow application of the standard expression.

The transistor model assumed in the calculations to follow is the low-frequency h-parameter model with $h_{ie} = 1500$ ohms, $h_{re} = 0$, $h_{fe} = 200$, and $h_{oe} = 0.5 \times 10^{-4}$ mhos. The driving source for the amplifier is assumed to have a 600-ohm internal impedance. No attempt will be made to design for any other performance parameter other than a lower 3-db frequency of 1.0 kHz.

2. \overline{TURC} . By comparing Figures 6-1(a) and (b) it is seen that in order for the \overline{TURC} to replace the lumped input

coupling/bias network it is convenient to make $R = R_{B_1} + R_{B_2} = 16989$ ohms. Additionally, N must equal 0.548 in order to maintain Q_1 at the same quiescent point.

Inspection of Figure G-1, Appendix G, shows the \overline{TURC} to have a lower ϕ_{3db} value of 11.675. Substitution of this value of ϕ along with the above value for R and $f_{3db} = 509.8$ Hz into equation (5.9a) yields the capacitance of the \overline{TURC} to be 0.215 μF .

The overall design parameters for the \overline{TURC} are now

$$R = 16989 \text{ ohms}$$

$$C = 0.215 \mu\text{F}$$

$$N = 0.548.$$

3. \overline{TDRURC} . The resistive layers of the \overline{TDRURC} must provide the proper D.C. bias and along with the distributed capacitance, the desired f_{3db} of 509.8 Hz. Therefore, let $N_1 R = R_C = 135$ ohms for Q_1 and $R = R_{B_1} + R_{B_2} = 16989$ ohms for Q_2 . These, along with the need for the proper ratio between $N_2 R$ and $(1-N_2)R$, yield $N_1 = 0.00795$, $N_2 = 0.548$, and $R = 16989$ ohms. From an inspection of Figure G-2, Appendix G, the lower ϕ_{3db} value is seen to be 21.0. This value, along with R , N_1 , and $f_{3db} = 509.8$ Hz, yields

$$C = \frac{\phi_{3db}}{2\pi f_{3db} (1+N_1)R} = 0.383 \mu\text{F}. \quad (6.1)$$

Therefore, the overall design parameters for the $\overline{\text{TDRURC}}$ become

$$R = 16989 \text{ ohms}$$

$$C = 0.383 \text{ } \mu\text{F}$$

$$N_1 = 0.00795$$

$$N_2 = 0.548.$$

4. $\overline{\text{URC}}$ (as in Figure 6-1). Routine analysis of the $\overline{\text{URC}}$ used as an output coupling network (see Figures 6-1(b) and 6-5(a)) yields the transfer impedance to be

$$\frac{V_0}{I_i} = \frac{Y_{21}}{Y_{12}Y_{21} - (Y_S + Y_{11})(Y_L + Y_{22})} \quad (6.2)$$

where I_i is I_4 in Figure 6-5(a) and the y parameters are those of matrix (2.18). Inspection of the magnitude of (6.2) versus ϕ (see Figure G-3, Appendix G) shows the lower $\phi_{3\text{db}}$ value to be 0.086. For the URC to replace R_C for Q_2 of Figure 6-1(a), R must equal 135 ohms. Substitution of $R = 135$ ohms, $\phi_{3\text{db}} = 0.086$, and $f_{3\text{db}} = 509.8$ Hz into $\phi_{3\text{db}} = 2\pi f_{3\text{db}} RC$ gives

$$C = \frac{\phi_{3\text{db}}}{2\pi f_{3\text{db}} R} = 0.1989 \text{ } \mu\text{F}. \quad (6.3)$$

The design parameters for the \overline{URC} are now

$$R = 135 \text{ ohms}$$

$$C = 0.1989 \text{ } \mu\text{F.}$$

5. \overline{DRURC} . Figure 6-2 shows an amplifier using JFET's instead of bipolar devices. The interstage coupling network is now a \overline{DRURC} with the resistive layers providing the needed D.C. bias for Q_1 and Q_2 . In order for the \overline{DRURC} to provide the proper bias, NR must equal R_D of Q_1 , and R must equal R_g of Q_2 . This yields $R = 1\text{M ohm}$ and $N = 0.00418$.

Inspection of Figure G-4, Appendix G, shows the lower $\phi_{3\text{db}}$ value to be 3.1. With $R = 1\text{M ohm}$, $N = 0.00418$, $\phi = 3.1$, and $f_{3\text{db}} = 509.8 \text{ Hz}$, the needed capacitance becomes

$$C = \frac{\phi_{3\text{db}}}{2\pi f_{3\text{db}}(1+N)R} = 963.8 \text{ pF.} \quad (6.4)$$

The design parameters for the \overline{DRURC} are, therefore,

$$R = 1\text{M ohm}$$

$$C = 963.8 \text{ pF}$$

$$N = 0.00418.$$

6. \overline{URC} (as in Figure 6-2). The input and output \overline{URC} 's of Figure 6-2(b) can be designed using a procedure similar to that used for the output \overline{URC} of Figure 6-1(b). The appropriate values must be substituted into the proper equations to generate a set of ϕ -response curves.

The two equations listed below are the proper voltage transfer equations needed for the generation of the ϕ -response curves.

input \overline{URC} :

$$\frac{V_g}{V_{in}} = \frac{Y_s Y_{42}}{Y_{42} Y_{24} - (Y_s + Y_{22})(Y_L + Y_{44})}$$

output \overline{URC} :

$$\frac{V_0}{V_{ds}} = \frac{Y_s Y_{24}}{Y_{42} Y_{24} - (Y_s + Y_{44})(Y_L + Y_{22})}$$

Note that V_g is the gate-signal voltage of Q_1 , and $V_{ds} = -g_m r_d V_g$ of Q_2 in Figure 6-2(b).

For the input \overline{URC} Y_s is the internal admittance of the signal source, and Y_L is the input admittance of Q_1 . For the output \overline{URC} Y_s is the output admittance of Q_2 , and Y_L is the load admittance for the amplifier. In both cases, the Y_{ij} 's are found in the matrix of (2.18).

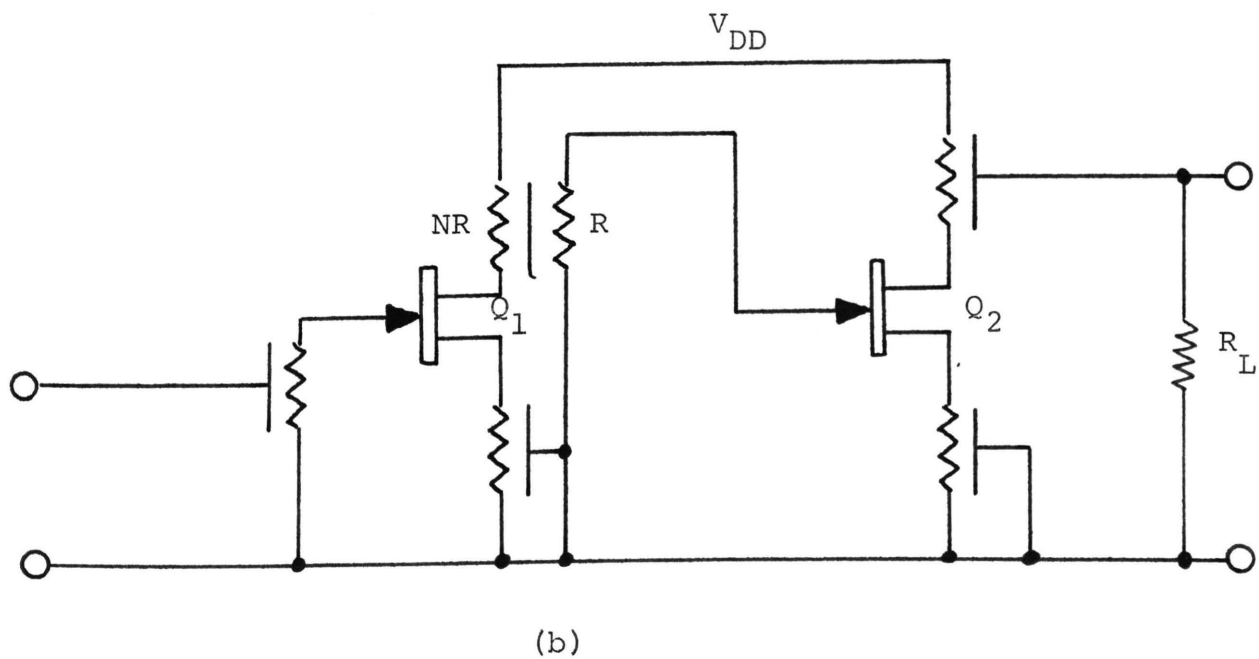
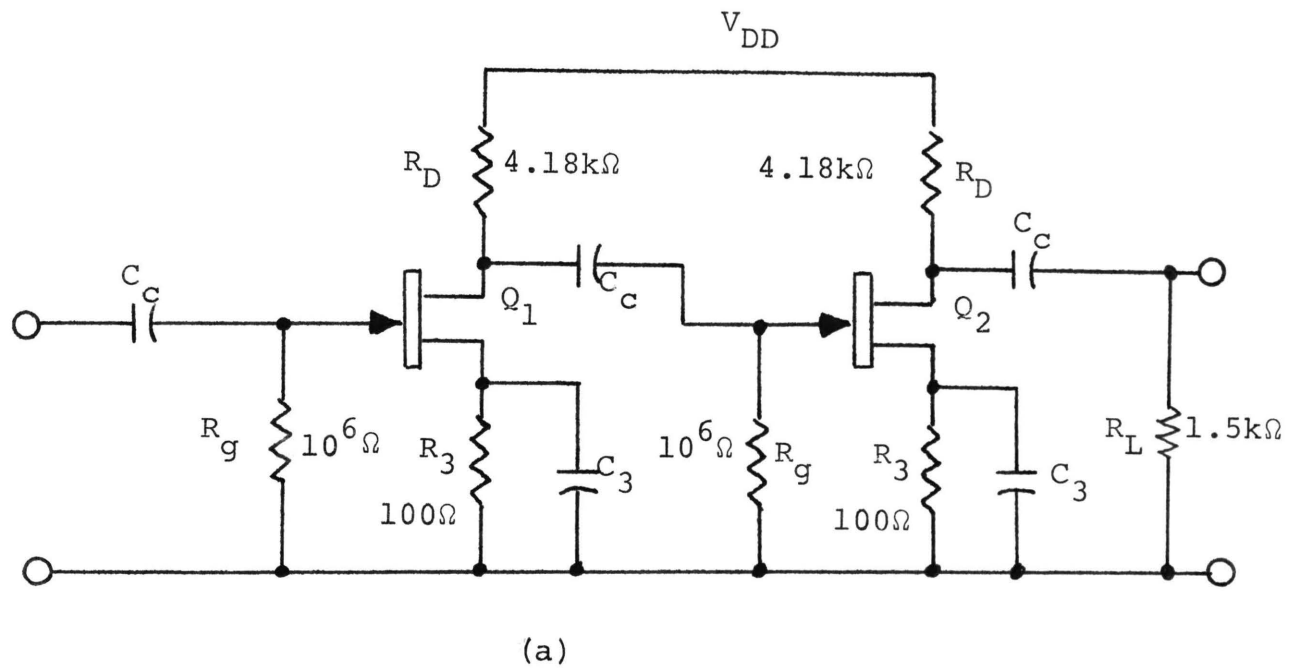


Figure 6-2. Typical RC-coupled two-stage JFET amplifier:
 (a) lumped RC version [36], (b) distributed
 RC version.

C. BY-PASS NETWORKS

For this particular design example each of the by-pass networks are designed to have a cutoff frequency of 0.1 times the cutoff frequency of the overall amplifier, i.e., 100 Hz. From equation (5.22a), the by-pass networks of Figure 6-1(b) have a capacitance of

$$C = \frac{2.61}{2\pi f R} = 4.15 \mu\text{F} \quad (6.5)$$

For the JFET amplifier of Figure 6-2(b), the capacitance value is 41.5 μF .

D. AMPLIFIER CHARACTERISTICS

1. Introduction. The design of the sub-networks of the distributed network amplifier is discussed in sections B and C. Discussion of the input and output impedances is presented in subsection 2 of this section, the frequency response of the amplifier in subsection 3, and a comparison of the lumped and distributed amplifiers in subsection 4.

2. Input and Output Impedances. The input impedance for the amplifier of Figure 6-1(b) is that of the input $\overline{\text{TURC}}$ (equation (6.6)). The load impedance for the $\overline{\text{TURC}}$ is the input impedance of Q_1 . Equation (6.6) comes from

equation (5.6b). The Z_L in equation (6.6) is the input impedance of Q_1 . Assuming that h_{re} of Q_1 is small

$$Z_{i\overline{\text{TURC}}} = \frac{1 + Y_{44}Z_L}{Y_{22}(1 + Y_{44}Z_L) - Y_{24}Y_{44}Z_L} \quad (6.6)$$

$$Z_{iQ_1} = h_{ie_1} \quad (6.7)$$

enough to be ignored, Z_{iQ_1} may be approximated by h_{ie_1} .

The output impedance of the amplifier is the output impedance of the output $\overline{\text{URC}}$. Equation (6.8) gives the output impedance of the $\overline{\text{URC}}$ where Z_s is the output impedance of Q_2 . With h_{re} again assumed small enough to be ignored, Z_{OQ_2} may be approximated by equation (6.9).

$$Z_{O\overline{\text{URC}}} = \frac{1 + Y_{11}Z_s}{Y_{22}(1 + Y_{11}Z_s) - Y_{12}Y_{21}Z_s} \quad (6.8)$$

$$Z_{OQ_2} = \frac{1}{h_{oe_2}} \quad (6.9)$$

Plots of the magnitude and phase of the input and output impedances for the amplifier of Figure 6-1(b) are shown in Figures 6-3 and 6-4. The data for these curves were computer generated from equations (6.6) and (6.8), for which the IAM parameters were computed by the programs listed in Appendices B and A, respectively.

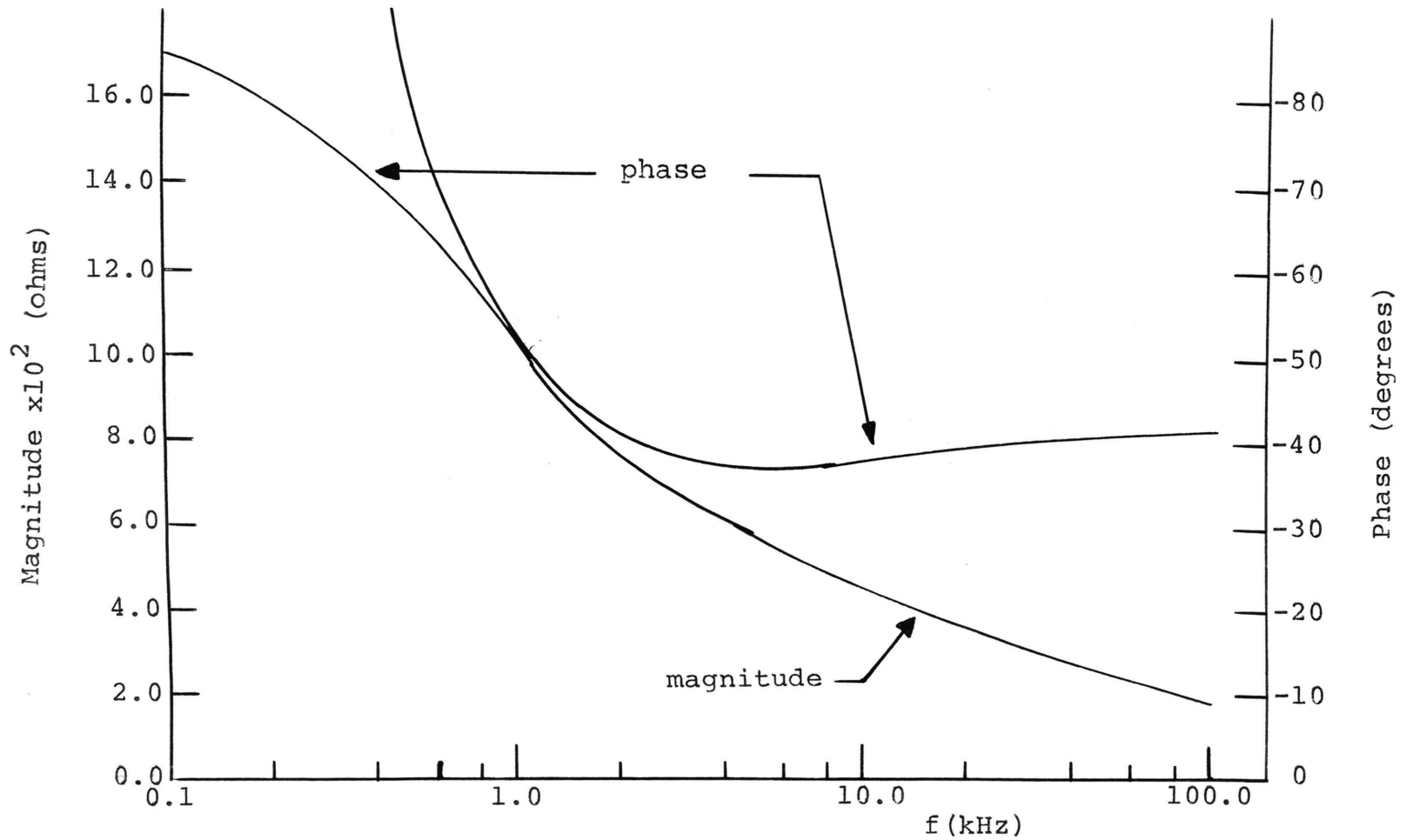


Figure 6-3. Magnitude and phase response for the input impedance of the distributed network amplifier shown in Figure 6-1(b).
 $h_{ie} = 1500\Omega$, $h_{re} = 0$, $h_{fe} = 200$, $h_{oe} = 0.5 \times 10^{-4}$ mhos.

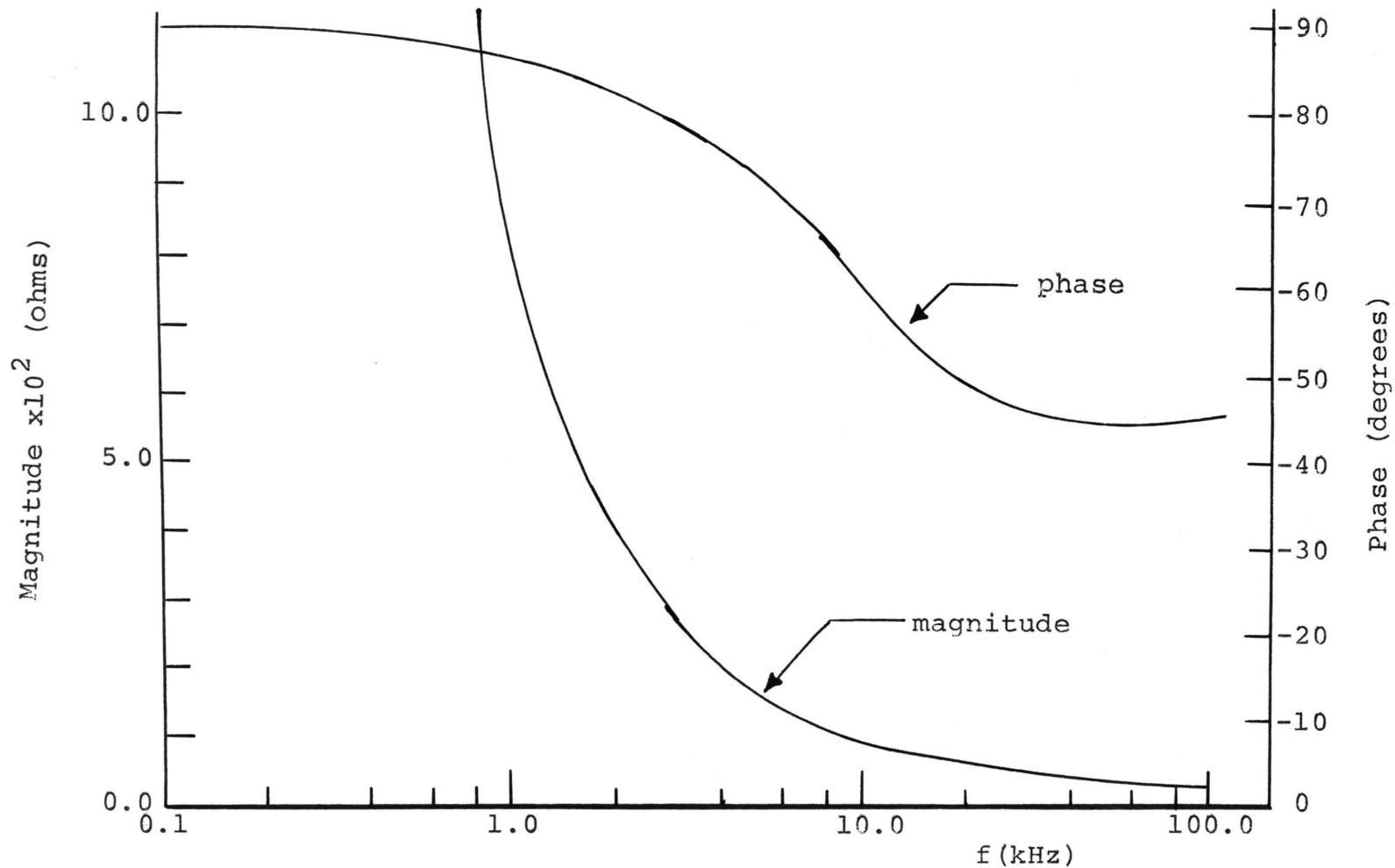


Figure 6-4. Magnitude and phase response for the output impedance of the distributed network amplifier shown in Figure 6-1(b).
 $h_{ie} = 1500\Omega$, $h_{re} = 0$, $h_{fe} = 200$, $h_{oe} = 0.5 \times 10^{-4}$ mhos.

3. Frequency Response. Use of the transfer immittances and ratios as well as the current gain expressions for Q_1 and Q_2 yield the voltage and current gain expressions for the amplifier of Figure 6-1(b).

$-h_{fe_1}$ and $-h_{fe_2}$ are assumed as the current gain expressions for Q_1 and Q_2 , respectively [44]. h_{ie} and h_{oe} of Q_1 and Q_2 are considered as the terminating immittances for the distributed network coupling components of the amplifier.

Figure 6-5(a) shows the equivalent circuit that is used for determining the frequency response characteristics of the amplifier. The overall voltage and current gain ratios are given by

$$\frac{V_0}{V_{in}} = (AVITUR) (-h_{fe_1}) (AITDR) (-h_{fe_2}) (AIVURC) \quad (6.10)$$

where

AVITUR is given by equation (4.8)

AITDR is given by equation (3.13)

AIVURC is given by equation (6.2)

$$\frac{I_0}{I_{in}} = (AITUR) (-h_{fe_1}) (AITDR) (-h_{fe_2}) (AIURC) \quad (6.11)$$

where

AITUR is given by equation (4.7)

AITDR is given by equation (3.13)

AIURC is given by equation (6.2) divided by Z_L

and

$$I_{in} = Y_s V_{in}.$$

Plots of the magnitude and phase of the voltage and current gains are shown in Figure 6-5(b). The data for these curves were computer generated from equations (6.10) and (6.11), for which the IAM parameters were computed by the programs listed in Appendices A, B, and D. Inspection of Figure 6-5(b) shows the mid-band voltage and current gain values to be 25.2 db and 17.2 db respectively. The upper and lower 3-db frequencies of the amplifier are 980 Hz and 30.5 kHz, respectively. Since equations (6.10) and (6.11) are related by a real constant, the phase-angle relationships for both are identical.

For the individual distributed networks, the upper 3-db frequencies are

$$\overline{TURC}: 32 \text{ kHz}$$

$$\overline{TDRURC}: 380 \text{ kHz}$$

$$\overline{URC}: 64 \text{ kHz}$$

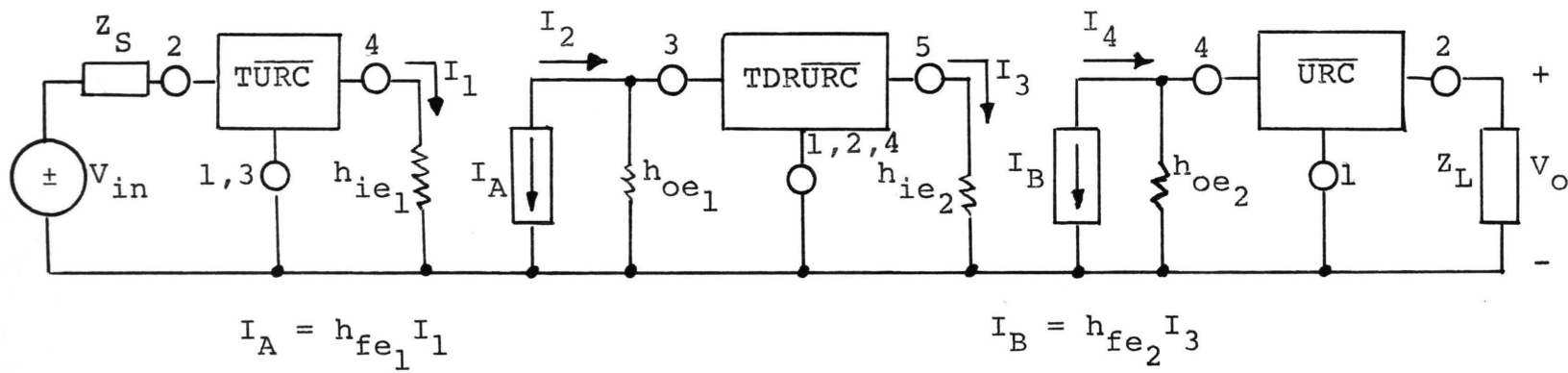


Figure 6-5(a). Equivalent circuit for Figure 6-1(b).

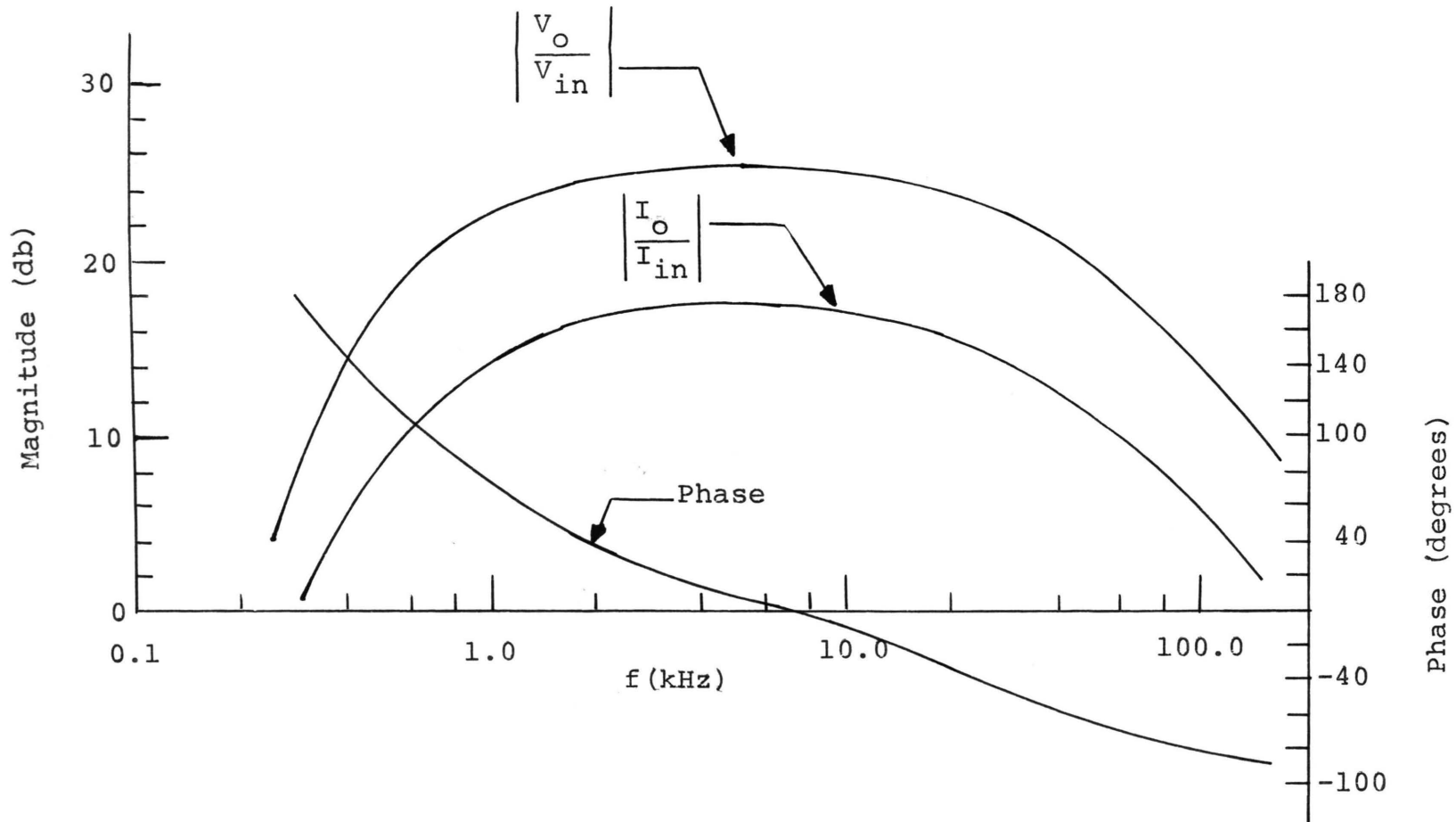


Figure 6-5(b). Magnitude and phase of voltage and current gain vs f (kHz) for the distributed network amplifier shown in Figure 6-1(b).
 $h_{ie} = 1500\Omega$, $h_{re} = 0$, $h_{fe} = 200$, $h_{oe} = 0.5 \times 10^{-4}$ mhos.

From the above data, it would appear that, for this particular case, the \overline{TURC} is the component that limits the bandwidth of the amplifier. The reader is cautioned to realize that this conclusion is for this example only and may not be a general rule.

As was pointed out previously (see Summary, Chapter V, Section C and Chapter VI, Section B) the capacitances needed for this design are not presently available. Using only those values that are, i.e., 0.03 μF , the mid-band gains change only a small amount while a significant change in bandwidth does occur.

With these changes in capacitance, the mid-band gains and upper and lower 3-db frequencies of the amplifier are as shown below. Since the by-pass networks were considered to be short circuits (see Figure 6-5(a)), only the coupling network capacitances were changed to 0.03 μF .

$$K_{V_{db}} = 24.1 \text{ versus } 25.2$$

$$K_{i_{db}} = 16.2 \text{ versus } 17.2$$

$$f_1 = 12.95 \text{ kHz versus } 0.98 \text{ kHz}$$

$$f_2 = 199.6 \text{ kHz versus } 30.5 \text{ kHz}$$

From these results it appears that the distributed network RC coupled amplifier is practical for use with frequencies above the audio frequency range.

4. Comparison of Distributed Network and Lumped

a. Introduction. The amplifier of Figure 6-1(a) was analyzed to compare its performance characteristics with those of the distributed network version of Figure 6-1(b). The items that are compared are: input and output impedances, coupling capacitor values, and the voltage gain. It was assumed that the transistors in the lumped network amplifier had terminal characteristics (h parameters, capacitances, etc.) identical to those of the distributed network amplifier. In particular, the input and output capacitances of the transistors are considered to have a value of zero. Three frequencies were used as comparison points: 1.0, 5.5, and 30.5 kHz. These represent the designed-for low-frequency 3-db point, the resultant mid-band frequency, and the resultant upper 3-db frequency of the distributed network amplifier, respectively. Additionally, the emitter RC network was assumed to have zero impedance at all the frequencies of interest.

b. Input and Output Impedances. The input and output impedances were calculated from a standard h-parameter equivalent circuit subject to the constraints stated in the

introduction to this subsection. The results of the comparison between the input and output impedances of the two amplifiers are shown in Table I. The magnitudes of the impedances are in ohms, and the phase angles are in degrees. Data for the distributed network impedances are taken from Figures 6-3 and 6-4.

c. Voltage Gain. The voltage gain for the lumped network amplifier was calculated from Figure 6-1(a) using a standard low-frequency, h-parameter, equivalent circuit with the same constraints as listed in the discussion on input and output impedances. The coupling capacitor values were calculated based on an assumed low-frequency 3-db point of 509.8 Hz for each of the three coupling networks.

The capacitances for the lumped coupling networks of Figure 6-1(a) are smaller in value than the capacitances for their distributed network counterparts of Figure 6-1(b). For the lumped networks, 0.182 μF , 0.252 μF , and 0.191 μF are the values needed for the input, interstage, and output coupling networks, respectively. These values are contrasted with 0.215 μF for the $\overline{\text{TURC}}$, 0.383 μF for the $\overline{\text{TDRURC}}$, and 0.1989 μF for the $\overline{\text{URC}}$ of Figure 6-1(b).

Since the frequency response shape of the distributed network RC amplifier is different from that of the lumped network version, a meaningful comparison between the two is difficult to make. Even though the input and output capacitances of the transistors are considered to be zero,

TABLE I. Input and output impedance comparison between the lumped and distributed network amplifiers of Figures 6-1(a) and (b).

FREQ.	LUMPED (Z_{in})	DIST. (Z_{in})	LUMPED (Z_{out})	DIST. (Z_{out})
1.0 kHz	$1.41 \times 10^3 / \underline{-38.3^\circ}$	$\cong 1.1 \times 10^3 / \underline{-53^\circ}$	$0.843 \times 10^3 / \underline{-80.85^\circ}$	$\cong 0.85 \times 10^3 / \underline{-87^\circ}$
5.5 kHz	$1.12 \times 10^3 / \underline{-8.17^\circ}$	$\cong 0.7 \times 10^3 / \underline{-38^\circ}$	$0.2 \times 10^3 / \underline{-48.4^\circ}$	$\cong 0.26 \times 10^3 / \underline{-80^\circ}$
30.5 kHz	$1.11 \times 10^3 / \underline{-1.48^\circ}$	$\cong 0.3 \times 10^3 / \underline{-40^\circ}$	$0.137 \times 10^3 / \underline{-11.5^\circ}$	$\cong 0.05 \times 10^3 / \underline{-46^\circ}$

there is a definite upper 3-db frequency for the distributed network amplifier (due primarily to the frequency response of the \overline{TURC}). For the lumped version, no such upper 3-db frequency exists. Because of the dissimilarity of the two response shapes, the voltage gains of the two amplifiers are compared at only the three frequencies specified in the introduction to this subsection. Table II shows the comparison between the voltage gain of the lumped network amplifier and the distributed network amplifier. The voltage-gain magnitude is given in decibels while the phase is given in degrees. Data for the voltage gain of the distributed network amplifier is taken from Figure 6-5(b).

TABLE II. Voltage gain comparison between the lumped and distributed network amplifiers of Figures 6-1(a) and (b).		
FREQ.	LUMPED	DIST.
1.0 kHz	41.55/ <u>81.15</u> °	≅ 23.0/ <u>73</u> °
5.5 kHz	44.45/ <u>15.9</u> °	≅ 25.2/ <u>0</u> °
30.5 kHz	44.56/ <u>2.9</u> °	≅ 22.2/ <u>-50</u> °

From Table II, it can be seen that if the same mid-band ($f = 5.5$ kHz) gain is to be obtained from both amplifiers, transistors with higher h_{fe} would be needed in the distributed network version. As a matter of comparison on that

point, the h_{fe} of the transistors in the lumped version was reduced to 100 (in place of the assumed 200), and the amplifier was analyzed at $f = 30.5$ kHz. The resultant gain was 32.6 db, 7.4 db above the maximum gain of the distributed network amplifier using transistors with $h_{fe} = 200$. This indicates that an increase in the h_{fe} of the transistors used in the distributed network RC amplifier (over those of the lumped amplifier) of greater than 100% would be needed to meet the gain characteristic of the lumped network amplifier.

5. Summary. Comparing distributed network RC coupled amplifiers with lumped RC versions, several differences become apparent. First, the distributed network version contains fewer components. Secondly, for frequencies below 10 kHz, the bandwidth is limited in the distributed network version. Thirdly, transistors with a higher h_{fe} are needed in the distributed network version to achieve the same mid-band gain as obtained in the lumped RC-coupled amplifier. These difficulties make the distributed network RC-coupled amplifier impractical for use at audio frequencies.

As stated in the abstract, no previous work has been done in applying distributed networks to electronic amplifiers. Therefore, no comparisons with previously obtained results can be made.

E. OSCILLATORS

1. $\overline{\text{DRURC}}$ Network Design. The phase-shift network for the oscillator shown in Figure 5-9 has element values determined by equation (5.36). Assuming $N = 0.08627$, $R = 15 \text{ k}$ ohms and a capacitance of 1700 pF , equation (5.36) yields a frequency of oscillation

$$f = \frac{30.75}{2\pi C(1+N)R} \approx 177 \text{ kHz.} \quad (6.12)$$

With the above element values the $\overline{\text{DRURC}}$ required is shown in Figure 6-6.

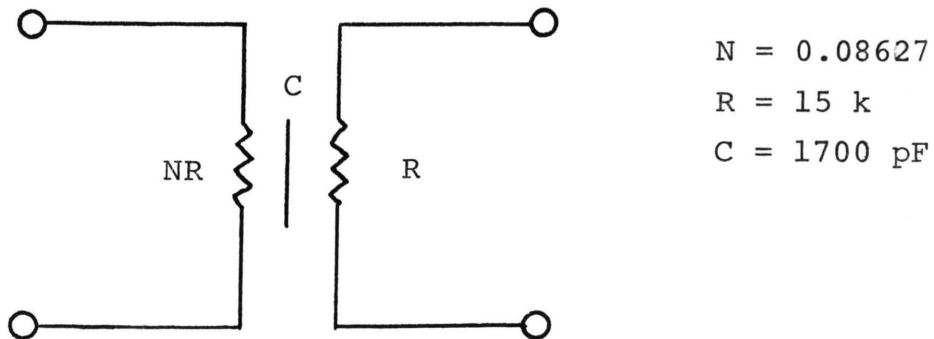


Figure 6-6. $\overline{\text{DRURC}}$ required for ICVS oscillator.

2. Active Block Design. Several realizations for the ICVS exist; the one used here is shown in Figure 5-12. The schematic diagram of a practical version is shown in Figure 6-7. The required gain for the ICVS is found from equation (5.35) and for this example becomes

$$K = 0.82(1+N)R = 13.35 \times 10^3 \text{ (volts/amp)} \quad (6.13)$$

where R and N are those connected with Figure 6-6.

The gain adjustment resistor can be calculated from equation (5.37) and is

$$R = \frac{K}{h_{fb1}} = \frac{13.35 \times 10^3}{0.98} = 13.6 \text{ k ohms.} \quad (6.14)$$

An oscillator constructed using the ICVS of Figure 6-7 produced a sinusoidal waveform with low (1.0%) distortion as measured on a spectrum analyzer. A photograph of the waveform is shown in Figure 6-8.

A monolithic version of the oscillator suitable for integration is shown in Figure 6-9. With proper design, theoretically all the design characteristics could be met.

F. FILTERS

1. Passive Band Reject. This filter has the same form

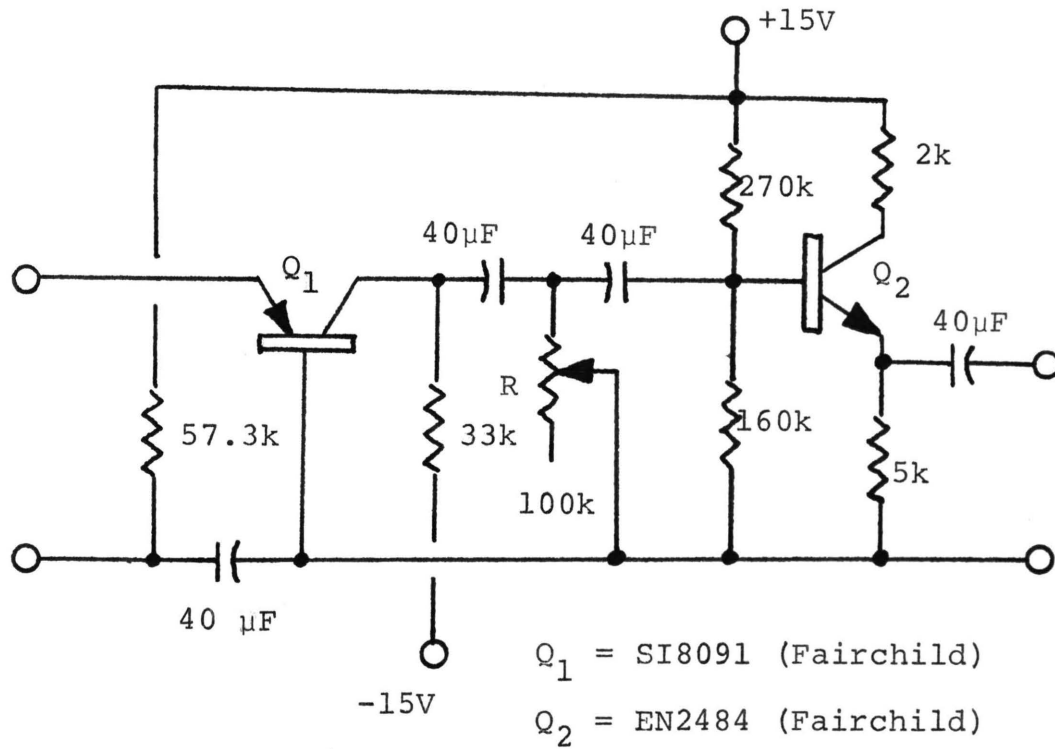
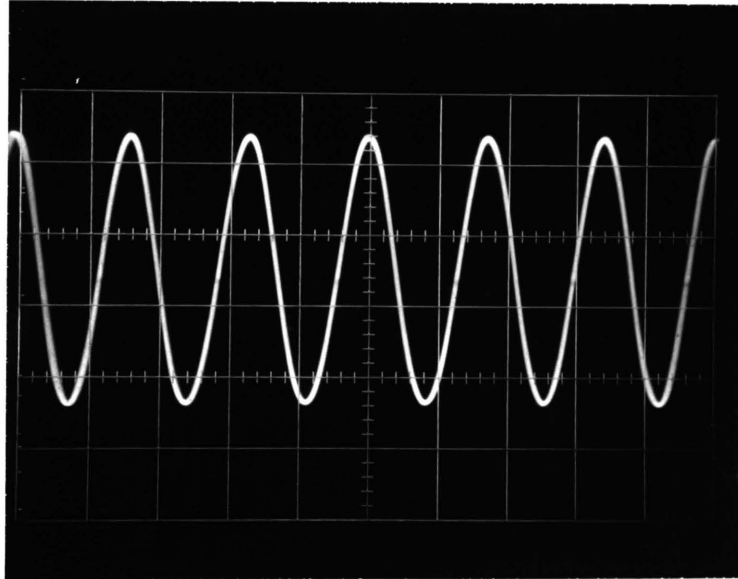


Figure 6-7. Bipolar transistor current-controlled voltage-source (ICVS). R provides the needed value from equation (6.14).



Horizontal - 5 $\mu\text{sec}/\text{cm}$, vertical - 0.5 v/cm.

Figure 6-8. Waveform of $\overline{\text{DRURC}}$ phase shift oscillator.

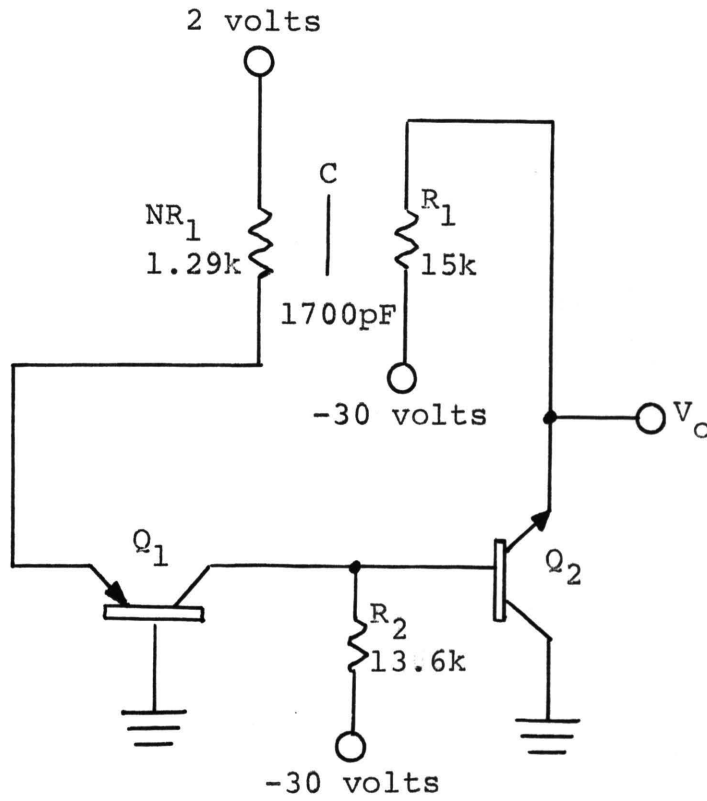


Figure 6-9. Example schematic diagram of a DRURC phase-shift oscillator suitable for integrated circuit design.

as that shown in Figure 2-6 [28]. The equations are exactly the same, including that for the necessary capacitance. Assuming a notch frequency is given, values for N , R , and C are required to complete the design.

The optimum value for N is 0.08627, R should be chosen to be very small in comparison to the terminating load into which the filter is supposed to feed, and C is calculated to complete the design. Assume that the load impedance is 10 k ohms and the desired notch frequency is 100 k Hz. In order to approximate an open-circuited load, R is chosen to be 1 k ohm.

Using equation (5.38) [28], C is calculated to be

$$C = \frac{19.75}{2\pi f(1+N)R} = 28,900 \text{ pF.} \quad (6.15)$$

The element values are, therefore,

$$R = 1 \text{ k ohm}$$

$$C = 0.0289 \text{ } \mu\text{F}$$

$$N = 0.08627$$

2. Active Bandpass. The equations describing the active bandpass filter are the same as those describing the passive notch filter [28]. This assumes that the gain of the active block is high, i.e.:

$$A \gg 1. \quad (6.16)$$

Assuming $f_0 = 100 \text{ k Hz}$ and A satisfies equation (6.16), the design proceeds as for the passive notch filter. The requirement on the value of R is not as restrictive as for the passive notch filter, however, due to the low output impedance of the total feedback amplifier [33]

$$Z_{0_T} \approx \frac{Z_0}{A\beta} \leq 1 \text{ ohm}. \quad (6.17)$$

Then, because of the relative independence of load impedance (the loading is not as critical), the value of R may be chosen to allow a smaller value of capacitance.

Let $R = 15 \text{ k ohms}$. This value is well within the range of resistance values obtainable in distributed networks. With this value of R the value of capacitance now becomes

$$C = \frac{19.75}{2\pi f(1+N)R} = 1925 \text{ pF}. \quad (6.18)$$

1925 pF is much more easily obtained in a distributed network than is the value given in equation (6.15).

As an example of active bandpass filter design where the amplifier gain is finite, consider the following. A typical FM tuner has an IF strip with these frequency characteristics: $f_0 = 10.7 \text{ MHz}$ and $BW = 150 \text{ kHz}$. The Q of the IF strip is, therefore, 71.4. From Figure 5-15, with a Q

of 71.4, the range of R is seen to be 100 ohms to 2 k ohms. Since both R = 1 k ohm and NR = 86.3 ohms are easily fabricated, R = 1 k ohm is chosen for the DR \overline{URC} . With this combination of R and Q, the needed amplifier gain is 975. Figure 5-16, with R = 1 k ohm and A = 975, yields $\phi_o = 19.6$. Substituting these values, along with N = 0.08627 and $\omega_o = 2\pi(10.7 \times 10^6)$ into

$$\phi_o = \omega_o(1+N)RC \quad (6.19)$$

yields the necessary capacitance of the DR \overline{URC} to be 279 pF.

In summary, the 10.7 MHz DR \overline{URC} bandpass filter with a 150 kHz bandwidth has the following element values

$$R = 1.0 \text{ k ohms}$$

$$C = 278 \text{ pF}$$

$$N = 0.08627$$

$$A = 975. \quad (6.20)$$

The work done here on the phase-shift oscillators and bandpass amplifiers had been suggested earlier [28], but no details of any work had been published. Furthermore, the oscillator shown in [28] uses the distributed network to provide feedback only whereas the oscillator shown in Figure 6-9 utilizes the DR \overline{URC} to provide most of the D.C.

bias circuitry as well as providing feedback. This results in a smaller, simpler circuit.

To design the bandpass amplifier, two of the following need be specified: Q , bandwidth, or center frequency. Some previous work had been done [1], but no details concerning design for a specific Q or bandwidth was given.

G. LABORATORY VERIFICATION

1. Capacitance Determination

a. \overline{DRURC} . A \overline{DRURC} was fabricated by the author in 1972 using thin-film techniques and has a resistance of 15 k ohms and an N of 0.08627. This value of N produces a notch that is quite easy to measure. The method from Chapter II, Section C, is used to determine the capacitance of the \overline{DRURC} . A check on the value obtained is made from the formula for capacitance of a parallel-plate capacitor,

$$C = \frac{\epsilon\epsilon_0 A}{d}, \quad (6.21)$$

where $\epsilon \approx 3.5$ (silicon monoxide), $A = 3.37 \text{ cm}^2$, $d \approx 65 \times 10^{-5} \text{ cm}$ and $\epsilon_0 = 8.85 \times 10^{-14} \text{ F/cm}$. These values substituted into equation (6.21) yield a capacitance of 1606 pF.

When the network described above is used in a passive notch filter such as the one in Figure 2-6, the measured frequency of the notch is 120 k Hz. This, along with

$N = 0.08627$ and $R = 15 \text{ k}$, when substituted into equation (2.34) yields

$$C = \frac{19.75}{2\pi f(1+N)R} \cong 1603 \text{ pF} \quad (6.22)$$

Since equations (6.22) and (6.21) give similar values for capacitance, the method from Chapter II, Section C is verified as a valid method of determining the capacitance of a $\overline{\text{DRURC}}$ type distributed network.

b. $\overline{\text{URC}}$. A $\overline{\text{URC}}$ having approximately the same physical dimensions as the $\overline{\text{DRURC}}$ above is tested to determine the capacitance. The value of R_{sh} is determined to be (see equations (4.10) and (4.12))

$$R_{\text{sh}} = \frac{R}{17.8} = \frac{4.7 \text{ k}}{17.8} = 264\Omega. \quad (6.23)$$

The measured notch frequency is 240 k Hz. Substituting $f = 240 \text{ k Hz}$ and $R = 4.7 \text{ k ohms}$ into equation (4.12) yields

$$C = \frac{11.2}{2\pi f R} = 1580 \text{ pF}. \quad (6.24)$$

Again, agreement is quite close, thereby verifying the notch-frequency method of capacitance determination. The difference is due to fabrication of the capacitance layer. Since the $\overline{\text{TURC}}$ and $\overline{\text{TDRURC}}$ are special cases of the $\overline{\text{URC}}$ and

\overline{DRURC} , respectively, the calculations are basically the same.

2. \overline{URC} By-pass. A \overline{URC} connected as a by-pass network functions as a low-pass filter. Investigation of the response curves shows that the \overline{URC} version is comparable to the lumped version. The 3-db frequency is higher than that of the lumped version for the same value of capacitance, and the magnitude of the slope is also less at that frequency. In order to meet the same 3-db requirement, a larger capacitance would be needed for the distributed network. Plots of the normalized frequency response are found in Castro, et al. [28] and Lin [25].

VII. FABRICATION

A. INTRODUCTION

The fabrication of distributed RC networks follows procedures similar to those used in the fabrication of integrated circuits [34-37]. Since the topic is covered in great detail in the texts noted above, no attempt is made to cover the process of fabrication exhaustively. The two processes discussed are thin-film deposition and diffusion of semiconductor p-n junctions. Both are used to produce the distributed RC network.

B. FABRICATION METHODS

1. Thin-film. The process of thin-film deposition is used extensively in depositing contacts and interconnecting networks on integrated circuits. The technique is one of heating the material to be deposited until it vaporizes. The resulting vapors are then allowed to condense onto a surface and form a thin or thick film; there is no clear-cut definition of what constitutes a thin or thick film. Generally, a layer more than a few microns ($1 \text{ micron} = 10^{-4} \text{ cm}$) thick is considered a thick-film. Typical thickness for a thin-film resistor is 80-100 angstroms ($1 \text{ angstrom} = 10^{-8} \text{ cm}$).

Figure 7-1 shows a typical system used for the deposition of thin films. The material to be evaporated is

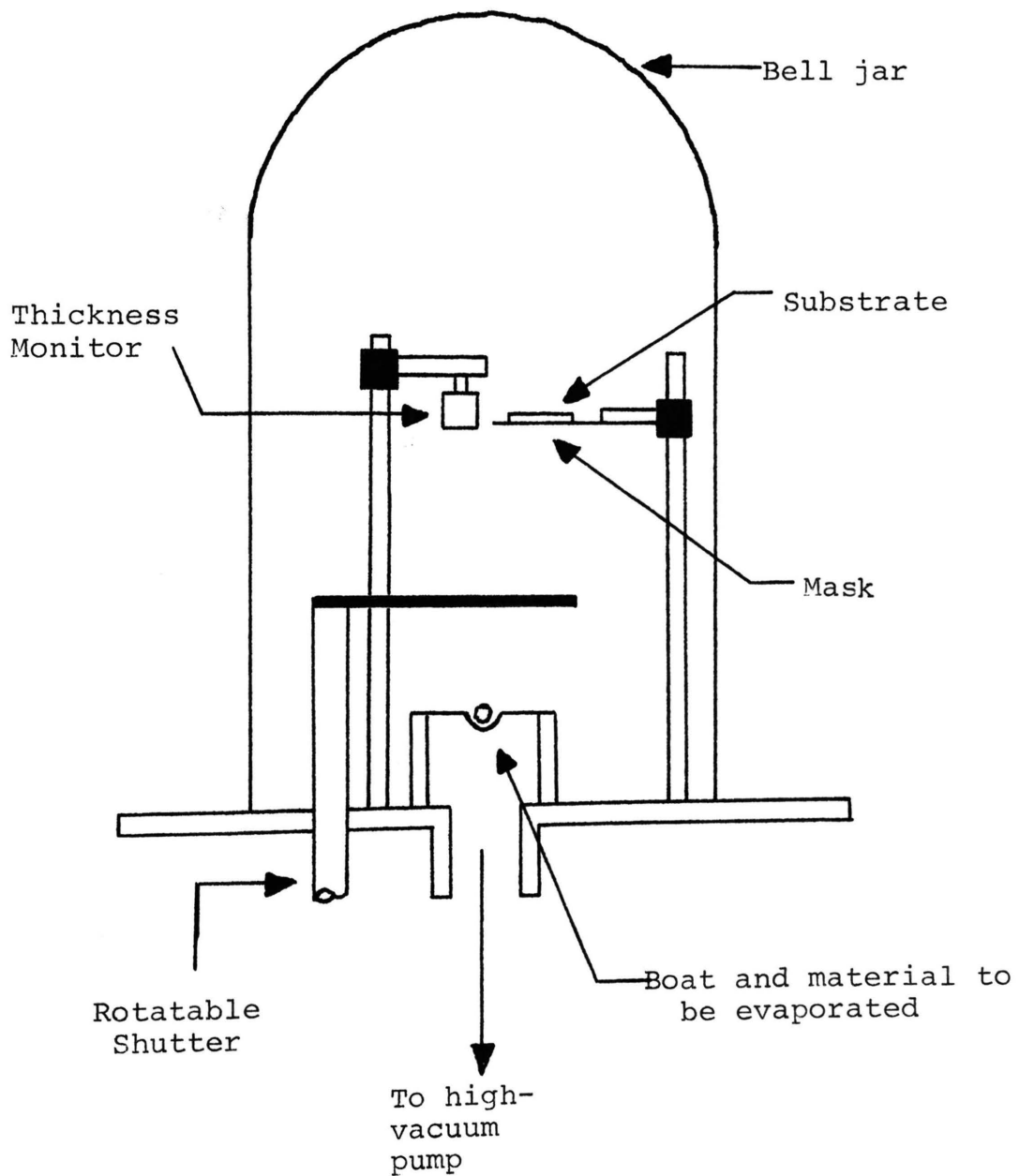


Figure 7-1. Principal parts of a system for thin-film deposition.

placed in a small "boat" made from a strip of refractory metal such as tungsten, molybdenum or tantalum. Alternatively the boat may be made by winding the refractory material into a coil-shaped basket. The material to be evaporated is then placed into the basket or attached to one of the edges. After the boat, or basket, and the substrate (the surface onto which the material is to be deposited) are mounted in the vacuum system, the system is evacuated to a low pressure.

When the desired vacuum has been achieved (10^{-5} to 10^{-7} mm Hg), the material is heated to the vaporization point by passing a current through the boat or basket. Table I. [38,43] shows several commonly used materials, the necessary temperature, and vacuum for proper evaporation.

TABLE III. Commonly used materials in thin-film deposition.		
MATERIAL	TEMPERATURE (°C)	PRESSURE (mm Hg)
Aluminum (Al)	812	10^{-6}
Nichrome (80% Ni, 20% Cr)	986	10^{-6}
Silver (Ag)	617	10^{-6}
Tantalum (Ta)	2240	10^{-6}
Silicon Monoxide (SiO)	1300	10^{-6}
Germanium (Ge)	957	10^{-6}

Initially, the material to be deposited is discharged in lumps. A shutter is interposed between the boat or basket and the substrate so as to block deposition onto the substrate until the rate of deposition approaches a steady value. After the rate attains a steady value, the shutter is moved, and the material is allowed to condense onto the substrate. Usually, some provision is made for heating the substrate so that the deposited material will form as smooth a layer as possible. If the substrate is considerably cooler than the material being deposited, the material is likely to deposit in lumps and form cracks or pin holes.

As is seen in sections C and D, the thickness of the material deposited is a critical factor in determining the value of the resistor or capacitor to be formed. Therefore some means of monitoring the thickness is required. Two popular methods for accomplishing this are the use of a rate monitor and optical interference methods. Both of these methods are discussed in considerable detail by Chopra [39] and Holland [40].

The first method, that of monitoring the rate at which the material is deposited, is often used as both monitor and controller. In other words, it can be used to monitor the film thickness and consequently regulate the rate of deposition. The rate of deposition is slowed down, and finally reduced to zero, as the desired thickness is approached. By using the deposited film as one arm of a

DC or AC Wheatstone bridge, the film resistance can be the controlling variable for the rate monitor [39]. When the desired value of resistance is attained, the bridge is balanced and signals the monitor to stop the deposition process. A similar procedure is to use the resistance of the film as the input resistor to a feedback operational amplifier. The output of the amplifier can be made a function of the film resistance [41] and used to control the rate of deposition.

The change in resonant frequency oscillation of a quartz crystal with change in mass can also be used to determine the film thickness [39]. This method, along with that of optical interference, is used to determine the thickness of films for which resistance measurements are difficult. For example, silicon monoxide is commonly used as the dielectric for thin film capacitors. The resistance is extremely high ($>10^{16}$ ohms) and is difficult to measure using the methods previously described.

The fundamental frequency for a quartz crystal is given by [40]

$$f = \frac{n}{2t} \times \left(\frac{C}{\rho}\right)^{\frac{1}{2}} \quad (7.1)$$

where n = overtone number, t = thickness of the crystal, C = shear elastic constant of the crystal, and ρ = density of the crystal. If the temperature of the crystal is accurately controlled, equation (7.1) may be rewritten as

$$f = \frac{N}{t} \quad (7.2)$$

where N is a constant depending upon the way the crystal is cut and the constants of equation (7.1).

From equation (7.2) it can be seen that if the thickness changes due to a deposited material, the resonant frequency of the crystal changes proportionately. This change in the resonant frequency provides the basis for the quartz-crystal monitor.

The sensitivity to change in mass deposited on the face of the crystal is more pronounced for higher-frequency crystals. For crystals in the 5-MHz range a 1-Hz change in frequency corresponds to a change in weight of about 1.8×10^{-8} grams/cm². This is translated into thickness by allowing only a small, accurately dimensioned space to be covered by the material being deposited. Knowledge of the density of the deposited material and the dimensions of the open area on the crystal face allow calculation of thickness from the change in the resonant frequency. Most quartz-crystal thickness monitors read out the thickness of the deposited film directly in angstrom units without the need for calculations by the observer.

The method of thickness determination by monitoring the reflected light intensity has also been used. The accuracy of measurement is dependent upon the accuracy of the knowledge of the frequency of the light source. With the advent of the laser as a practical tool in the

laboratory, the frequency of the light source is accurately known.

Thickness monitoring by use of light reflection is one of depositing the desired film onto a suitable substrate for which the refractive index is known and different from that of the deposited film. A monochromatic light is shone onto the surface, and the intensity of the reflected light is monitored. The intensity level is oscillatory with increasing film thickness. Film thickness is determined from the maxima or minima of the intensity of the reflected light. These maxima and minima occur at intervals given by [40]

$$2m \cdot \frac{\lambda}{4} = n_f t \quad (7.3)$$

where $2m$ = number of the maxima or minima, λ = wavelength of the reflected light (in microns), n_f = refractive index of the film, and t = film thickness (in microns).

As an example, the distributed networks built as part of this dissertation use SiO (silicon monoxide) as a dielectric; assume the desired thickness to be 1000 angstroms (0.1 microns) and the light source to be a helium-neon laser ($\lambda = 0.6328$ microns). Substitution of these values into equation (7.3) yields $2m = 12.64$. Physically, this value of $2m$ means that one would look for the 6th maximum and 0.32 of the way toward the next maximum. Most optical thickness monitors, like the quartz crystal monitors read

thickness directly.

2. Semiconductor p-n Junction. Since the author has not had the opportunity to work with the preparation of p-n junction devices by the diffusion process, the following discussion is intended to serve as an introduction to the topic. As is pointed out in Chapter I, if the distributed RC network is to be an integral part of an integrated circuit, the method of semiconductor fabrication of the network is preferable. The network can be formed using the same process as used for the rest of the integrated circuit [10,35,37].

The process discussed is only one of several in common use throughout the industry. However, since it is one of the easiest to use in terms of equipment needed and reproducibility of results, this discussion centers on the diffusion process. This process is called "open tube" diffusion due to the construction of the apparatus needed.

In a p-n junction device formed using silicon as the substrate, two semiconductor types, p and n, must be diffused. The process for diffusing the two are slightly different. The process starts with a silicon wafer, as pure as possible. The pure silicon wafer is obtained by a process known as "zone refining". If a thin molten region is made to pass down the length of a rod of impure silicon, the impurities in the silicon have a tendency to concentrate in the molten region. Thus, as the molten

region moves along the length of the rod, the impurities are swept out of the rod. After several passes the impurities are concentrated at one end, which is then cut off. What remains is a silicon rod of extremely high purity (less than one part per billion of impurity atoms).

This rod of highly purified silicon is then melted and a single crystal grown from it. The process is one of inserting a small crystal of silicon into the molten silicon. It is then slowly rotated and withdrawn; the molten silicon then solidifies onto the small crystal forming a much larger crystal of highly pure silicon.

The diffusion process of forming a p-n junction assumes the silicon to be already either p or n type. During the "pulling" process described above, an impurity is added to the molten silicon. Donor (for p-type) or acceptor (for n-type) impurities are added, depending upon the type of semiconductor material desired.

After a crystal has been formed of the desired length and diameter (8-10 inches and 1-2 inches, respectively), the crystal is cut into wafers about 0.01 inch thick. The wafers are then polished to a high level of smoothness and prepared for the diffusion process.

The diffusion process is one of diffusing a layer of impurity of the type opposite to that of the wafer into the wafer. A simplified diagram of a system used for the diffusion of n-type material into a p-type silicon wafer is shown in Figure 7-2. The silicon wafers are placed in a silica

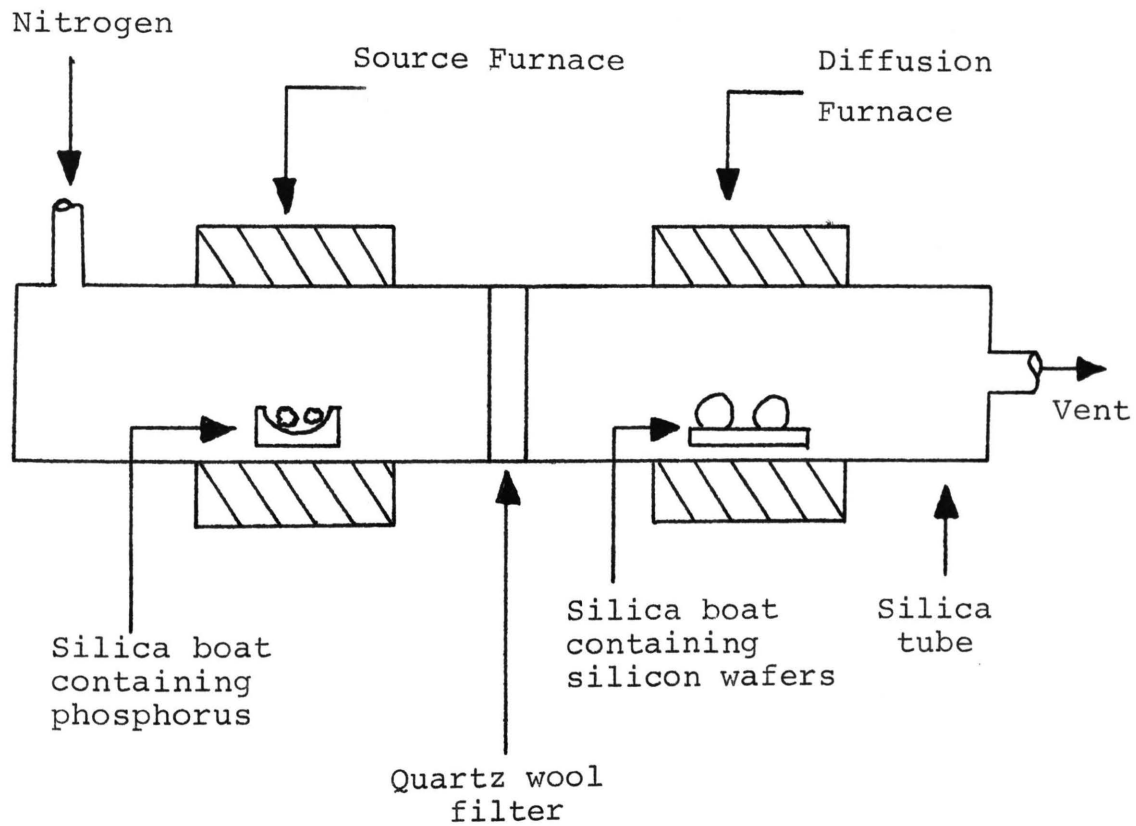


Figure 7-2. A simplified diffusion system for phosphorus.

boat and inserted into the silica tube which passes through the diffusion furnace. Another silica boat is loaded with the desired source material (commonly either solid-or-liquid-phosphorus) and placed into the source furnace. This method is called a two-zone system. The silicon wafers are held at about 2000°C, and the source at about 200°C. The nitrogen gas acts as the carrier for the phosphorus vapor. This saturated gas then passes into the diffusion furnace through the filter, which screens out any solid particles, over the silicon and finally out through the vent. The amount of phosphorus diffused into the silicon wafer is an approximate exponential function of the source and wafer temperatures.

When a layer of phosphorus has been diffused into the silicon wafer, an oxidizing gas, such as dry oxygen, is pumped into the diffusion furnace. The temperature of the diffusion furnace is unchanged during this process so that the depth of diffusion can be accurately controlled. The originally p-type silicon wafer now has a layer of n-type material diffused on one side such that the desired p-n junction has now been formed.

C. RESISTORS.

1. Introduction and Design Equations. The procedure for fabrication of a thin-film nichrome resistor is described by Herzog [42]. The equipment used by Herzog is similar in all important aspects to that used by the author (and

several undergraduates working on special problems under the direction of the author) for fabrication of thin-film resistors. Because of this similarity, the reader interested in the details is referred to Herzog's thesis.

a. Thin-Film. If thin-film resistors are to be used as part of an integrated circuit, additional steps are required. However, they do offer a much wider range of values, reduced temperature coefficients, and, since the resistivity of the layer may be selected independently, much closer tolerances are possible.

The resistance of a thin-film resistor is specified in terms of sheet resistance. The sheet resistivity [37] is the resistance of a square of the material used when one contact is along one side, and the other contact is along the other side. The resistance of this square is specified in ohms per square (ohms/sq) and is independent of the size of the square. An isolated segment of a thin film resistor has the resistance

$$R = \frac{\rho l}{A} = \frac{\rho l}{w t} \quad (7.4)$$

where ρ = resistivity of the material in ohms-cm, l = length of the segment, w = width of the segment, and t = thickness of the segment. If $w = l$ (i.e., a square is formed out of the segment), then w and l cancel leaving

$$R = \frac{\rho}{t} \text{ (ohms/square)}. \quad (7.5)$$

Using a material with a given sheet resistivity, the resistance of a given strip of the material is determined by use of the length to width ratio. Multiplication of the length to width ratio by the sheet resistivity yields the resistance of the strip of material. For example, if a resistor is formed from nichrome (sheet resistivity = 300 ohms/sq), and the length-to-width ratio is 100, the resistor has a value of

$$R = (300 \text{ ohms/sq})(100 \text{ squares}) = 30 \text{ k ohms}. \quad (7.6)$$

Most integrated circuit applications are limited to materials having sheet resistivities between 100 and 300 ohms per square because of fabrication costs and/or accuracies involved. Nichrome is one of the few exceptions. Several others are listed in Table II below.

TABLE IV. Sheet resistivities for materials used for thin film resistors. Thickness ranges from 200°A down to 1°A respectively.	
MATERIAL	SHEET RESISTIVITY (OHMS/SQ)
Nichrome (NiCr)	54-108,000
Tantalum (Ta)	7-1400
Aluminum (Al)	1.5-300
Cumet (Cl-SiO)	200-2500

b. Diffused Semiconductor. The resistance mechanism in a semiconductor resistor is entirely different from that in a thin-film resistor. Thin-film resistors have a large number of free electrons available for conduction, and, as a result, temperature has only a very slight effect on the value of resistance. However, the number of free electrons in a semiconductor is small, and temperature has a marked effect on the resistance. The lower the sheet resistivity, the less dependence the value has upon temperature.

Sheet resistivity for a semiconductor-diffused-resistor is given by [34]

$$R_s = \frac{1}{q \int_0^x \mu N dx} , \quad (7.7)$$

where q = electron charge = 1.6×10^{-19} coulombs, μ = mobility of the material, N = concentration of impurities, and x = diffusion depth. As might be expected, the resistance of the semiconductor resistor varies inversely with the number of free carriers available. The usual value of sheet resistance is approximately 100 to 200 ohms per square, which reflects a compromise between resistance values obtainable and a desirable temperature coefficient.

Even though the diffused semiconductor resistor has an undesirable temperature coefficient of resistance (up to $\pm 2,000$ ppm/ $^{\circ}$ C), it does have the desirable attribute of

"tracking". If two resistors are diffused on the same chip, the values may vary from the desired value, but the ratio of the resistances remains fixed, despite the large temperature coefficient.

The quantities associated with equation (7.7) are much more difficult to control in practice than those of equation (7.5). Therefore, the semiconductor resistor, although quite attractive from an integrated circuits point of view, is more difficult to fabricate with the same close tolerances as those of the thin-film variety.

2. Geometry. In order to achieve the resistance desired, it is quite often impossible to fabricate the resistor in a single straight strip. Both equations (7.5) and (7.7) may require that the length be so long as to not fit in the allocated area for the resistor. Recourse may be made to a material with a higher resistivity, or a smaller number of free carriers, but the best solution often lies in letting the resistor assume another shape. One possibility is shown in Figure 7-3 [34].

The cross-hatched areas are conducting strips made of a material with a resistivity much lower than that of the resistor. This geometry (with metallized horizontal edges) has a resistance quite easy to calculate, being merely the sum of the resistance squares in each vertical arm multiplied by the number of vertical arms. The current density in the resistive portion is uniform. Unfortunately,

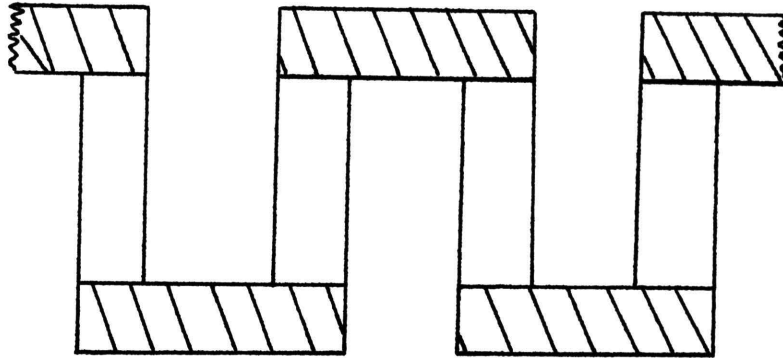


Figure 7-3. Typical geometry for uniformly distributed resistance.

there is quite an amount of wasted space due to the low resistance of the metallized horizontal segments.

The geometry can be modified such that the horizontal end segments are made of the same material as the rest of the network. Camenzind [34] discusses this situation and shows that if the end segments are made resistive, then the corners must be rounded in order to maintain a reasonable current density. If square inside corners are maintained, exceptionally high current densities occur with the result that the resistance around that portion of the network

becomes highly nonlinear. The recommended curvature for the loop is to make the radius of curvature for the inside edge

$$r_i = \frac{w}{2} \quad (7.8)$$

where w = width of the strip used as a resistor, and r_i = radius of curvature of the inside edge of the loop. Occasionally the outside edge of the loop is also rounded to have a radius of

$$r_o = \frac{3w}{2} \quad (7.9)$$

where w is again the width of the strip, and r_o is the radius of the outside edge of the loop.

D. CAPACITORS

1. Introduction and Design Equations. In the fabrication of a distributed RC network, the capacitor is formed as an integral part of the network. For example, a DRURC is formed by sandwiching a dielectric between two resistive layers. Therefore, after the geometry for the resistive layers has been decided upon, the capacitance of the distributed network is determined by the dielectric and the thickness of the dielectric. The plate area (A) of equation (7.10) has already been determined

$$\frac{C}{A} = \frac{\epsilon \epsilon_r}{t} = 8.85 \times 10^{-14} \frac{\epsilon}{t} \quad (\text{Farads/cm}^2) \quad (7.10)$$

by that area required for the resistance. However, as in all practical design situations, some trade-offs do occur. In this case, the trade-off comes between resistance (area and thickness) and capacitance (plate area, dielectric constant, and dielectric thickness). The thin-film varieties are the easier to design and fabricate, but, as with the resistors, the semiconductor version is more practical for use with integrated circuits.

a. Thin-Film. Since the area available for a distributed network in a typical microelectronic circuit application is limited, it is necessary to resort to the use of very thin (<500 angstroms) films formed of materials having as high a dielectric constant as possible. Occasionally, it is even necessary to stack several networks on top of one another and interconnect them such that the capacitances add together.

Equation (7.10) indicates that in order to obtain a large capacitor, the dielectric must be very thin. Unfortunately, films much thinner than 500 angstroms do not yield uniformly continuous layers. They tend to be thin in some spots and very thick in others; they are also easily damaged by structural faults and have low breakdown voltages

Table III [35] lists several common materials that are useful for the dielectric layer in a thin-film distributed network. The last entry in Table III must be flash evaporated [38-40], and, as a result, the film

thickness, as well as uniformity, is extremely difficult to control. Obviously, when the process is improved to the point where good yields were possible, BaSrTiO₃ would hold the key to large capacitances in distributed networks.

MATERIAL	ϵ	ELECTRICAL PERFORMANCE
SiO	5	0.005 μ F/cm ² (1 μ)
Al ₂ O ₃	8	0.31 μ F/cm ² (1 μ)
Ta ₂ O ₅	22	0.31 μ F/cm ² (1 μ)
BaSrTiO ₃	10 ³ -10 ⁴	8.85 μ F/cm ² (1 μ)

b. Diffused Semiconductor. The diffused semiconductor capacitor, although convenient for integrated circuits, exhibits several disadvantages. If high doping is used, the breakdown voltage is quite small (<10 volts), and these capacitors are polarity sensitive since they must be operated with a given amount of reverse bias. Still another disadvantage is the nonlinearity of the capacitance variation with applied voltage (see equation (7.11)).

The parameters of the p-n junction that yield a given capacitance are not as easily determined as they are for a thin-film capacitor. The capacitance of a p-n junction varies with the area and the dielectric constant of the material used just as with the thin-film capacitor. However, the distance between the conducting layers does not

remain constant as it does with the thin-film capacitor. This distance is the width of the depletion region surrounding the p-n junction. The thickness of this region changes with the square root of the applied voltage across the junction.

The capacitance of a semiconductor p-n junction distributed network is dependent upon the width of the depletion region. Since this width depends upon both the quantity of impurities on each side of the junction as well as the applied bias voltage, the expression for the capacitance will be considerably more complicated than equation (7.10).

It can be shown [35] that the width of the depletion region is given by

$$d = \left[\frac{2\epsilon\epsilon_0 (V_a + V_d) (N_a + N_d)}{qN_a N_d} \right]^{\frac{1}{2}} \quad (7.11)$$

where

N_d = concentration of donors in the n region

N_a = concentration of acceptors in the p region

q = electronic charge

ϵ = dielectric constant of material used

ϵ_0 = permittivity of free space

V_d = junction potential

V_a = applied bias across the junction.

The capacitance of the p-n junction now becomes

$$C = \frac{\epsilon \epsilon_0 A}{d} \quad (7.12)$$

or

$$C = A \left[\frac{q \epsilon \epsilon_0 N_a N_d}{2(V_a + V_d)(N_a + N_d)} \right]^{\frac{1}{2}} \quad (7.13)$$

As the applied bias voltage, V_a , is decreased, the capacitance across the p-n junction increases. In theory, at least, the capacitance approaches infinity as $V_a = -V_d$; however, at $V_a = -V_d$ the potential barrier across the junction is eliminated, and the resultant flow of carriers across the junction neutralizes the space charge, decreasing the voltage difference to zero. At this point, no capacitance exists across the junction.

Capacitances on the order of 10^4 pF per cm^2 can be achieved. These capacitors are, however, extremely nonlinear and, as a result, do not serve satisfactorily as coupling capacitors, since the signal voltage change across the junction changes the value of the capacitance. The nonlinearity can be used to cause a change in capacitance with applied voltage. This change in capacitance may be used to change the frequency of oscillation of an oscillator or cause the oscillator to start oscillating as a given capacitance is achieved.

E. THIN-FILM DESIGN EXAMPLE

As an example of the design of a uniformly distributed thin-film RC network, assume the desired R to be 30 k ohms and the capacitance to be 1000 pF. The largest space available for the network is 4 square centimeters. Choose NiCr with a sheet resistivity of 300 ohms/square for the resistive strip and assume the strip is 1 mm (=0.1 cm) wide. The number of squares needed for the resistor is therefore

$$\# \text{ of sq's} = \frac{R}{\text{ohms/sq}} = \frac{3 \times 10^4}{3 \times 10^2} = 100 \text{ squares.} \quad (7.14)$$

The area available for the capacitor plates is $lxw = (0.1)(100)(0.1) = 1 \text{ cm}^2$. Choosing SiO from Table II shows that the dielectric constant is 6 and the capacitance per square is $0.005 \mu\text{F/cm}^2$. This information into equation (7.10) gives the needed thickness to be

$$t_{\text{cm}} = 8.85 \times 10^{-14} \frac{\epsilon A}{C} = 53.1 \times 10^3 \text{ A}^\circ. \quad (7.15)$$

In summary, the resistive strip is 0.1 cm wide and 10 cm long, and the dielectric is $53.1 \times 10^3 \text{ A}^\circ$ thick. The 10 cm length is obtained by depositing the resistive strip in a pattern similar to Figure 7-3. The remainder of the problem involves the fabrication, and since many processes and equipment types exist, nothing is gained by a detailed discussion of the process. Details are given in several of the references already cited in this chapter.

VIII. CONCLUSIONS

A. SUMMARY

In conjunction with the rising interest in microelectronics and integrated circuits, much interest has been displayed in distributed-parameter networks. Since the RC distributed network may be fabricated using the same techniques, use of it in integrated circuits appears to be advantageous. The application of distributed networks has been hindered by the lack of a systematic set of design equations or a detailed procedure for application.

This dissertation attempts to overcome these difficulties by applying the IAM for each of four networks (\overline{URC} , \overline{TURC} , \overline{DRURC} , and \overline{TDRURC}) in deriving a set of equations that allows the designer to apply these networks to amplifier design; other sets of equations apply to the design of band-pass filters and phase-shift oscillators. Several examples illustrate the applications of these networks to various electronic circuits.

The \overline{URC} and \overline{DRURC} have already been discussed in detail by previous authors. The modification of these networks to yield the \overline{TURC} and the \overline{TDRURC} has not been covered before in much detail. The \overline{TURC} has been previously applied in a synthesis procedure, but no work (such as the development of the IAM) has been presented to extend its usefulness.

The $\overline{\text{TDRURC}}$ is a new network that has never been discussed or applied before. The IAM's of both the $\overline{\text{TURC}}$ and the $\overline{\text{TDRURC}}$ are contributions, therefore, to the state of the art in network design.

Since one of the goals of this dissertation is the application of uniformly distributed RC networks, it was necessary to derive the needed equations. Equations describing the input and output immittances, voltage and current transfer ratios, and transfer immittances were derived and applied to RC-coupled amplifiers. Equations necessary to the design of band-pass amplifiers and phase-shift oscillators were also derived.

The work on band-pass amplifiers and phase-shift oscillators has been previously suggested, but no details have been published. A set of curves allowing the design of a band-pass amplifier using a high-gain operational amplifier and a single $\overline{\text{DRURC}}$ is developed; to design the desired band-pass amplifier, the designer need specify only two of three variables: center frequency, bandwidth, or quality factor (Q). Previously published design procedures have not treated the problem of design where bandwidth or Q has been specified.

The $\overline{\text{DRURC}}$ may also be applied to the design of phase-shift oscillators. This is not, in itself, a new idea, but the use of the $\overline{\text{DRURC}}$ to replace some (or all) of the passive biasing elements in the single gain block, as well as the detailed design procedure, is new.

All of the previously mentioned applications have been illustrated by way of detailed example. Some of the circuits, such as the phase-shift oscillator, have been built and tested. Each of the test circuits gave good response and met all expectations.

The above applications lend themselves to integrated-circuit fabrication since each of the distributed networks may be constructed using basically the same techniques applied to integrated circuits. However, the problem of obtaining large capacitance (above several hundred pico-Farads) does remain a problem, especially for low-frequency RC-coupled amplifiers. A review of the methods of fabricating a distributed RC network is included because of the need for completeness, as well as the lack of material covering the fabrication of distributed networks per se.

The method of semiconductor p-n junction fabrication appears to be the most convenient in the sense that the distributed network can be formed at the same time as the rest of the integrated circuit. In situations where the distributed network alone is of interest, thin-film deposition is the most convenient. A chapter is included which reviews both fabrication processes including the methods and equipment used in each.

The analysis of any system containing distributed networks can be difficult at best, especially when the system contains lumped as well as distributed networks. The analysis of such a system is facilitated by decomposing the system

into separate, simpler mathematical models that are inter-related. The method of multiple-plane root locus, as is applied to the analysis of the $\overline{\text{DRURC}}$ phase-shift oscillator, may be used as well as the computer programs listed in the appendices.

B. SUGGESTIONS FOR FURTHER RESEARCH

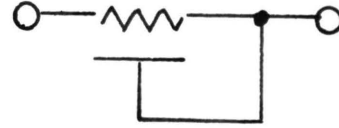
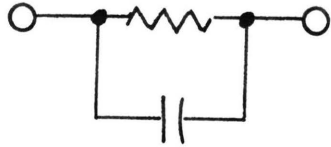
One suggestion is to have the results of this dissertation compared with the results obtained from using non-uniformly distributed RC networks. Several authors have reported sharper roll off characteristics obtained in low-pass filters by using exponentially tapered RC distributed networks. Perhaps for some of these specific applications a smaller total capacitance is required by using one of the tapered networks.

Another problem is the determination of the exact nature of the network. In other words, the design may specify a uniformly distributed network, but the fabrication process may yield a network with some slight deviation. Does this deviation radically change the performance of the distributed network? Some work should be done in the area of parameter identification.

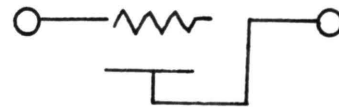
In the same vein as the previous paragraph, what happens to the performance of the network as the signal frequency is increased? Throughout this research the assumption of the ideal RC distributed network has been made. By ideal

it is meant that the network exhibits no inductive effects along the resistive layer(s) and that the dielectric has no loss. However, due to the geometry of the resistive layer(s) at some relatively high frequency the inductance may become appreciable, perhaps even resonant with the capacitance layer. The frequency of resonance and effect on the operation of the network should be investigated.

The frequency-response characteristics of the $\overline{\text{TURC}}$ may allow it to be used as a lead or lag compensation network. Figure 8-1 illustrates the idea by making use of the series and parallel replacement for the RC lumped networks. Figure 8-2 shows a lead and a lag network realization utilizing the $\overline{\text{TURC}}$.

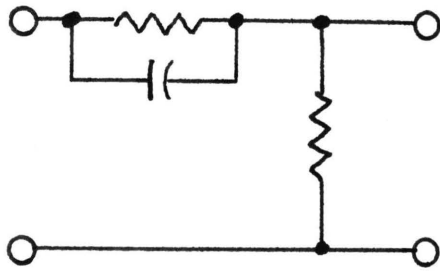


(a)

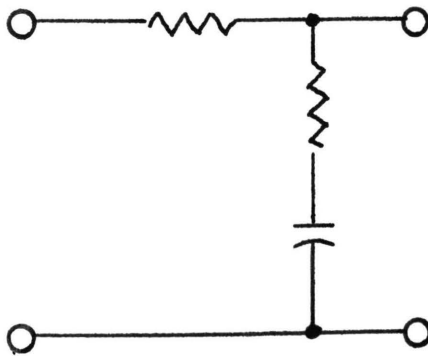
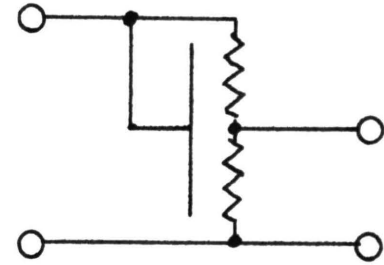


(b)

Figure 8-1. (a) Distributed RC parallel and (b) Distributed RC series replacement networks and the lumped RC counterparts.



(a)



(b)

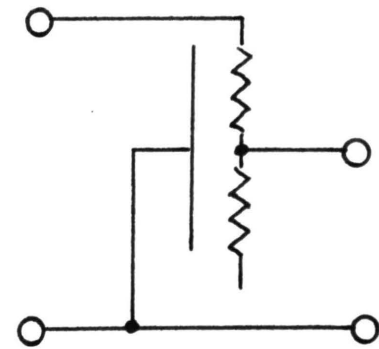


Figure 8-2. Suggested RC distributed network replacements for (a) lead and (b) lag compensation networks.

BIBLIOGRAPHY

1. Ghausi, M. S., Kelly, J. J.. Introduction to Distributed-Parameter Networks. New York: Holt, Rinehart, and Winston, 1968.
2. Holt, A. G. J., Bowron, P., "The General Realization of Rational Transfer Functions Using Single-and Double-Contoured Heizer Distributed Networks," IEEE Trans. on Circuit Theory, Vol. CT-16, No. 1 (February 1969), pp. 76-81.
3. Peirson, R. C., Bertnolli, E. C., "Numerical Calculation of Distributed-Network Transfer Matrices," IEEE Trans. on Circuit Theory, Vol. CT-16, No. (November 1969), pp. 579-581.
4. Hensley, R. D., "Distributed Network Realizations for the Simulation of Partial Differential Equations," UMR Ph.D. Dissertation, 1972.
5. Happ, W. W., Castro, P. S., "Distributed Parameter Circuits and Microsystem Electronics", Proc. National Electronics Conference (1960), pp. 448-460.
6. Wyndrum, R. W., Jr., "The Exact Synthesis of Distributed RC Networks," Technical Rep. 400-76, Lab. for Electro-science Research, Dept. of Electrical Engineering, New York Univ., May 1963.
7. Smith, A. B., Cooper, G. F., "Printed Distributed RC Networks," Electrical Manufacturing, Vol. 58, No. 5 (November 1958), p. 121.
8. Smith, A., "Rejection Filters With Distributed R and C", Proc. 1960 Electronics Components Conf. (May 1960).
9. Archer, F., "Stability and Synthesis of Transfer Functions in $\omega = e^{\sqrt{T}(s^2+bs+c)}$ and $\theta = \sqrt{T}(s^2+bs+c)$ ", UMR Master's Thesis, 1971.
10. Gray, P. E., Searle, C. L.. Electronic Principles: Physics, Models, and Circuits. New York: John Wiley and Sons, 1969.
11. Chirlian, P. M. . Integrated and Active Network Analysis and Synthesis. Englewood Cliffs, New Jersey: Prentice-Hall, 1967.
12. Newcomb, R. W.. Active Integrated Circuit Synthesis. Englewood Cliffs, New Jersey: Prentice-Hall, 1968.
13. Weinberg, L.. Network Analysis and Synthesis. New York: McGraw-Hill,

14. Kaupman, W. M., Garrett, "Tapered Distributed Filters", IRE Trans. on Circuit Theory, Vol. CT-9, No. 4 (December 1962), pp. 329-336.
15. Walsh, J., Giguere, J. C., Swamy, M. N. S., "Active Filter Design Using Exponentially Tapered RC Lines", IEEE International Symp. on Circuit Theory, Symp. Digest (December 1969), p. 110.
16. Hayes, R. A., "Distributed RC Circuits in Multi-vibrations," Tenth Annual Allerton Conf. on Circuit and System Theory (October 1972).
17. Ruston, H., Bordogna, J.. Electric Networks: Functions, Filters, Analysis. New York: McGraw-Hill, 1966.
18. Balabanian, N., Bickert, T. A.. Electrical Network Theory. New York: John Wiley and Sons, 1969.
19. Leon, B. J., Wintz, P. A.. Basic Linear Networks for Electrical and Electronics Engineers. New York: Holt, Rinehart, and Winston, 1970.
20. Strauss, L.. Wave Generation and Shaping. New York: McGraw-Hill, 1970.
21. Wylie, C. R., Jr.. Advanced Engineering Mathematics. New York: McGraw-Hill, 1960.
22. Bertnolli, E. C., "Analysis of the n-Wire Exponential Line," Proc. IEEE, Vol. 55, p. 1225, 1967.
23. Mahdi, H., "Synthesis of Low-Pass Linear Phase Active Circuits Using Distributed RC Networks," IEEE International Symp. on Circuit Theory, Symp. Digest (December 1969), pp. 102-104.
24. Kerwin, W. J., "RC Active Networks," in Papers on Integrated Circuit Synthesis, compiled by R. W. Newcomb and T. Rao, Stanford Electronics Laboratories, Technical Report No. 6560-4, June 1966.
25. Lin, H. C.. Integrated Electronics. San Francisco: Holden-Day, 1967.
26. Carson, J. A., et al., "Effects of Dielectric Laser on the Performance of Thin Film Distributed Notch Filters," Journal Solid State Circuits, June 1971.
27. Lemke, P. B., "A Distributed RC Network Broadband F.M. Discriminator in Thin Film," Conference on Integrated Circuits, Congress Theatre, Eastborne, Sussax, England (May 1967).

28. Castro, P. S., Nichols, A. J., Kaiser, H. R., "Distributed Parameter Circuit Design Techniques," IRE Wescon Convention Record, 1962.
29. Happ, W. W., Fuller, W. D., "Design Procedures For Film Type Distributed Parameter Circuits," Proc. National Electronics Conf. (1961), pp. 597-610.
30. Kaufman, W. M., "Theory of a Monolithic Null-Device and Some Novel Circuits," IRE Proc., Vol. 48 (September 1960).
31. Bourquin, J. J., "Stability of a Class of Lumped-Distributed Systems," Journal of the Franklin Institute, Vol. 287, No. 5, (May 1969).
32. Mitra, S. K., Analysis and Synthesis of Linear Active Networks. New York: John Wiley and Sons, 1969.
33. Tobey, G. E., Graeme, J. G., Huelsman, L. P., Ed's. Operational Amplifiers: Design and Applications. New York: McGraw-Hill, 1971.
34. Camenzind, H. R., Circuit Design for Integrated Electronics. Massachusetts: Addison-Wesley, 1968.
35. Levine, S. N., Principles of Solid-State Microelectronics. New York: Holt, Rinehart, and Winston, 1963.
36. Chirlian, P. M., Electronic Circuits: Physical Principles, Analysis and Design. New York: McGraw-Hill, 1971.
37. Doyle, J. M., Thin Film and Semiconductor Integrated Circuitry. New York: McGraw-Hill, 1966.
38. Maissel, L. I., Handbook of Thin Film Technology. New York: McGraw-Hill, 1970.
39. Chopra, K. L., Thin Film Phenomena. New York: McGraw-Hill, 1969.
40. Holland, L., Thin Film Microelectronics. New York: John Wiley and Sons, 1965.
41. Turner, J. A., et al., "A Method for Continuous Measurement of Thickness and Deposition Rate of Conducting Films During A Vacuum Deposition," J. Sci. Instruments, Vol. 40, (1963), pp. 557-561.
42. Herzog, R. R., "Thin Film Resistor Deposition," Umr Master's Thesis, 1965.

43. "The Sloan Notebook of Thin Film Technology,"
Sloan Technology Corp., Santa Barbara, California.
44. Haykin, S. S., Active Network Theory. Massachusetts:
Addison-Wesley, 1970.

VITA

Michael Flynn Kavanaugh was born on March 23, 1940, in Little Rock, Arkansas. He received his primary and secondary education in Henderson, Kentucky, Webster Groves, Missouri, and graduated from high school in Hattiesburg, Mississippi. He received his undergraduate education from Mississippi State University, in State College, Mississippi and received a Bachelor of Science degree in Physics and Applied Mathematics from the University of Southern Mississippi, in Hattiesburg, Mississippi, in 1962. From 1962 to 1964 he was employed by Lockheed Missiles and Space Company.

In 1964, he enrolled in the Graduate School at the University of Arkansas, Fayetteville, Arkansas and was awarded the Master of Science degree in Electrical Engineering in 1966. From 1967 to 1971 he was Assistant Professor of Electronic Engineering at Northrop Institute of Technology, Inglewood, California. In 1971 he was awarded an Academic Leave Grant to complete the work on his Ph.D. From August 1971 to August 1973 he was employed as an Instructor in the Electrical Engineering Department, University of Missouri - Rolla, Rolla, Missouri.

He and his wife, Nancy, are the parents of three daughters (Joyce, Catherine, and Melinda) and one son (David).

APPENDICES

- A. $\overline{\text{URC}}$ IAM
- B. $\overline{\text{TURC}}$ IAM
- C. $\overline{\text{DRURC}}$ IAM
- D. $\overline{\text{TDRURC}}$ IAM
- E. $\overline{\text{TURC}}$ VOLTAGE RATIO AS ϕ APPROACHES INFINITY
- F. MANUAL VERIFICATION OF THE LOWER 3-db FREQUENCY
OF THE DISTRIBUTED NETWORK RC COUPLED AMPLIFIER
- G. FREQUENCY RESPONSE CURVES OF THE DISTRIBUTED NETWORKS
IN FIGURE 6-1 AND THE $\overline{\text{DRURC}}$ IN FIGURE 6-2

A. $\overline{\text{URC}}$ IAM

The program below is used to calculate the numerical values of the elements of indefinite admittance matrix, (2.18). The program is to be used with the program in Appendix B.

```

1.  COMPLEX RTPH1, CSQRT, CMLPX, THETA1, THETA2,
    CEXP, X1, X2, Z1, Z2, RATIO1, RATIO2,
    RATIO3, RATIO4, Y11A, Y12A, Y13A, Y21A,
    Y22A, Y23A, Y31A, Y32A, Y33A, Y11B, Y12B,
    Y13B, Y21B, Y22B, Y23B, Y31B, Y32B, Y33B
2.  REAL*4 N, K1, K2
C   PUT IN HERE THE DESIRED VALUES FOR N AND R
C   PH1 =  $\omega RC$ 
3.  K1 = 1.0/((1.0-N)*R)
4.  K2 = 1.0/(N*R)
5.  RTPH1 = CSQRT(CMLPX(0.0,PH1))
6.  THETA1 = (1.0-N)*RTPH1
7.  THETA2 = N*RTPH1
8.  X1 = CEXP(THETA1)
9.  X2 = CEXP(THETA2)
10. Z1 = CEXP(2.0*THETA1)
11. Z2 = CEXP(2.0*THETA2)
12. RATIO1 = THETA1*(Z1+1.0)/(Z1-1.0)
13. RATIO2 = 2.0*THETA1*X1/(Z1-1.0)
14. RATIO3 = THETA2*(Z2+1.0)/(Z2-1.0)
15. RATIO4 = 2.0*THETA2*X2/(Z2-1.0)
16. Y11A = K1*RATIO1
17. Y12A = K1*(RATIO2-RATIO1)
18. Y13A = K1*(-RATIO2)
19. Y21A = Y12A
20. Y22A = K1*2.0*(RATIO1-RATIO2)
21. Y23A = Y12A
22. Y31A = Y13A
23. Y32A = Y12A
24. Y33A = Y11A
25. Y11B = K2*RATIO3
26. Y12B = K2*(RATIO4-RATIO3)
27. Y13B = K2*(-RATIO4)
28. Y21B = Y12B
29. Y22B = K2*2.0*(RATIO3-RATIO4)
30. Y23B = Y12B
31. Y31B = Y13B
32. Y32B = Y12B
33. Y33B = Y11B

```

B. $\overline{\text{TURC}}$ IAM

This WAT5 program can be used for the numerical calculation of the IAM parameters for a $\overline{\text{TURC}}$. It gives the numerical values for the elements of (4.1) for given N, R, and ϕ . The main part of the program is composed of the program shown in Appendix A.

1. **COMPLEX** The complex statement here is the same as that for the $\overline{\text{URC}}$ program of Appendix A. With the additions shown below it serves as the complex statement for the $\overline{\text{TURC}}$ program.

Y11, Y12, Y13, Y14, Y21, Y22, Y23, Y24, Y31,
Y32, Y33, Y34, Y41, Y42, Y43, Y44

2. **REAL*4** N, K1, K2

Since this is a program for the calculation of the $\overline{\text{TURC}}$ IAM parameters, a value for N must be inserted as well as values for PH1, R, and Y_L .

3. $K1 = 1.0 / ((1.0 - N) * R)$
4. $K2 = 1.0 / (N * R)$
5. $RTPH1 = \text{CSQRT}(\text{CMPLX}(0.0, \text{PH1}))$
6. $\text{THETA1} = (1.0 - N) * RTPH1$
7. $\text{THETA2} = N * RTPH1$
8. $X1 = \text{CEXP}(\text{THETA1})$
9. $X2 = \text{CEXP}(\text{THETA2})$
10. $Z1 = \text{CEXP}(2.0 * \text{THETA1})$
11. $Z2 = \text{CEXP}(2.0 * \text{THETA2})$
12. $\text{RATIO1} = \text{THETA1} * (Z1 + 1.0) / (Z1 - 1.0)$
13. $\text{RATIO2} = 2.0 * \text{THETA1} * X1 / (Z1 - 1.0)$
14. $\text{RATIO3} = \text{THETA2} * (Z2 + 1.0) / (Z2 - 1.0)$
15. $\text{RATIO4} = 2.0 * \text{THETA2} * X2 / (Z2 - 1.0)$
16. $Y11A = K1 * \text{RATIO1}$
17. $Y12A = K1 * (\text{RATIO2} - \text{RATIO1})$
18. $Y13A = K1 * (-\text{RATIO2})$
19. $Y21A = Y12A$
20. $Y22A = K1 * 2.0 * (\text{RATIO1} - \text{RATIO2})$
21. $Y23A = Y12A$
22. $Y31A = Y13A$
23. $Y32A = Y12A$
24. $Y33A = Y11A$
25. $Y11B = K2 * \text{RATIO3}$
26. $Y12B = K2 * (\text{RATIO4} - \text{RATIO3})$
27. $Y13B = K2 * (-\text{RATIO4})$
28. $Y21B = Y12B$

29. $Y22B = K2 * 2.0 * (RATIO3 - RATIO4)$
30. $Y23B = Y12B$
31. $Y31B = Y13B$
32. $Y32B = Y12B$
33. $Y33B = Y11B$
34. $Y11 = Y11A$
35. $Y12 = Y12A$
36. $Y13 = (0.0, 0.0)$
37. $Y14 = Y13A$
38. $Y21 = Y12$
39. $Y22 = Y22A + Y22B$
40. $Y23 = Y23B$
41. $Y24 = Y23A + Y21B$
42. $Y31 = Y13$
43. $Y32 = Y23$
44. $Y33 = Y31B$
45. $Y34 = Y13B$
46. $Y41 = Y14$
47. $Y42 = Y24$
48. $Y43 = Y34$
49. $Y44 = Y33A + Y11B$

C. DRURC IAM

The program shown below can be used for the calculation of numerical values for the elements of the indefinite admittance matrix (2.11). This program forms the basis for the program shown in Appendix D. It is for use in the next program, and that is the reason for the A and B subscripts on each of the Y terms.

1. COMPLEX RTPH1, CSQRT, CMLPX, GAMMA1, GAMMA2,
CEXP, X1, X2, Z1, Z2, RATIO1, RATIO2,
RATIO3, RATIO4, Y11A, Y12A, Y13A, Y14A, Y21A,
Y22A, Y23A, Y24A, Y31A, Y32A, Y33A, Y34A,
Y41A, Y42A, Y43A, Y44A, Y11B, Y12B, Y13B,
Y14B, Y21B, Y22B, Y23B, Y24B, Y31B, Y32B,
Y33B, Y34B, Y41B, Y42B, Y43B, Y44B, DELTA
2. REAL*4 N1, N2, K1, K2
PUT IN HERE THE DESIRED VALUES FOR Y_s , Y_L , N1, N2, R, AND
PH1 ($=\omega(1+N1)RC$). IF THE Y PARAMETERS FOR THE DRURC ALONE
ARE DESIRED, PUT N2=0.
3. K1 = 1.0/((1.0+N1)*(1.0-N2)*R)
4. K2 = 1.0/((1.0+N1)*N2*R)
5. 20 RTPH1 = CSQRT(CMLPX(0.0,PH1))
6. GAMMA1 = (1.0-N2)*RTPH1
7. GAMMA2 = N2*RTPH1
8. X1 = CEXP(GAMMA1)
9. X2 = CEXP(GAMMA2)
10. Z1 = CEXP(2.0*GAMMA1)
11. Z2 = CEXP(2.0*GAMMA2)
12. RATIO1 = GAMMA1*(Z1+1.0)/(Z1-1.0)
13. RATIO2 = 2.0*GAMMA1*X1/(Z1-1.0)
14. RATIO3 = GAMMA2*(Z2+1.0)/(Z2-1.0)
15. RATIO4 = 2.0*GAMMA2*X2/(Z2-1.0)
16. Y11A = K1*(RATIO1+N1)
17. Y12A = K1*(1.0-RATIO1)
18. Y13A = K1*(RATIO2-1.0)
19. Y14A = K1*(-RATIO2-N1)
20. Y21A = Y12A
21. Y22A = K1*(RATIO1+1.0/N1)
22. Y23A = K1*(-RATIO2-1.0/N1)
23. Y24A = Y13A
24. Y31A = Y13A
25. Y32A = Y23A
26. Y33A = Y22A

27. Y34A = Y12A
28. Y41A = Y14A
29. Y42A = Y24A
30. Y43A = Y34A
31. Y44A = Y11A
32. Y11B = $K2 * (RATIO3 + N1)$
33. Y12B = $K2 * (1.0 - RATIO3)$
34. Y13B = $K2 * (RATIO4 - 1.0)$
35. Y14B = $K2 * (-RATIO4 - N1)$
36. Y21B = Y12B
37. Y22B = $K2 * (RATIO3 + 1.0 / N1)$
38. Y23B = $K2 * (-RATIO4 - 1.0 / N1)$
39. Y24B = Y13B
40. Y31B = Y13B
41. Y32B = Y23B
42. Y33B = Y22B
43. Y34B = Y12B
44. Y41B = Y14B
45. Y42B = Y13B
46. Y43B = Y34B
47. Y44B = Y11B
48. DELTA = Y33A + Y22B

D. $\overline{\text{TDRURC}}$ IAM

The program below applies the program shown in Appendix C and adds to it. It can be used to find numerical values for the elements of the $\overline{\text{TDRURC}}$ indefinite admittance matrix shown in (3.1).

1. COMPLEX The complex statement here is the same as for the program in Appendix C except for the additions shown below.

Y11, Y12, Y13, Y14, Y15, Y21, Y22, Y23, Y24, Y25,
Y31, Y32, Y33, Y34, Y35, Y41, Y42, Y43, Y44, Y45,
Y51, Y52, Y53, Y54, Y55

Since this is a program for the calculation of $\overline{\text{TDRURC}}$ IAM parameters, a value for N2 must be inserted between steps 2 and 3 of the program in Appendix C. This is the same location as that for the values for N1, R, and PH1 for the previous program.

2. REAL*4 N1, N2, K1, K2
3. K1 = 1.0/((1.0+N1)*(1.0-N2)*R)
4. K2 = 1.0/((1.0+N1)*N2*R)
5. 20 RTPH1 = CSORT(CMPLX(0.0,PH1))
6. GAMMA1 = (1.0-N2)*RTPH1
7. GAMMA2 = N2*RTPH1
8. X1 = CEXP(GAMMA1)
9. X2 = CEXP(GAMMA2)
10. Z1 = CEXP(2.0*GAMMA1)
11. Z2 = CEXP(2.0*GAMMA2)
12. RATIO1 = GAMMA1*(Z1+1.0)/(Z1-1.0)
13. RATIO2 = 2.0*GAMMA1*X1/(Z1-1.0)
14. RATIO3 = GAMMA2*(Z2+1.0)/(Z2-1.0)
15. RATIO4 = 2.0*GAMMA2*X2/(Z2-1.0)
16. Y11A = K1*(RATIO1+N1)
17. Y12A = K1*(1.0-RATIO1)
18. Y13A = K1*(RATIO2-1.0)
19. Y14A = K1*(-RATIO2-N1)
20. Y21A = Y12A
21. Y22A = K1*(RATIO1+1.0/N1)
22. Y23A = K1*(-RATIO2-1.0/N1)
23. Y24A = Y13A
24. Y31A = Y13A
25. Y32A = Y23A
26. Y33A = Y22A

```

Y34A = Y12A
Y41A = Y14A
Y42A = Y24A
Y43A = Y34A
Y44A = Y11A
Y11B = K2*(RATIO3+N1)
Y12B = K2*(1.0-RATIO3)
Y13B = K2*(RATIO4-1.0)
Y14B = K2*(-RATIO4-N1)
Y21B = Y12B
Y22B = K2*(RATIO3+1.0/N1)
Y23B = K2*(-RATIO4-1.0/N1)
Y24B = Y13B
Y31B = Y13B
Y32B = Y23B
Y33B = Y22B
Y34B = Y12B
Y41B = Y14B
Y42B = Y13B
Y43B = Y34B
Y44B = Y11B
DELTA = Y33A+Y22B
Y11 = Y11A-Y13A*Y31A/DELTA
Y12 = Y12A-Y13A*Y32A/DELTA
Y13 = -Y13A*Y23B/DELTA
Y14 = -Y13A*Y24B/DELTA
Y15 = Y14A-Y13A*(Y34A+Y21B)/DELTA
Y21 = Y12
Y22 = Y22A-Y23A*Y32A/DELTA
Y23 = -Y23A*Y23B/DELTA
Y24 = -Y23A*Y24B/DELTA
Y25 = Y24A-Y23A*(Y34A+Y21B)/DELTA
Y31 = Y13
Y32 = Y23
Y33 = Y33B-Y32B*Y23B/DELTA
Y34 = Y34B-Y32B*Y24B/DELTA
Y35 = Y31B-Y32B*(Y34A+Y21B)/DELTA
Y41 = Y14
Y42 = Y24
Y43 = Y34
Y44 = Y44B-Y42B*Y24B/DELTA
Y45 = Y41B-Y42B*(Y34A+Y21B)/DELTA
Y51 = Y15
Y52 = Y25
Y53 = Y35
Y54 = Y45
Y55 = (Y44A+Y11B) - (Y42A+Y21B) * (Y34A+Y21B)/DELTA

```

E. $\overline{\text{TURC}}$ VOLTAGE RATIO AS ϕ APPROACHES INFINITY

For the $\overline{\text{TURC}}$, the voltage transfer ratio is given by

$$\frac{V_0}{V_i} = \frac{Y_s Y_{42}}{Y_{42} Y_{24} - (Y_L + Y_{44})(Y_s + Y_{22})} \quad (\text{E.1})$$

Using equation (4.2) and investigating only the numerator of (E.1) (Y_L and Y_s are assumed to be passive circuit element combinations)

$$Y_s Y_{42} = Y_s \left[\frac{\theta^*}{R^*} \left(\frac{1 - \cosh \theta^*}{\sinh \theta^*} \right) - \frac{\theta^{**}}{R^{**}} \left(\frac{1 - \cosh \theta^{**}}{\sinh \theta^{**}} \right) \right] \quad (\text{E.2})$$

Since,

$$\frac{\theta^*}{R^*} = \frac{(1-N) \sqrt{j\phi}}{(1-N)R} = \frac{\sqrt{j\phi}}{R} \quad (\text{E.3a})$$

$$\frac{\theta^{**}}{R^{**}} = \frac{N \sqrt{j\phi}}{NR} = \frac{\sqrt{j\phi}}{R} \quad (\text{E.3b})$$

these terms may be factored out of (E.2). Assuming Y_s is not zero, only Y_{42} need be investigated.

$$Y_{42} = \frac{\sqrt{j\phi}}{R} \left[\left(\frac{1 - \cosh \theta^*}{\sinh \theta^*} \right) - \left(\frac{1 - \cosh \theta^{**}}{\sinh \theta^{**}} \right) \right] \quad (\text{E.4})$$

As ϕ approaches infinity, both θ^* and θ^{**} approach infinity as well. Therefore,

$$\frac{1 - \cosh \theta^*}{\sinh \theta^*} \Bigg|_{\theta^* \rightarrow \infty} = \frac{-e^{\theta^*}}{e^{\theta^*}} = -1 \quad (\text{E.5a})$$

and

$$\frac{1 - \cosh \theta^{**}}{\sinh \theta^{**}} \Bigg|_{\theta^{**} \rightarrow \infty} = \frac{-e^{\theta^{**}}}{e^{\theta^{**}}} = -1. \quad (\text{E.5b})$$

These values substituted into equation (E.4) yield the desired result of forcing the numerator of (E.1) to zero as ϕ approaches infinity.

F. MANUAL VERIFICATION OF THE LOWER 3-db FREQUENCY OF THE
DISTRIBUTED NETWORK RC COUPLED AMPLIFIER

The following is presented as a manual verification of the computer program used for developing the response curve and 3-db values given in Chapter VI.

Using the expression for V_0/I ; (see equation (6.2)), the magnitude is found manually at both the lower 3-db frequency and the midband gain frequency of the amplifier (i.e., 980 Hz and 5500 Hz).

<u>f (Hz)</u>	<u>Magnitude</u>
980.0	57.533
5500.0	64.550

The ratio of the magnitude at 980 Hz to the magnitude at 5500 Hz is 0.89129. This value cubed is 0.70804.

This value is close (within 0.14%) to the desired value of 0.70711 and therefore verifies the 3-db frequency of the amplifier.

G. FREQUENCY RESPONSE CURVES OF THE DISTRIBUTED NETWORKS
IN FIGURES 5-3 AND 6-1 AND THE DR \overline{URC} IN FIGURE 6-2

The frequency response curves on the following pages represent the magnitudes of the indicated equations versus ϕ . The values of R , Y_L , Y_S , and N (or N_1 and N_2) are listed on the figures.

The values of the ϕ_{3db} points are indicated on each figure. This is to aid the reader in locating the ϕ_{3db} values for use with the appropriate network.

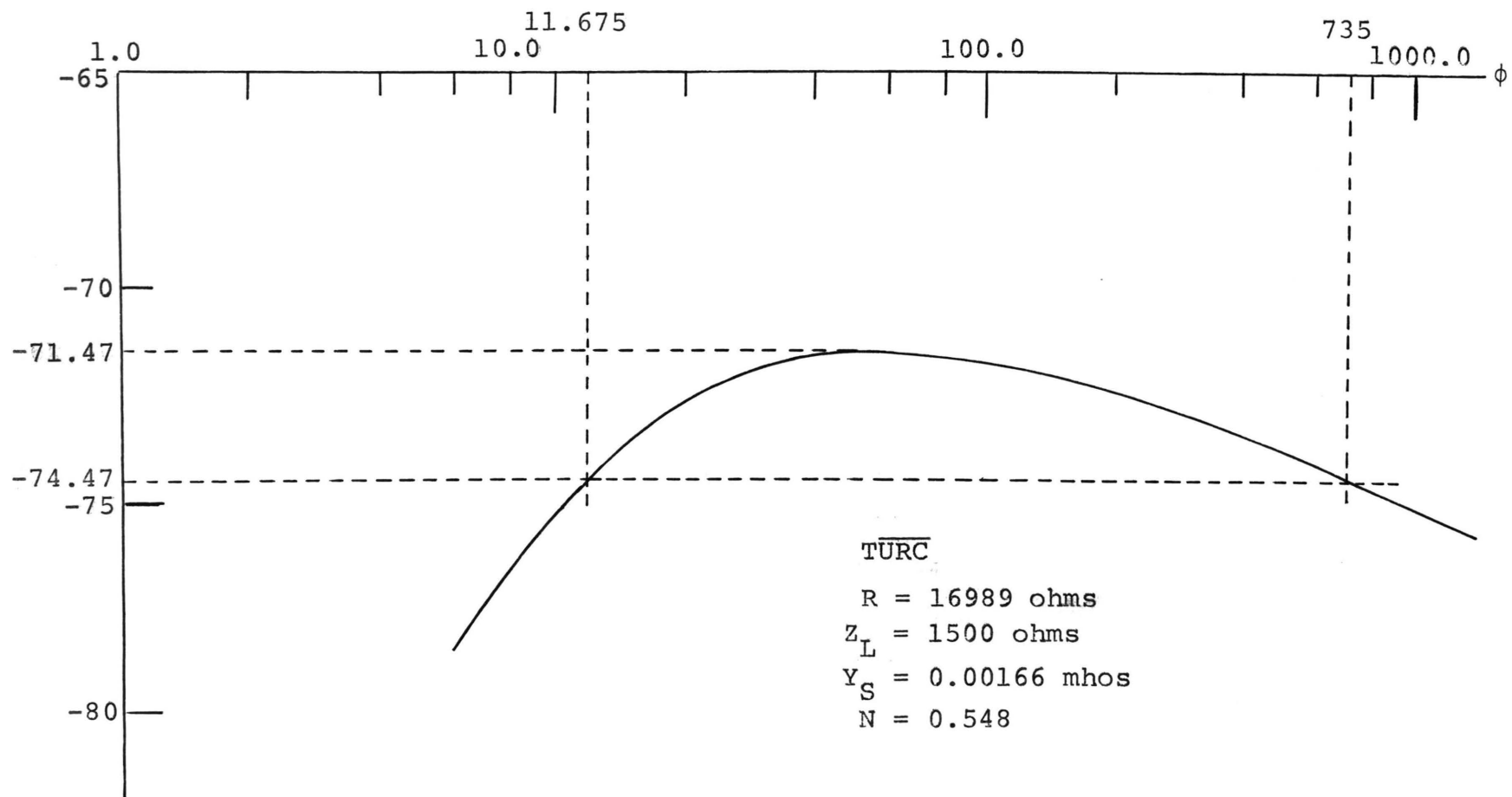


Figure G-1. Magnitude of equation (4.8) versus $\phi = \omega RC$.

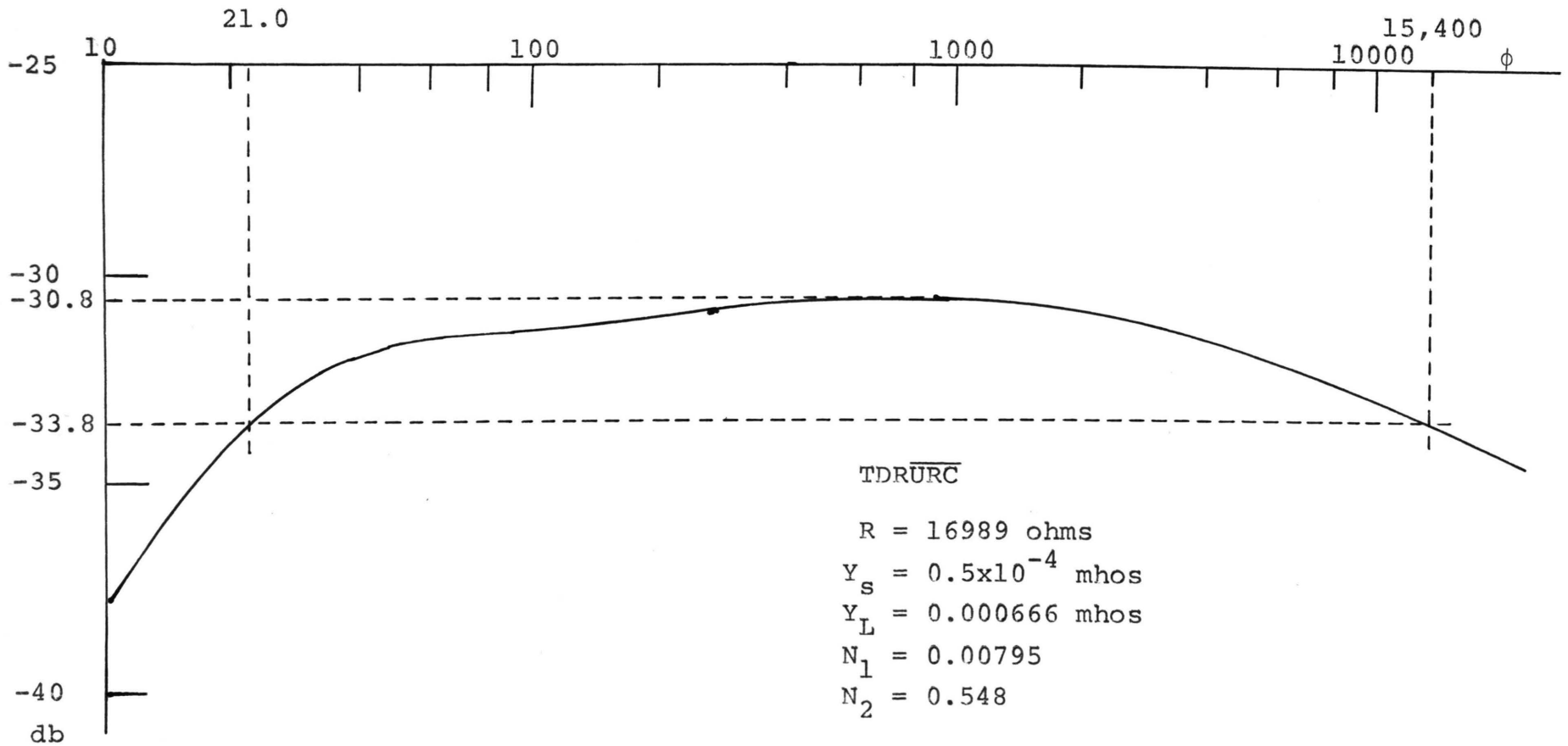


Figure G-2. Magnitude of equation (3.13) versus $\phi = \omega(1+N)RC$.

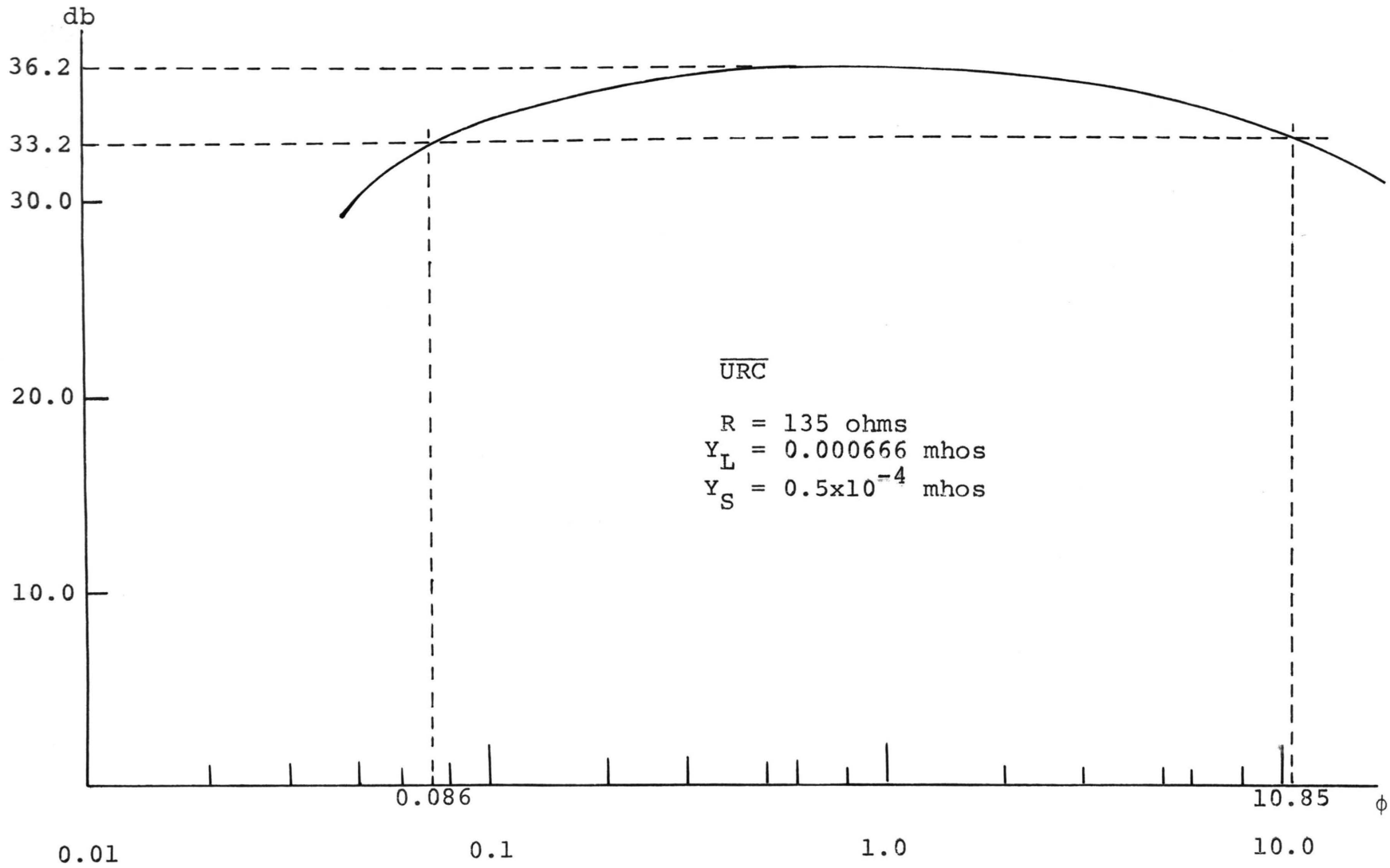


Figure G-3. Magnitude of equation (6.2) versus $\phi = \omega RC$.

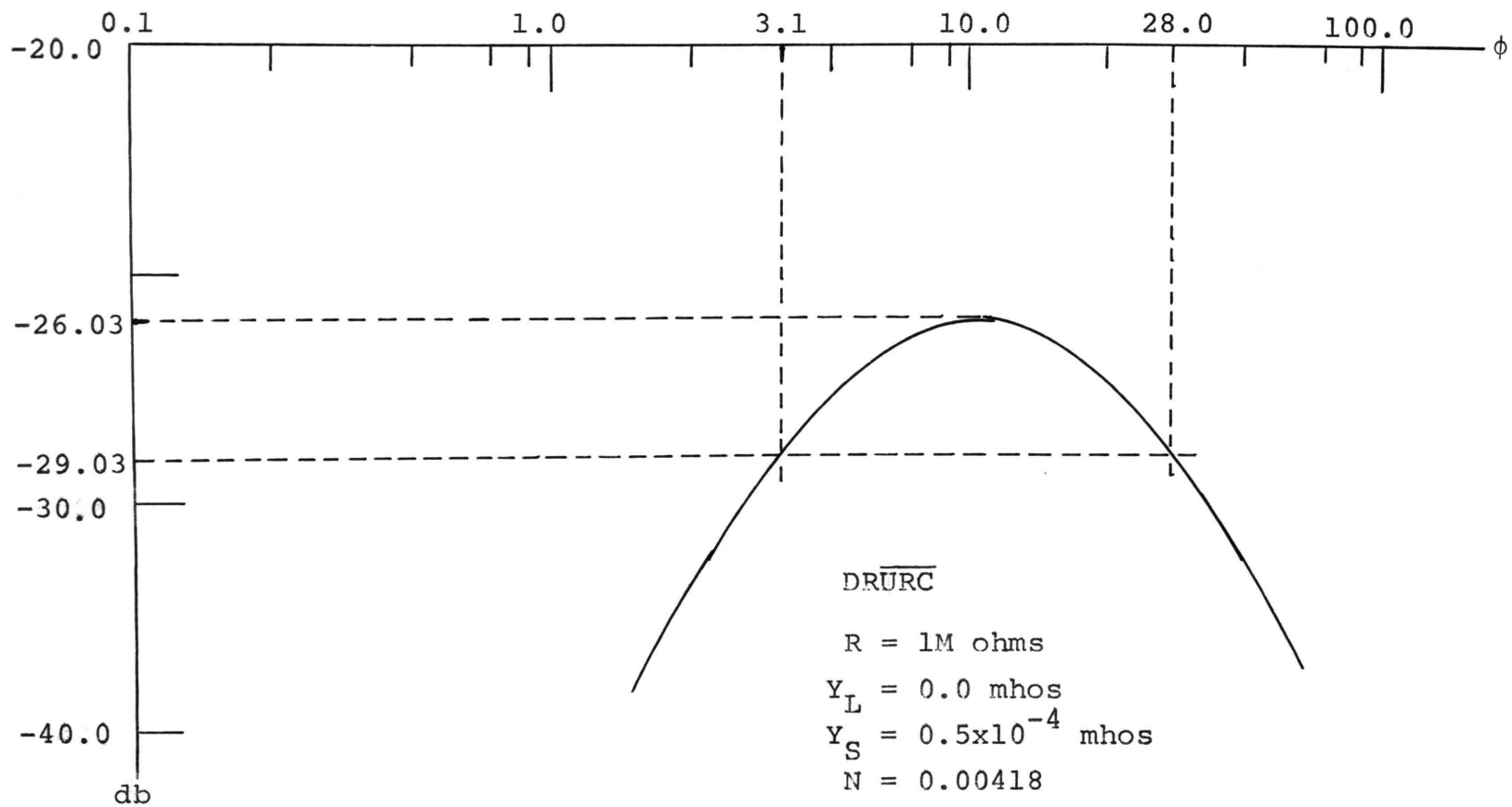


Figure G-4. Magnitude of equation (2.15) versus $\phi = \omega(1+N)RC$.